DISS. ETH No. 16219

Electrostatic Field Guided Assembly of Nanoscale Objects in Nonpolar Liquids using Local Surface Charges

-

Creating Patterned Arrays of Functional Biomolecules

A dissertation submitted to the
SWISS FEDERAL INSTITUTE OF TECHNOLOGY
ZURICH

for the degree of
Doctor of Technical Sciences

presented by
Nicola Naujoks
Dipl.-Ing.
born 08.06.1977
citizen of the Federal Republic of Germany

accepted on the recommendation of
Prof. Dr. A. Stemmer, examiner
Dr. P. Hoffmann, co-examiner

Zurich, 2005

Acknowledgements

This thesis is the result of my research at the Nanotechnology Group at the Swiss Federal Institute of Technology in Zurich (ETHZ).

First of all, I would like to thank Prof. Dr. Andreas Stemmer for supervising my thesis and for allowing me great freedom in conducting research at his lab.

Much appreciation is due Dr. Patrik Hoffmann from the Swiss Federal Institute of Technology in Lausanne (EPFL) for accepting the role as co-referee of this thesis.

I appreciated very much the discussion with Dr. Patrick Mesquida and Dr. Robert Stark, who introduced me in the exciting field of scanning probe microscopy.

Very special thanks go to Guy Birrer and Ralph Friedlos not only for invaluable electronic support, but also for their patience in trying to share their knowledge with me. Furthermore, I would like to thank my office-mates – Bohu, Roxana, and Dominik – for interesting conversation also on non-scientific topics.

All actual and former members of our group contributed to the nice time I had in the lab. Thanks go to (in the order of appearance): Dr. Patrick Mesquida, Dr. Robert Stark, Dr. Georg Schitter, Dr. Iouri Beliaev, Guy Birrer, Dr. Daniel Häfliger, Dr. Brian Cahill, Stefan Lengweiler, Dr. Bohuslav Rezek, Roman Fedosseev, Altan Gürsel, Miho Sakai-Stalder, Ralph Friedlos, Dr. Roxana Stoenescu, Manuel Aschwanden, Dominik Ziegler, Markus Beck, Dr. Andreas Vonderheit.

Finally, very special thanks go to Martin Seemann for his constant encouragement and support, especially during the time while I was writing down this thesis.

Nicola Naujoks
Zurich, November 2005

Contents

Abstract

The ability to selectively position nanoscale objects on a solid surface is a key factor for the success of nanotechnology. Novel techniques are required to assemble nanoparticles and biomolecules – serving as building blocks – into devices, thereby enabling the fabrication of quantum devices, bioelectronics systems, or novel chemical and biological sensors. Biomolecular patterns may for example be used to direct cell growth, and may also serve as templates to create other nanostructured materials.

Nanoscale objects are preferably handled in a parallel fashion based on self-assembly. Since classical self-assembly processes offer only limited control for positioning particles on a substrate, guiding the assembly proves necessary. One way to direct self-assembly processes is to use electric fields that allow for parallel manipulation of a large number of components. Electric fields may be generated by localized surface charges that may serve as templates for particle assembly, or as nucleation or reaction sites, allowing molecules to deposit in a predefined geometric pattern.

This thesis concentrates on the selective assembly of nanoscale particles and proteins on a solid surface guided by electrostatic forces that are generated by local surface charges written by an atomic force microscope (AFM) tip. The driving forces of the deposition process are studied in detail and the process is applied to selectively position proteins, thereby creating a basis for site-directed layered assembly of biomolecular structures.

The charge patterns are written into a thin polymer film by applying voltage pulses to a conductive AFM tip while scanning over the sample in ambient conditions. The same tips are used for characterizing the charge patterns by means of Kelvin probe force microscopy (KFM). As the charges are rapidly neutralized upon contact with water and polar solvents in general, insulating nonpolar fluorocarbon liquids are used for the subsequent development step. To this end, the samples are immersed into a water-in-oil emulsion, consisting of a dispersed aqueous phase containing particles or proteins, and a continuous fluorocarbon oil

phase. The electrostatic fields cause a net force of (di)electrophoretic nature on the droplets, thereby guiding the particles to the predefined locations.

As model system to study the deposition characteristics, we use 50 nm silica and latex nanoparticles dispersed in aqueous suspensions, taking advantage of the positive charge at the surface of the water droplets that spontaneously forms in nonpolar media. We find that the right choice of the substrate material offers additional control over the process, due to interfacial potentials that may appear in nonpolar media. While the deposition on FC-layers is shown to be dominated by Coulomb interactions, positive charges induced at the PMMA-oil-interface shift the balance of dielectric and Coulomb forces acting on the droplets in the direction of dielectric interaction, as manifested in the deposition on charge patterns of both polarities. Furthermore, the overall repulsive forces between PMMA surfaces and water droplets lead to very low background coverages. With these insights, we are able to significantly improve pattern definition on FC layers.

Protein patterns deposited by the same method are utilized as docking sites for functionalized particles and molecules to create layered biomolecular structures. By binding 40 nm sized biotin-labelled beads to predefined locations via a streptavidin linker, we verify the functionality of the previously deposited IgG-biotin. All assembly steps following the initial deposition of the docking proteins can conveniently be conducted in aqueous solutions.

Using emulsified water droplets as transporters offers great flexibility in the choice of particles and biomolecules to be deposited, since most nanoparticles and especially biomolecules are water-soluble. They neither have to show special affinity to the substrate material, nor do they have to be dispersible or even soluble in the oil. The resolution achievable with this method mainly depends on the emulsion droplet size. Although we observe individual 50 nm sized particles deposited onto single charge dots, the resolution in terms of pitch or minimal distance between objects depends on the droplet size, which is currently limited to a few hundred nm.

In this thesis, we investigate the mechanism of electric field guided assembly of nanoscale objects on solid surfaces. Due to its great flexibility, the process developed may offer a promising approach in nanoscale fabrication.

Kurzfassung

Das genaue Positionieren nanoskaliger Objekte auf Oberflächen ist von zentraler Bedeutung für den Erfolg der Nanotechnologie. Um Nanopartikel und Biomoleküle wie Bausteine zu Strukturen zusammenzufügen zu können, bedarf es innovativer Methoden, die die Fabrikation von Quanten- oder bioelektronischen Systemen, sowie von neuartigen chemischen oder biologischen Sensoren ermöglichen könnten. Strukturen aus Biomolekülen beispielweise finden Anwendung sowohl als Gerüste für die Herstellung anderer nanoskaliger Materialien, als auch zur Steuerung und Untersuchung von Zellwachstum.

Am besten geeignet zur Manipulation von Objekten mit Grössen im Nanomaterbereich snd parallele Methoden basierend auf kontrolliertem, oder gerichtetem, *self-assembly*, die, im Gegensatz zum klassischen *self-assembly*, mehr Kontrolle über den Prozess erlauben. Eine Möglichkeit zur Steuerung des assembly Prozesses ist der Einsatz elektrischer Felder, die beispielsweise durch Ladungsmuster auf Oberflächen erzeugt werden können, welche somit das geometrische Muster für die Anlagerung von Partikeln oder Molekülen vorgeben.

Im Rahmen dieser Arbeit präsentieren wir eine Methode zur exakten Positionierung von Partikeln und Proteinen auf Oberflächen mit Hilfe von via Ladungsmuster generierter elektrischer Felder. Neben der Untersuchung der treibenden Kräfte des Anlagerungsprozesses, zeigen wir, wie diese Methode zur lokalen Fabrikation von mehrschichtigen Strukturen aus Biomolekülen verwendet werden kann.

Auf dünnen Polymerfilmen werden Ladungsmuster erzeugt, indem bei Umgebungsbedingen eine Spannung an eine über die Probe scannende Rasterkraftmikroskopspitze angelegt wird. Die gleiche Spitze wird zur Charakterisierung der Ladungsmuster mittels Kelvin probe force microscopy (KFM) verwendet. Da wässrige Lösungen, sowie polare Lösungsmittel im allgemeinen die Ladungsmuster schnell neutralisieren, werden für die folgende Entwicklung der Proben unpolare, elektrisch hochisolierende Öle auf Fluorkohlenstoffbasis verwendet. Hierfür werden die Proben in eine Wasser-in-Öl

Emulsion getaucht, welche in ihrer dispersen, wässrigen Phase Nanopartikel oder Proteine enthält. Die Tropfen werden von den vom elektrischen Feld erzeugten Kräften zu den vordefinierten Positionen auf der Probe geleitet.

Zur Untersuchung des Anlagerungsprozesses wird eine Suspension mit 50 nm grossen Silica und Latex Partikeln als wässrige Phase verwendet. Befindet sich ein Wassertropfen in einem unpolaren Medium, wie Öl oder Luft, entstehen an seiner Oberfläche spontan positive Ladungen, welche hier genutzt werden, um die Tropfen selektiv einzufangen.

Die richtige Wahl des Probenmaterials bietet eine weitere Möglichkeit zur Kontrolle des Prozesses: An der Grenzfläche zwischen der Probe und dem unpolaren Oel können aufgrund der Interaktion beider Materialien elektrische Potentiale entstehen, welche das Verhältnis von Coulomb- und dielektrischen Kräften verschieben können. Während auf Fluorkarbonschichten (FC) Coulomb-Kräfte vorherrschen, verschiebt ein positives Potential an der PMMA-Oel Grenzfläche das Verhältnis zugunsten dielektrischer Kräfte. Ausserdem bewirken die abstossenden Kräfte zwischen Wassertropfen und Probe eine sehr geringe Hintergrundbelegung auf PMMA. Mit diesen Erkenntnissen ist es uns gelungen, die Definiton der Strukturen auf FC-Schichten deutlich zu verbessern.

Mit der gleichen Methode werden Strukturen von Proteinen erzeugt, welche nachfolgend als „Andockstellen“ für funktionalisierte Partikel und Moleküle verwendet werden, und somit eine Basis für mehrschichtige biomolekulare Strukturen bilden. Die Funktionalität von Strukturen bestehend aus mit Biotin modifiziertem IgG wurde durch Anlagerung von 40 nm grossen Polymerpartikeln via Streptavidin nachgewiesen. Alle Modifikationen können in wässrigen Lösungen durchgeführt werden.

Das Verwenden von Wassertropfen als Transportmittel bietet grosse Flexibilität in der Wahl der zu positionierenden Partikel, da die meisten Nanopartikel und Biomoleküle wasserlöslich sind. Die Auflösung dieser Methode wird hauptsächlich durch die Tropfengrösse in der Emulsion bestimmt. Obwohl es möglich ist, einzelne 50 nm grosse Partikel zu positionieren, hängt der minimale Abstand einzelner Punkte zueinander direkt von der Tropfengrösse ab, die zur Zeit bei einigen hundert nm liegt.

In dieser Arbeit wird der Mechanismus des durch elektrische Felder kontrollierten *self-assembly* untersucht. Ihre grosse Flexibilität könnte die Methode zu einem vielversprechenden Ansatz in der Nanotechnologie machen.

1 Introduction

1.1 Particle Assembly at the Nanoscale

The ability to selectively position nanoscale objects on a solid surface is a key factor for the success of nanotechnology. Molecular- or nm-scale objects with a variety of electrical, chemical, and optical properties are routinely synthesized today. These nanoparticles are generally considered as building blocks for future nanoscale devices. The challenge remains to assemble these particles in two or three dimensions in predefined arrangements, thereby enabling the fabrication of quantum devices, bioelectronics systems, or novel chemical and biological sensors.

Conventional lithographic methods as applied in microtechnology and –electronics usually follow the top-down approach. Their use in nanoscale fabrication is limited not only due to the resolution achieved, but also because of expensive and demanding clean room technologies. The harsh process conditions, such as vacuum, high temperatures, and the use of strong etchants in classical lithographic technologies prohibit their application in the fabrication of molecular structures, especially when working with biomolecules.

Novel techniques are required to assemble the building blocks into devices: Single particle manipulation does not prove suitable due to low yield and extremely slow fabrication speed. Thus, one would prefer to handle the particles in a parallel fashion based on self-assembly. In nature, self-assembly causes the build-up of structures on a cellular scale, without being externally controlled. However, in view of technical applications, guiding or directing the assembly proves necessary, since classical self-assembly processes offer only limited control for positioning particles on a substrate.

Various approaches for guided self-assembly have emerged recently, be it capillary forces that direct colloidal particles into lines [Ray2005] or two- and three-dimensional arrays [Deegan2000a; Maillard2001], or a selectively patterned

surface, either chemically, electrically, or structurally [Garno2002]. Chemical patterns on a nanometer scale typically are achieved by structuring self-assembled monolayers (SAM) by means of elimination or by inducing changes in the head groups, typically by oxidation [Maoz1999]. Nanoscale charge patterns on surfaces may be used as nucleation or reaction sites or for preferential adsorption of particles [Garno2002; Hoeppener2002]. Electrostatics may also be applied for particle assembly in terms of dielectrophoretic forces [Suzuki2004]. Zheng et al. used nanotubes as templates for dielectrophoresis-based particle deposition [Zheng2004].

A variety of SPM-based techniques have been introduced for patterning surfaces on the nanoscale. As scanning probes are often operated under ambient conditions, be it in air or in liquids, they are particularly suited for fabricating molecular structures. Furthermore, pattern resolution depends to a large extent on the probe geometry, which theoretically enables resolutions of a few nm. A review on SPM-based fabrication methods in general is given in [Nyffenegger1997], whereas a recent overview on electrical SPM-based techniques can be found in [N. Naujoksto be published in 2005].

Patterning might be based e.g. on pure mechanical effects [Garno2002], such as scratching or indentation, on thermomechanical effects [Mamin1992], or on local oxidation of semiconductors [Dagata1998; Dagata2004a; b] or SAMs [Maoz1999]. Molecules or particles can be delivered to a target substrate in a direct-write fashion by dip-pen lithography (DPN), first demonstrated by Piner et al. [Piner1999], where capillary forces transport molecules from an AFM tip to the substrate. Since its first invention, the use of dip-pen lithography has been extended to the deposition of biomolecules [Agarwal2003] and to electrochemically induced deposition of metallic lines [Li2001; Maynor2001]. The water nanocapillary that forms between tip and sample in humid atmosphere acts like an electrochemical nanocell, reducing metal salts locally to pure metal on a Si surface (E-DPN). A review on various DPN methods can be found in [Ginger2004].

Electric fields have proven suited for parallel and contactless handling of small particles by using long-range (di)electrophoretic forces, like in xerography, where charged toner particles are attracted to light-generated charge patterns. Already in 1976, Feder has reported the attachment of carbon particles to electron-beam charged patterns on Teflon foils with a resolution in the micrometer range

[Feder1976]. Roughly 20 years later, Wright and Chetwynd discussed the use of SPM-generated charge patterns as templates for nano-assembly [Wright1998].

Local surface charging for particle deposition has been achieved by various routes, be it conductive stamps [Jacobs2001], focused ion and electron beams [Fudouzi2001; 2002a; b], or SPM-based techniques [Mesquida2002c; d; Naujoks2004; 2005]. Just like the charging mechanism, the deposition of the particles or molecules also offers several possibilities: Nanoparticles could be deposited directly after creation from the gas phase in an aerosol process [Krinke2002; Krinke2001]. For the deposition of particles from the liquid phase, suspensions in fluorocarbon liquids have been used to large extent [Fudouzi2002a; b; Jacobs2001], although emulsions also found their applications in electrostatic field guided particle assembly [Mesquida2002d].

Electric fields are particularly suited for directing particle assembly due to various reasons: The electrostatic force is one of the significantly effective forces at the nanoscale. Polarity and strength of the field can easily be adjusted, enabling selective manipulation. Regarding the materials, electric fields also offer great flexibility, since electrostatic forces act on charged and uncharged as well as dielectric and conducting particles suspended in a medium. Charge sites, acting as self-assembly targets, may also be created by mixed monolayers [Tzeng2002], providing charge heterogeneity.

SPM-based local charging of surfaces has been investigated since the first years of scanning probes. Stern reported on charge patterning of insulating thin films [Stern1988]. Since then, most studies focused on high-density data storage, employing the SPM tip as the read/write head. Although the first proposals for using SPM-generated charge patterns for nanoscale assembly appeared rather late at the end of the 1990s [Wright1998], the number of studies increased recently [Mesquida2001; Wilks2004], including investigations of different substrates for charge writing.

A crucial requirement for using these charge patterns in nanofabrication is the stability of the charge patterns. Using either a gas–phase environment or an insulating, nonpolar medium has one simple reason: The charges on the substrates are not stable in aqueous solutions and polar solvents in general, probably because the charge is trapped at the surface, rather than in the bulk of the material. Nonpolar liquids, such as hydro- or fluorocarbon oils, have much higher resistivity and provide better stability of the charge patterns.

Biomolecular patterns not only find applications in the field of biosensors, but may also be used to direct (patterned) cell growth [Bouaidat2004], or directing the motion of kinesin by patterning microtubules – their tracks – onto substrates. Various strategies for patterning surfaces with biomolecules that are currently under investigation involve classical lithographic methods [Falconnet2004; Kane1999], as well as dip-pen- [Lee2003] and E-DPN-based approaches [Garno2002], and sphere based lithography [Garno2002].

1.2 Motivation and Outline of the Thesis

Achieving controlled assembly of systems in the nanoscale regime opens new possibilities in fields ranging from molecular electronics to biomedical and bioelectronics applications to catalysis. This creates a need for new routes to selectively pattern surfaces either chemically, structurally, or electronically. Positioning and immobilizing biomolecules, e.g. oligonucleatides or proteins, in an array on a surface could help in the fabrication of biosensors. Biomolecular patterns are used to direct cell growth, and may also serve as templates to create other nanostructured materials

One way to guide or direct self-assembly processes is to use electrostatic fields that allow for parallel manipulation of a large number of components. Localized surface charges may serve as templates for particle assembly, or as nucleation or reaction sites, allowing molecules to deposit in a predefined geometric pattern.

Nanoscale objects have been selectively positioned on a surface using local surface charges. Though, the exact deposition mechanism is not fully understood, especially when working in nonpolar liquids, and more profound understanding of the driving forces is necessary to render this technology suitable for nanoscale manufacturing. Besides gaining a basic understanding of the process itself, the application of this method for creating arbitrary nanoscale patterns of biomolecules is to be investigated, too. These particle or biomolecular patterns may for example serve as docking sites in molecular sensors design or as building blocks in the fabrication of new materials and electronic devices.

The simple, xerography-like, process presented here is based on electrostatic field guided deposition of objects to charge patterns previously generated on the substrate using the lithographic capability of an atomic force microscope (AFM)

(Fig. 1.1A). As the local surface charges do not provide enough charge stability in aqueous solutions, the particles are deposited from a water-in-oil emulsion, consisting of (particle loaded) water droplets dispersed in a nonpolar oil phase (Fig. 1.1B). Electrostatic fields cause a net force of (di)electrophoretic nature on the disperse phase of the emulsion, which transports the nanoscale objects to the patterns (Fig. 1.1C). The choice of the substrate material significantly influences the forces acting on the droplets during deposition, leading to qualitatively and quantitatively different deposition results. The deposited biomolecules subsequently act as docking sites for functionalized molecules or particles. All further modifications can be conducted in aqueous solutions.

One great advantage of this method is that processing can be done without exposing the samples and the molecules to harsh conditions usually found in standard lithographic processes. Guiding particle assembly via electric forces enables a large number of objects to be processed simultaneously. The use of water droplets as transporters for the particles offers great flexibility in the choice of particles or molecules to be deposited, since they do not have to be dispersed in the oil directly [Stemmer2002]. Furthermore, organic molecules, especially proteins require an aqueous environment to maintain functionality. The method takes advantage of a number of "naturally" occurring phenomena, such as the positive charge at the surface of water droplets that establishes when they are dispersed in nonpolar media, or the capacity of proteins to serve as natural emulsifying agents. Furthermore, the right choice of substrate material offers additional control over the interaction forces during deposition.

This thesis is organized in three major parts:

- ◊ SPM-based charge writing is described in Chapter 2: Besides a general overview, experimental details of the charge writing process are given.
- ◊ Chapter 3 elucidates the deposition characteristics and driving forces: The chapter starts with short introductions to interactions in nonpolar media, and to emulsions, with focus on charging phenomena. After investigating the properties of the emulsion we are working with, the electret-oil interface is studied regarding overall interactions and charge stability. Results of particle deposition help to complete the understanding of the deposition mechanism [Naujoks2005]

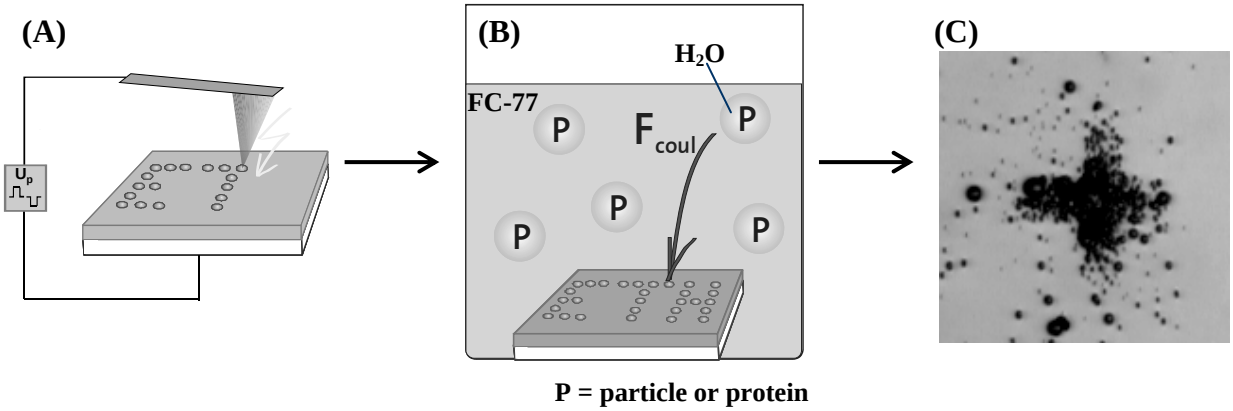

Figure 1.1 Process scheme. Patterns of local surfaces charges are written into the substrate by applying voltage pulses to an AFM tip (A). The sample is subsequently developed in a water-in-oil emulsion, were water droplets (containing particles or molecules) are attracted to the patterns by the electrostatic field generated by the surface charges (B). Water droplets selectively deposit on the preselected region, resulting in structures of particles or proteins (C) that may serve as templates for further assembly.

◊ Results of the selective deposition of proteins onto charge patterns are presented in Chapter 4. After checking the biomolecular patterns regarding their functionality and activity, we show how layered biomolecular structures can be created via specific antigen-antibody reactions [Naujoks; 2004], [Naujoks].

2 Charge Writing

Charge writing has to be performed with materials that can trap charges for a sufficiently long time, so called electrets. According to the definition of Sessler [Sessler1987] an electret is a dielectric material exhibiting a quasi-permanent electric charge usually characterised by an external, electric field. The term quasi-permanent means that the time constant for charge decay is longer than the time required for the experiment [Sessler1987]. This very general definition includes "real"-charge electrets, in which surface or space charges occupy trapping-sites, as well as piezo- or ferroelectric materials. In general, dielectrics are characterized by a large bandgap of more than 4 eV, which leads to a very small conductivity at ambient temperature [Sessler1987]. In the case of electrets, defects in the crystalline structure such as impurities or interfaces offer trapping-sites for holes or electrons within the bandgap [Sessler1987].

Charges are trapped either by redistributing electrons within the material or by injecting excess charge carriers into the volume or trapping them at the surface, keeping them spatially localized for a certain time. Technically, charges can be generated by contact electrification with or without applied voltage, by corona charging and by using e-beams or ion-beams. The most widely known electrets are carnauba wax, fluorocarbon or hydrocarbon polymers and silicon based multilayer systems [Kressmann1996]. In this study the deposition characteristics have been analyzed for fluorocarbon and PMMA layers on silicon wafers.

2.1 Scanning-Probe-Microscopy-Based Charge Writing

Shortly after the invention of scanning-probe microscopy (SPM) in the 1980's these microscopes were utilized to perform charge-writing (SPM-CW) on the nanometer scale on dielectric materials. With this method, positive (holes) or negative (electrons) charges are injected into or deposited on the surface of a dielectric by applying a bias voltage to a conductive SPM tip in close proximity or

contact with the sample. SPM-CW has the great advantage that *in-situ* studies can be carried out conveniently by performing the charge injection and the subsequent charge pattern-imaging using the same tip and instrument.

One of the main motivations for performing SPM-CW was the potential applicability to high-density data storage using charge "dots" as data bits. Encoding digital information in electrostatic instead of magnetic form seemed promising due to the small size of the charge patterns. On poly(methyl methacrylate) (PMMA) for example, 70-nm-diameter charge dots could be created [Schönenberger1992]. There is no a-priori physical restriction of the size of the charge patterns. This is different from magnetic recording-techniques, where the finite size of magnetic domains or the superparamagnetic effect limit the resolution. In principle, the smallest charge pattern would be generated by a single elementary charge at a fixed position. However, limiting factors such as diffusion and recombination of charge carriers leading to decay of the charge patterns have to be taken into account.

A newer application, which was increasingly reported in the literature in the last 5-6 years, is the use of nanoscale charge patterns as local attachment sites for nanoparticles or molecules. Because of the analogy to the working-principle of photocopiers and laser printers it is often referred to by the term micro- or nano-xerography.

SPM-CW has been applied to thin-film electrets of a thickness ranging from a few nanometers to several hundred micrometers. Typical materials are polymer layers or oxides. If the tip is in direct mechanical contact with the surface true contact-charging occurs, whereas a corona discharge can occur if the tip is held at some distance (several 100 nm) from the surface. Because of this short distance between tip and surface or back-electrode the electric field is often very high even at low bias voltage and the breakdown field strength of the electret can easily be reached. The quantity of charge transferred does not only depend on the material properties of the electret, i.e. the number, location and energy levels of the trapping sites, but also on parameters such as the applied voltage, its polarity, the film thickness, the pretreatment of the electret, etc.

As the tips must be conductive, full-metal, metal-coated or highly doped semiconductor tips are used for SPM-CW. Examples are etched STM tips made of W- or Ni-wires or metal-coated (Au, Pt, PtIr, TiPt, Co) AFM tips. Doped Si tips

with a resistivity of the order of 0.001 Ohm·cm are sometimes considered better than metal-coated tips because the latter can show abrasion of the metal layer during SPM-CW. An additional metal-coating also increases the tip radius.

Besides pure charge transfer and trapping, unwanted effects may occur, which are often difficult to control and separate from the charge-writing process. For example, material can be transferred between tip and sample due to the current and topographic or chemical modifications can be induced when applying a voltage. In an ideal case, the process consists exclusively of the creation of net surface or space charge areas of the sample.

Polymeric materials

Polymers were amongst the first materials investigated by SPM-CW, mainly because they are known to exhibit very good charge storage properties [Sessler1987] and because thin-films can easily be produced by spin-coating or gas phase deposition methods. The first example was PMMA, which is commonly used as resist in electron beam lithography and which can be spin-coated to form very thin (< 100 nm) and smooth films. Stern and co-workers were the first to create and image charge patterns using Ni-wires as SPM tips and a 1-mm-thick PMMA-layer as electret [Stern1988]. Voltages of more than 100 V were applied for several milliseconds in air at ambient conditions and the charge dots obtained were about 2 µm in diameter. They decayed within about 1 h but showed very little lateral spread. Positive and negative charge patterns could be discriminated by imaging with a suitable detection voltage applied to the tip and it was shown that the sign of the charge depends on the polarity of the voltage pulse applied during SPM-CW [Terris1990]. Although PMMA is a promising material for SPM-CW systematic investigations of the influence of, e.g., film thickness or of structural parameters such as the molecular weight of the polymer are scarce.

Other polymers, which are known to exhibit excellent charge storage properties with respect to amount and charge retention time are polytetrafluoroethylene (PTFE) and related fluorocarbon-based materials [Sessler1987]. Spin-coated, perfluorinated films have been contact-electrified by SPM-CW using relatively high voltages of up to 300 V and long pulse lengths of several seconds [Umeda1994]. The resolution achieved was ca. 280 nm and the patterns decayed

after about 8 h. Layers of PTFE-like fluorocarbon films deposited by plasma-enhanced chemical vapor deposition have been investigated systematically by SPM-CW [Mesquida2002a; Mesquida2002b]. Charge patterns of positive and negative sign, with a resolution of about 100 nm in the best case and 200 nm on average, could be created using commercial, highly-doped Si AFM tips.

In polymers, the cause of localized charges are chemical or structural anomalies such as impurities, defects, chain irregularities or imperfections in crystalline regions, which are often located at the electret surface.

Inorganic materials

The electret most widely investigated by SPM-CW is SiO_2 because of its high availability and its outstanding importance as dielectric material in microelectronics. However, a disadvantage of SiO_2 as electret is the formation of silanol groups on the surface and its hydrophilicity, which leads to adsorption of ambient water causing a high lateral surface conductivity [Olthuis1992]. Morita et al. reported contact electrification of a 5.3 nm thin SiO_2-film by combined AFM/STM [Morita1993a]. A voltage of -4 V was applied using an ion-implanted diamond tip, which was brought into contact with the sample for 20 s resulting in negative charge dots of a diameter of about 1 µm. The time course of the charge decay was extensively investigated and showed 3 phases of different decay speeds, which was attributed to solid-liquid-like phase transitions of negative surface charges [Morita1993b; Sugawara1994; Uchihashi1994a]. Surface charge dissipation was also shown to be affected by environmental conditions and pretreatment of the sample [Uchihashi1994a]. As expected, charge decay was higher at higher humidity and preheating the sample made charge patterns more stable. The decay could be reduced considerably by coating the SiO_2 with silane monolayers or hexamethyldisilazane before SPM-CW [Enikov2004; Uchihashi1994b]. The best resolution reported was ca. 200 nm [Uchihashi1997].

Promising systems from the point of view of charge pattern stability and resolution are nitride-oxide-silicon (NOS, $Si_3N_4/SiO_2/Si$) and oxide-nitride-oxide-silicon (ONOS, $SiO_2/Si_3N_4/SiO_2/Si$) layers. Charges trapped in NOS-layers showed a high stability at temperatures up to 300°C and in high humidity [Amjadi2001]. It is generally assumed that charges are trapped in the bulk of the

nitride and at the nitride/oxide interface. The first actual high-resolution charge image has been shown by Barrett and Quate using etched W-wires and Ir-coated SiO_2 tips to which voltage pulses of -40 V and 20 µs length were applied in mechanical contact with the sample surface [Barrett1991]. The smallest dot size obtained was 75 nm full width at half maximum (FWHM) and the dots could be "erased" by voltage pulses of opposite sign. No lateral spread was observed and further ageing experiments performed at elevated temperature showed that charge retention times of 30 years could be extrapolated from the decay curves [Terris1995]. With ONOS structures a resolution of 80 nm FWHM was reported [Fujiwara1996].

The resolution was increased even further by Tzeng and co-workers using SPM tips to which carbon nanotubes were attached [Tzeng2002]. Charge-writing and imaging could be performed with these extremely sharp and high-aspect-ratio tips on 4-nm-thin NOS-samples in high-vacuum. Patterns of 50 nm resolution were reported with an imaging-resolution of 5 nm.

Several other, inorganic electrets have been used for SPM-CW. Charge patterns of 60 nm feature size were reported on $SrTiO_3$ [Uchihashi1994b]. The patterns were stable for at least 23 min. Multilayers of CeO_2/Si/CeO_2/Si(111), which are interesting for Si-heterojunction technology because of the small lattice mismatch of CeO_2 with Si, could be used to write charge dots of 60 nm FWHM with a stability of 24-40 h [Jones1999]. Lambert and co-workers reported recently a detailed investigation and discussion of the charge transfer mechanism into Al_2O_3, which is attractive for microelectronics because of its high dielectric constant [Lambert2004]. The feature size of charge patterns produced in N_2-atmosphere was 100-200 nm FWHM; no decay studies were reported.

A novel and promising route to create very small and stable charge patterns is to confine space charges in nanometer scale structures. Gemma et al. charged small droplets of TTPAE, a molecule used as donor in organic electroluminescent devices [Gemma1995]. Only positive charges could be transferred, which is consistent with the electronic properties of the molecule. The size of the charge patterns appeared to be 30-70 nm, which was slightly larger than the size of the domains. No significant decay was observed after 10-20 h and the authors estimated that only a few elementary charges were transferred per droplet. Boer et al. charged individual Si-nanocrystals of 28 nm diameter embedded in a 100-nm-thick SiO_2-layer and observed that the charge patterns are confined in individual

crystallites [Boer2001b]. They estimated the number of transferred elementary charges to a few hundred [Boer2001a]. Recently, Wilks and co-workers showed localized, 10-nm-size charge patterns imaged by STM on samples of 8-nm-diameter SnO_2-nanoparticles deposited on a ceramic substrate. These features were created by applying negative voltage pulses to an STM tip scanning the sample in UHV [Maffeis2004]. The features could be erased by applying an opposite voltage and were stable for more than 1 week [Maffeis2004].

The two most widely accepted „benchmark“ criteria for electrets in SPM-CW are charge pattern resolution and decay time. However, one has to be careful when comparing results in the literature as experiments by different groups were often performed under conditions that cannot be compared directly, e.g. ambient air, inert atmosphere, vacuum, corona-charging or contact-electrification. From the recent literature, one can to some extent infer that a practical resolution of about 100 nm can be achieved with most electrets. A higher resolution is conceivable but it would be very likely limited by the finite resolution of imaging-methods rather than the actual charge-writing process. The question whether long decay times are needed at all depends on the application. For data storage, long decay times of the order of years are necessary. However, for nanoxerography processes the attachment of particles or molecules on the charge patterns takes place within a few minutes and long charge retention times are therefore less crucial [Mesquida2002d; Naujoks2003; 2004].

2.2 Kelvin-Probe Force Microscopy

SPM-CW has the great advantage that in-situ studies can be carried out conveniently by performing the charge injection and the subsequent charge pattern-imaging using the same tip and instrument. Electric force microscopy and its variants such as Kelvin-probe force microscopy (KFM) are typically used to image and quantify the charge patterns [Fujihira1999; Nonnenmacher1991]. An important, common characteristic of these methods is that the spatial, electrical resolution is considerably lower than the topographical one. This is due to the long-range of electrostatic forces and the large interaction area caused by the finite geometry of the tip [Jacobs1998]. In practice, the best resolution with standard SPM-tips is in the range of 50 -100 nm. STM-based imaging methods, which record currents instead of electrostatic forces, achieve a higher resolution but STM is difficult to perform on insulating surfaces and the interpretation of the data is not straightforward [Wilks2004].

KFM allows for quantative measurements of the surface potential distribution on arbitrary samples in non-contact mode. Since Nonnenmacher et al. first introduced the KFM in 1991 [Nonnenmacher1991], the principle was used for various applications ranging from the detection of material contrasts [Jacobs1997], to dopant profiling [Kikukawa1995], to imaging of biological samples [Knapp2002]. For a review the reader is referred to [Fujihira1999].

Since the measurement principle has already been described numerous times, we will concentrate on the main characteristics here. KFM measurements are typically performed in the so-called lift mode. In consequence, each scan line is traced twice: After acquiring the topography in a first tapping mode scan, the tip is lifted, and performs the KFM scan at a constant lift height above the sample surface (Fig. 2.1). When lifted above the sample, the mechanical excitation of the tip is switched off, and the tip is electrically excited at its mechanical resonance frequency ω. To this end, an AC voltage $U(t)$ is applied to the cantilever, with amplitude U_{AC} and DC offset U_{DC}:

$$U(t) = U_{AC}\cos(\omega t) + U_{DC}.$$

Kelvin-probe force microscopy is a nulling technique: The ω component of the force acting between tip and sample is recorded by a lock-in amplifier, and used as a feedback signal to adjust the offset voltage U_{DC}, so that the F_ω=0:

$$F_\omega = \frac{\partial C}{\partial h} U_{AC}(U_{DC} - \Phi_S)\cos(\omega t)$$

leading to U_{DC}=Φ_S. Under experimental conditions the tip has its own potential Φ_T depending on the material. The Kelvin signal, U_{DC}, then corresponds to the local contact potential difference between tip Φ_T and sample Φ_S:

$$U_{DC} = \Phi_T - \Phi_S.$$

By performing the measurements in lift mode artifacts occurring due to the tip geometry are minimized, and also the influence of non-electrostatic forces, such as van-der-Waals forces is kept constant during a single measurement.

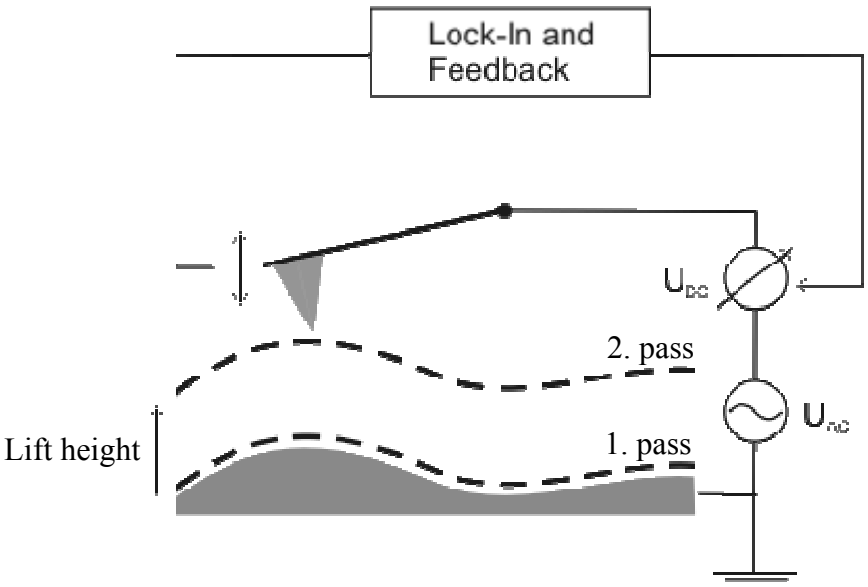

Figure 2.1 Principle of KFM measurements. After acquiring surface topography in the 1st scan, the tip lifted by a certain height to record the local surface potential in a second pass. The oscillation of the cantilever is used as a feedback signal to adjust the DC voltage U_{DC}.

2.3 Experimental Details

2.3.1 Samples

Due to the excellent charge storage properties of PTFE, its long decay times, as well as its remarkable inertness against almost all kinds of chemicals, fluorocarbon layers are used as substrates for particle deposition in this work. Charge writing in PTFE foils and subsequent attachment of micrometer sized particles was already performed in 1976 by Feder using electron beam irradiation [Feder1976]. As second type of electret layer we used poly(methyl methacrylate) (PMMA), also known for its excellent charge storage properties. The samples consist of polished p-doped Si wafers as conductive support, coated with a thin electret layer.

The fluorocarbon (FC) layers were produced by plasma-enhanced chemical vapour deposition (PECVD) from C_4F_8 precursor gas in a Deep Reactive Ion Etching (DRIE) set-up, leading to 300 nm thick layers (in the following termed FC-layers). Alternatively, thin fluorocarbon layers have been prepared from hexafluoropropene (CF_3-CF=CF_2) (HFP) as precursor gas according to [Mesquida2002b] in a custom-built plasma chamber (FC-HFP). 150 nm thick PMMA layers were spin-coated from a 3.5% solution of PMMA (M_W=350kDa) in toluene.

2.3.2 Technical Details of the Charge-Writing Process

We used a Nanoscope MultiMode atomic force microscope with a NanoScope IIIa Controller (Digital Instruments Veeco Metrology Group, Santa Barbara, CA, USA) for the charge writing and charge pattern imaging. By operating the same instrument in KFM mode (using the phase extender capabilities), the generated local surface charges were detected. Charges of either polarity were written by applying voltage pulses to the conductive tip while scanning over the surface (Fig. 2.2). N-doped silicon tips with a resistivity of 0.01 – 0.025 Ωcm were used throughout the experiments. Length t_p and height U_p of the voltage pulses were set by a custom-built pulse generator.

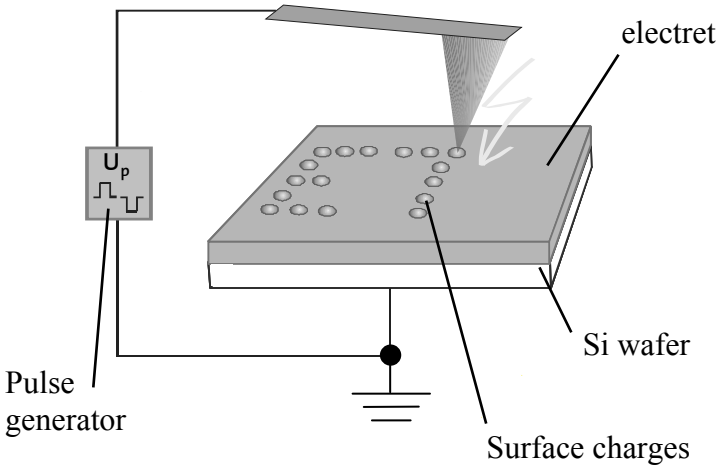

Figure 2.2 Charge writing procedure. While the AFM tip is scanning over the sample surface, voltage pulses, generated by a custom-built pulse generator, are applied between the tip and the conductive backside of the sample. Local surface charges are stored in the electret layer.

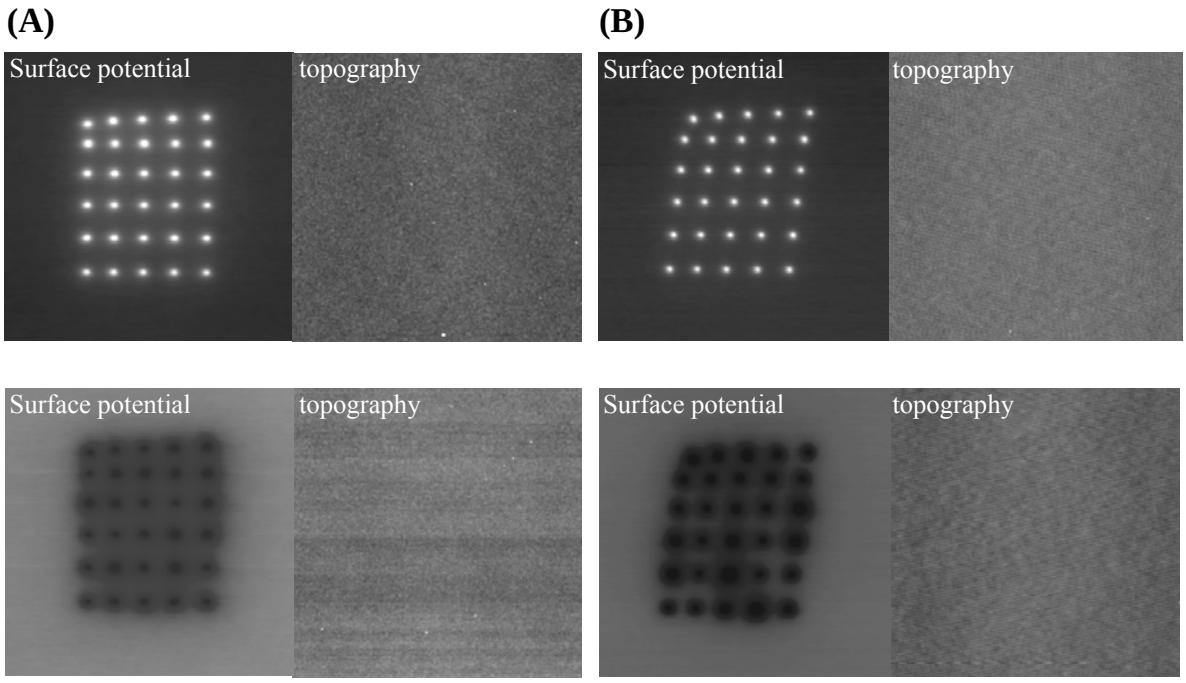

Figure 2.3 Patterns of local surface charges. KFM (left) and topography (right) images of positively (top) and negatively (bottom) charged dots on FC-layers (A) and PMMA samples (B). Charge pattern: 30 dots (6x5) with 2 μm pitch. Samples were charged by 1 ms voltage pulses of +/- 60 V (PMMA) and +/- 70 V (FC) pulse height. The z-scale in all KFM images is 2 V, with brighter regions corresponding to higher potential. Scale bar: 2 μm.

The voltage applied to the tip, and the pulse length were varied between 30 and 80 V and 1 and 3 ms, respectively, resulting in different surface potentials. Due to the short voltage pulses, topographic modifications of the films can be excluded, as no features are revealed in the topography images in Figure 2.3.

Two different kinds of charge patterns have been used to study particle deposition: Large scale cross patterns helped to determine the selectivity of the process during deposition, while deposition onto small scale dot patterns was better suited for studying pattern definition (Fig. 2.4). The small structures (Fig. 2.4A) were written with the help of the internal lithography mode of the Nanoscope software, which was used to laterally move the tip to the specified location. After applying a single voltage pulse, the tip was moved to the next location. The voltage pulses were triggered using the pulse generator. As the internal lithography mode showed too much drift and hysteresis for larger scanning areas, the large scale structures were generated in a more simple fashion: Charges were applied by turning the pulse generator on and off manually when the tip was normally scanning over the surface. This approach only allowed for writing simple geometric structures (Fig. 2.4B). In any case, charge writing was performed in tapping mode with z-feedback turned on, since applying voltage pulses in contact mode often leads to a damaged tip or sample surface.

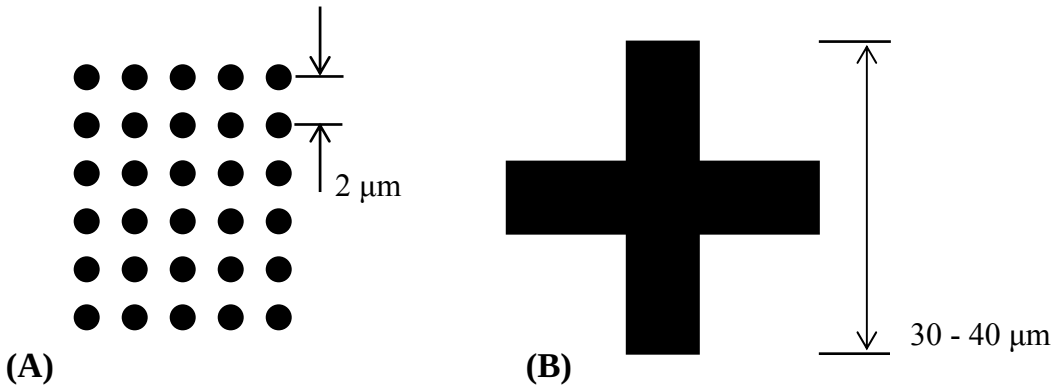

Figure 2.4 Charge pattern geometries. Small scale patterns consist 6 rows of 5 dots 2 µm apart (A) and are generated by applying one pulse per dot. Larger patterns are charged by applying a voltage to the cantilever during scanning, resulting in up to 40 µm large crosses (B).

3 Deposition of Particles

After writing the charge patterns, these surface charges have been used as templates to guide particle deposition. To this end, the samples are immersed into a so-called development solution, according to the process scheme presented in the Introduction (Fig. 1.1). The solution is actually an emulsion, consisting of water droplets dispersed in an insulating oil. The need for an insulating medium for particle deposition is determined by the poor stability of the surface charges when immersed into polar liquids. Though, most particles are difficult to disperse in nonpolar media, but are commercially available in form of a powder, or, in the case of nanoparticles and biomolecules, in aqueous solutions. By dispersing the particle solutions into the oil, the particles stay in their "natural" environment, while at the same time the charges on the sample are retained.

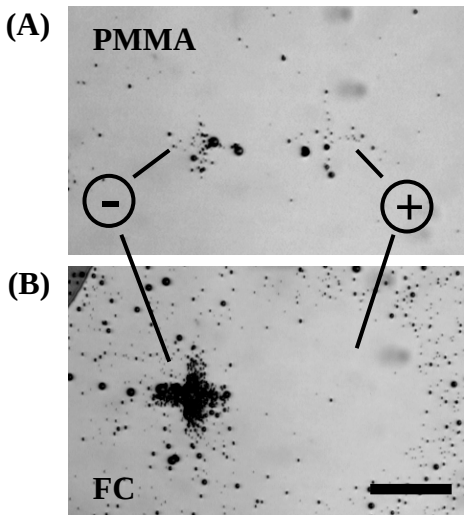

Figure 3.1 Influence of substrate material on particle deposition. Reflected light microscopy images of 330 nm silica beads on PMMA (A) and FC-samples (B) deposited from emulsion. Surface potential: +/- 3V, charge pattern: 40µm wide cross. Samples were mounted on the same sample holder and processed simultaneously. Scale bar: 40 µm.

The choice of the substrate material showed to have a significant influence on the interaction forces between the water droplets and the surface charge patterns, since the deposition results on PMMA and FC-layers display fundamental differences (Fig. 3.1): While the water droplets selectively get attracted to negative charges on FC-samples, we found deposition on both polarities on PMMA.

As we are working in nonpolar liquids, we will open the chapter with a brief overview on the characteristics of interactions in *nonpolar media*. Since the substrate material plays a crucial role in particle deposition, we first study the materials themselves including their interactions: the *emulsion* (corresponding to an oil-water-interface), and the *electret-oil interface*, followed by an investigation of the interaction between them (*emulsion-electret*). Based on insights regarding the driving forces gained in these investigations, we will conclude this chapter with a discussion on the *bead deposition* characteristics.

3.1 Electrical charges in nonpolar media

At first sight, surface charging is not thought to be of significance for materials in contact with nonpolar liquids. The reason is that ions have a very low solubility in nonpolar liquids and hence a diffuse layer of charge cannot form. However, the presence of electrical charges in nonpolar media was experienced very early [Fowkes1982], especially in the petroleum processing industry. The flow of petroleum generated large unwanted electrostatic potentials, which occasionally led to explosions. Klinkenberg et al. [A. Klinkenberg1958] showed that trace compounds present in the oil are responsible for the large potentials: Ions preferentially adsorbed to metal surfaces. The flow of liquid then separated the charges, building up electric fields that could discharge by sparking. A higher concentration of the same ions increased the conductivity of the oil sufficiently to prevent the build-up of large electrical potentials.

Besides petroleum processing, the phenomenon of surface charging in nonpolar liquids is of importance in many other practical situations including various imaging process technologies (liquid toner), manufacture of organic coating materials, and finely controlled synthesis of particulate materials. In most cases, charging is facilitated by enhancing the solubility of ions in the nonpolar liquid.

For general reviews on electrical charges in nonaqueous media please refer to [H.F. Eicke1987; Kitahara1984; Morrison1993; 2002].

Although the first studies on ionic dissociation of electrolytes in low dielectric constant liquids and on the formation of double layers in nonaquoeous media appeared already in the 1960s [Fowkes1972], the answer to how charged species are created and how they remain charged is still debated. One generally accepted model is that the electric charges are stabilized against neutralization by separating them in larger structures, such as micelles or complex macroions. Before describing this mechanism in more detail, let us first take a look on some very basic properties of dispersions in nonpolar media.

The dielectric constant for nonpolar solvents, like hydrocarbons, typically falls into the range of 2 to 4, which is a factor of 20 to 40 smaller than the permittivity of water. This explains the low concentration of ions we have in the solvent: The coulomb attraction between an ion and its counterion is strengthened 40 times, leading to minimal dissociation of molecules. The Debye length can easily reach a few tens of μm, in some cases even some hundred μm [Briscoe2002a]. Although particles suspended in nonpolar media are observed to carry considerable surface potentials, the repulsion between charged particles is generally observed to be weak and long-ranged [Briscoe2002b], with screening lengths at least one order of magnitude larger than in aqueous media.

Direct experimental determination of interaction forces in nonpolar media is difficult due to the following reasons: The interaction forces are generally very weak, but at the same time the extraordinary large diffuse double layer results in long-range interaction. Briscoe et al used a modified surface force apparatus (SFA) setup to directly determine the electric double layer interaction in nonpolar liquids [Briscoe2002b; W.H. Briscoe2004].

The evidence of colloidal stability even without the addition of polymeric steric stabilizers points towards a stabilizing force of electrostatic origin between the particles, although the magnitude is still unknown [Briscoe2002b]. In polar solvents, like water or ethanol, electrostatic stabilization of colloidal dispersions is calculated using the DLVO theory. For nonpolar liquids, there are serious questions about the applicability of this theory. The very low concentration of ions would induce a very large Debye length. However, due to the low surface charge the total number of counterions is so small that the continuum model of

charge density does not hold anymore, onto which part of the DLVO theory is based.

Briscoe et al. have developed an alternative model for describing the "electrostatic vicinity" of charged particles based on a counterion-only double layer approach [Briscoe2002a]. The ion reservoir in the bulk phase, onto which the definition of the Debye length is based, can be neglected in nonpolar media. The concentration of counterions between two surfaces in close proximity is most likely far greater than the concentration of the background ions. The authors found dispersions containing the ionic surfactant AOT (Aerosol OT, sodium bis(2-ethylhexyl)sulfosuccinate) being well represented by the counterion-only model in the case of low water content. Increasing water content enhanced the conductivity of the dispersions and their characteristics were then better described by a classical double-layer model.

Both research and industrial applications provide evidence that solids in nonpolar media can become charged in presence of amphiphilic electrolytes [Keir2002; Kitahara1984; Vellenga1965]. Mica particles, for instance, have been found to be unstable in distilled decane while upon addition of AOT they are stable and also show electrophoretic motion [W.H. Briscoe2004]. The addition of stabilizers or other additives such as salts can also induce a charge reversal, as has been reported for PMMA in hydrocarbons [Perez2004] and the air-water interface [Exerowa2003].

In aqueous solutions surface charges originate from the adsorption of ions or the dissociation of surface groups. The charging mechanism in nonpolar media is not the same as in aqueous suspensions. Fowkes et al [Fowkes1982] have shown that in organic media the mechanism of particle charging is based on donor-acceptor (or acid-base) interactions between the particle and the dispersing agent. Surface charges develop when adsorbed dispersants are desorbed into the organic medium, where they form the diffuse double layer. The dispersants are adsorbed as neutral molecules onto basic or acidic surface sites on the particle, where protons are transferred from the particle to the dispersant or vice versa. Therefore, basic dispersants induce exactly the opposite effect as in water: they produce a negative charge on the particles, while positive charge is achieved by acidic dispersants. Thus, the charge of a particle in nonpolar media is only determined by the interaction between particle and additive, without contribution of the solvent. After desorption from the surface, the charged polymer – the counterion –

is often incorporated into a reverse micelle. This assures that the charge is kept at distance from the oppositely charged surface, thus reducing the force of attraction sufficiently to prevent the counterion being drawn into the Stern layer.

Water can change the properties of particle surfaces even in the ppm concentration range when it adsorbs onto hydrophilic surfaces [Kitahara1984; McGown1966]. Trace amounts of water influence both the formation of micellar structures, the dissociation of ionic molecules, and reactions on particle surfaces. By reacting with the surface ions of the particle, it can enhance the acid-base character of the solid, or even change it.

Nonpolar dispersions are characterized by weak, long-ranged interactions in a medium of very low ionic strength. The large Debye length easily leads to an overlap of single double layers, especially when the concentration of particles is increased. Thus, the effective potential is decreased and electrostatic charges do not sufficiently stabilize the dispersion anymore. Hence, concentrated dispersions require the use of steric stabilizers, while dilute systems may be electrostatically stabilized. The electrical properties of dispersions in nonpolar liquids can be controlled by the addition of surfactants, polymers, or even water. A number of AFM and SFA studies appeared on the long-range forces between solids immersed in nonpolar media for both different [Kanda2002] and identical materials [Briscoe2002b; Israelachvili1984; W.H. Briscoe2004] interacting with each other.

3.2 The Emulsion

3.2.1 Fundamentals

Emulsions

An emulsion is a heterogeneous system of two immiscible liquids, such as oil and water, where one liquid is dispersed in the other in form of droplets. They can broadly be classified into two types: oil-in-water (O/W) (direct emulsions) and water-in-oil (W/O) (reverse emulsions), depending on the nature of the disperse phase. Though, multiple emulsions are also frequently used, where the disperse phase contains droplets of the continuous medium. Emulsions may also be

classified regarding a thermodynamic point of view: Generally, emulsions are thermodynamically unstable but, by adding an appropriate emulsifier, thermodynamically stable states can be achieved, the so-called microemulsions. The thermodynamically unstable macroemulsions typically involve larger droplet sizes than microemulsions, easily exceeding 1 μm. However, there are macroemulsions consisting of smaller droplet size, called nano- or miniemulsions. General introductions into emulsions and their stability can be found in references [D. F. Evans1999; H.F. Eicke1987; Petsev2004; Sjöblom1996].

Generally, emulsion stability can be achieved by various additives which adsorb to the oil-water-interface. These additives may be small solid particles, polymers, or surfactants. Polymers and solid particles prove to be most effective if the continuous medium is the better solvent or the particle is wetted mostly by the continuous phase. Surfactants and other forms of amphiphiles, form a dense layer at the interface preventing direct contact between two droplets. A special case of polymeric stabilization is the use of certain proteins as emulsifiers, which, due to their amphiphilic character, show surface-active behaviour and adsorb at the interface [Kamyshny1997].

Emulsion properties - such as emulsion type, stability, and phase inversion - strongly depend on the static and dynamic properties of the surfactant film, especially on its hydrophile-lipophile characteristics. By choosing an appropriate surfactant a microemulsion may form. Microemulsions consist of one thermodynamically stable phase, essentially the same as a swollen micellar solution phase. In contrast to macroemulsions, bicontinuous structures may also form, rather than droplets in a continuous medium.

While microemulsions provide long-term stability, macroemulsions are not stable and, after a certain amount of time, the phases will separate into two or more equilibrium phases. Minimal stability lasting from minutes to even days can be achieved by the emulsifiers mentioned above. Macroemulsions can be prepared either by dispersion (producing larger interfacial area by break-up of bulk phases induced by mechanical energy), or by condensation (using chemical energy). Destabilization typically occurs in different steps: creaming (due to density differences between droplet and medium), flocculation (secondary minimum), coagulation (primary minimum), Ostvald ripening (size distribution moves to larger drops), coalescence (two droplets merge into one).

Charges at the oil-water interface

Water was early assumed to play an important role in the charging of solids in nonaqueous media (see also section 3.1). For example, transport pipes are charged by flowing petroleum, the degree of charging varying remarkably with content of water and contaminants. But water does not only influence the charging of solids, water droplets themselves acquire a charge in nonpolar media. Shaking a water-in-kerosene emulsion was reported to result in charged droplets.

The fact that the oil-water-interface can establish a charge in the absence of surfactants has been known for a long time. Though, the origin of these interfacial charges remained unclear until the last few years, when improved experimental techniques offered new insights into the characteristics of interfaces. During the last three years, numerous publications appeared providing experimental evidence of charges at the pristine oil-water-interface [Beattie2004; Marinova1996; Mishchuk2004; Sakai2004]. However, the total number of publications dealing with pristine oil-water-interface is by far outnumbered by studies involving any kind of surface active species.

Independent of the experimental system – oil droplets in water, water droplets in oil, or the interaction of planar surfaces – qualitatively similar results were reported. While an oil droplet in water carries a negative surface potential, water domains in apolar media generally appear positively charged. Some studies are dealing with an air-water system instead of oil and water. In the following we will not differentiate between air/water and oil/water, as both air and oil can be considered as nonpolar and hydrophobic [Ciunel2005], resulting in basically the same interactions at the interface.

Although the charging mechanism cannot be explained to full extent by now, one theory is widely accepted: Exerowa et al. were the first to propose that charging occurs due to preferential adsorption of hydroxide (OH^-) ions to the oil-water interface [Exerowa1969]. This theory has been extended by Marinova [Marinova1996], who found a strong pH dependence of the negative potential of oil droplets in water and, more recently, by a number of further authors [Mishchuk2004; Sakai2004] [Beattie2004]. While the preferential adsorption of hydroxide ions to the interface can be taken for granted, the origin of this adsorption process is still under investigation. Very recent studies on the adsorption of hydroxide ions to hydrophobic surfaces suggest the preferential

orientation of water molecules in the first two layers at the interface to be the driving force for adsorption. The molecules in the topmost water layer (towards the hydrophobic phase) are found to be oriented with the hydrogen atom pointing away from the aqueous phase [Ciunel2005; Mamatkulov2004; Sakai2004]. This orientation causes a strong dipole moment, which also explains the positive surface potential (+ 0.5 V) of the water surface observed by Mamatkulov et al. [Mamatkulov2004].

3.2.2 Experimental Details

The emulsion that we use for developing our samples has to fulfil two basic requirements: it has to be a *water-in-oil* emulsion which is *sufficiently stable* over the time needed for particle deposition. Bead deposition experiments showed that good attachment is achieved within less than a minute (section 3.5). Thus, the time required for the emulsion to be stable is so short, that we opted for working with macroemulsions without adding stabilizers. Although these kinds of emulsions do not provide long-term thermodynamic stability, their preparation is significantly easier than the formation of microemulsions. An additional difficulty arises due to the use of perfluorinated oils (which are needed because of charge pattern stability): water-in-FC-oil emulsions are poorly studied, compared to other kinds of W/O emulsions. Thus, surfactants stabilizing water-in-FC-oil emulsions are not commercially available.

Therefore, we are working with emulsions exhibiting a pure water-in-oil interface. An aqueous suspension of silica or latex particles is dispersed into FC-77 by sonication, either in an ultrasonic cleaner bath or by an ultrasonic probe (Fig. 3.2). A 20 µl droplet of bead suspension is typically placed on 2 to 3 ml of FC-77 in a small beaker and sonicated for a time period ranging from 20 seconds to 2 minutes, depending on the experiment. (For details please refer to section 3.5.) Following this procedure, we prepared emulsions consisting of a nonpolar continuous phase, and an aqueous disperse phase with particles suspended therein. We always observe a certain amount suspension that did not disperse in the oil. Hence, we can estimate a maximum volume fraction φ of disperse phase in our emulsions by assuming the 20 µl of suspension to be completely emulsified in 2 ml FC-oil, resulting in $\varphi=0.01$.

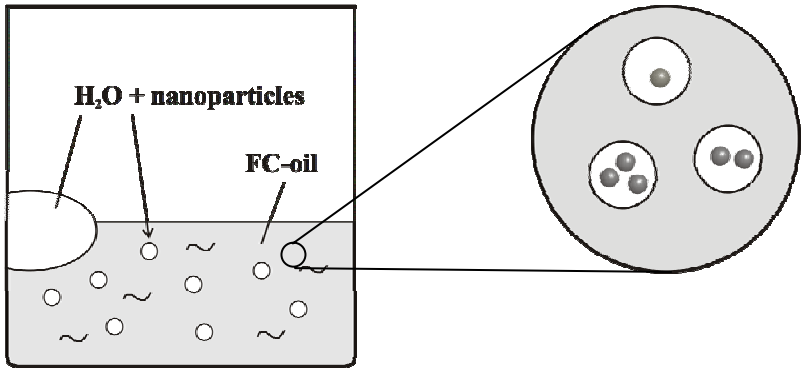

Figure 3.2 Preparation of the emulsions. Emulsions were prepared by mixing a small amount of aqueous particle suspension with FC-oil in an ultrasonic cleaner bath. The process results in dispersed water droplets that contain a certain amount of particles, depending on the concentration in suspension.

One question that arises is the following: where are the particles located in the droplet? Are they really located inside, or do they adsorb at the oil-water interface? Nanoparticles are known to be good stabilizers for certain kinds of emulsions [Binks2000; 2001; Pickering1907]. The silica and latex beads used in this study are supplied in pure UHQ-water and do not contain stabilizers on their surface nor do the solutions contain any additives. Though, the ionic strength might differ from UHQ to some extent due to dissociation of surface groups on the particles, resulting in an electrostatically stabilized suspension. The beads can be considered as hydrophilic due to the dissociation of the surface groups. Hence, they most probably do not show affinity for the oil surface, and are assumed to be located inside the water droplet. This assumption is confirmed by KFM images obtained of droplets after they have landed on the PMMA surface and evaporated. The water from the droplet locally changed the surface potential of the sample as revealed in Fig. 3.3. The particle, appearing as lower surface potential, is typically located in the centre of the circular droplet residue, rather than at the edges. The amount of particles per droplet differs depending on the dilution of the bead solution (see App. C.2).

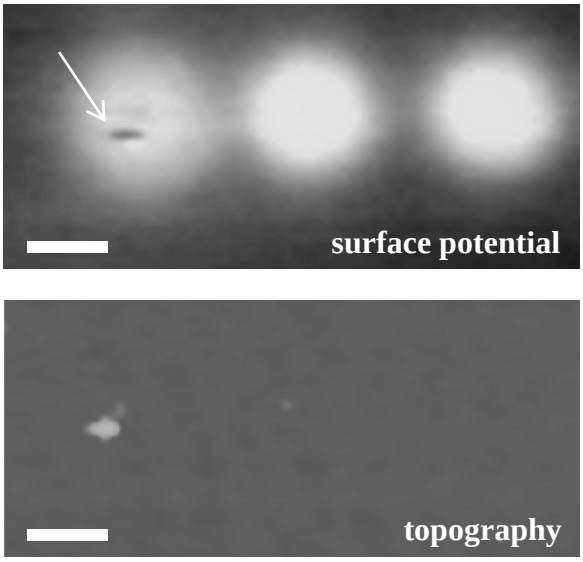

Figure 3.3 Charge pattern after deposition of water droplet. The surface potential image shows three positively charge dots, one being covered by a 100 nm particle. Around the particle, the surface potential has changed, due to the water droplet that has transported the particle to the pattern. The bead is roughly located in the middle of the circular water "footprint", indicating that the beads stay within the water phase when being emulsified in the oil. Scale bar: 1 µm.

The interaction between two neighbouring water droplets can generally be divided into three major parts:

- van der Waals attraction,
- electrostatic repulsion,
- steric repulsion.

While van der Waals attraction will always be present in this kind of emulsions, the effect of steric repulsion can be neglected here since we are working without additional stabilizers. As the beads are suspended in pure UHQ water, we assume to have a pure oil-water interface at our emulsion droplets. In accordance with the charging mechanism of the pristine oil-water interface discussed above, we observed our droplets to be positively charged during our experiments (see section 3.5).

The charge on the droplets might also lead to a certain degree of emulsion stability. We did not exactly determine the time our emulsions are stable, since they showed sufficient stability for conducting the experiment. Although a creaming effect has been observed already after less than a minute, the emulsions were still turbid for about 15 minutes after preparation. Knowing the exact time constant for demulsification was not crucial for a further reason: When the emulsion destabilizes, droplets grow - we observed them to coalesce – and rise up due to the difference in density between the oil phase and the water phase. The bigger a droplet gets, the faster it will move upwards. As we immerse our sample into the beaker with the electret surface facing upwards, all growing droplets migrate away from the sample, and will not hit the sample. Thus, mainly small droplets should come into close vicinity of the sample, leaving the sample surface free of unwanted deposition of large droplets.

Although both the theory and our experiments indicate the water droplets carrying a positive surface potential, the emulsion does not seem to be electrostatically stabilized in terms of long-term stability. Two effects might be responsible for that: First of all, the large density difference between the two liquids causes strong buoyancy forces facilitating the separation of the two phases. Secondly, the double layer in nonpolar media can easily extend over a few tens of µm due the low charge and only little ion dissociation. Already at relatively small volume fractions of the water phase the double layers of individual droplets will easily overlap, leading to rapid destabilization [Mishchuk2004]. A higher water volume fraction means more contacts between the water droplets. Upon contact, the droplets will rapidly coalesce and rise upwards, which acts against the emulsion formation process. However, regarding the extremely low volume fractions of the emulsions applied in the deposition process, we assume the density difference to be the main driving force for emulsion destabilization.

By using a simple water-in-oil emulsion we can take advantage of the positive potential that naturally establishes on water droplets to transport particles to predefined spots on the sample.

3.3 The Electret-Oil-Interface

As already mentioned in the introduction, we obtained different deposition characteristics on the various kinds of substrates used. The most striking difference is the polarity of charges to which the emulsion droplets are attracted during development: While on FC samples they deposit exclusively onto negative charge patterns, they do not show a clear preference for neither polarity on PMMA (Fig.3.1). As it is obviously the substrate material that determines the interaction forces, this section is used to elucidate the characteristics of the electret-oil-interface, also with respect to the stability of the charge patterns written into the electret layer.

3.3.1 The Pristine Electret-Oil-Interface

All substrates show comparable characteristics regarding charge writing with the AFM. But according to the differences in deposition results between PMMA and FC layers, the electrostatic field generated by the charge patterns when immersed into the FC-oil varies with the substrate material, resulting in different forces acting on the water droplets. The light microscopy images in Fig. 3.1 give an impression of typical *background coverage* (the amount of beads deposited all over the sample). Assuming a positive droplet charge, as discussed in section 3.2, the fact that we obtain less background coverage on PMMA could indicate a charging effect at the electret-oil-interface. One might think of two scenarios: (a) The FC layer acquires a negative charge and therefore attracts the water droplets while the PMMA stays neutral, and (b) the PMMA surface charges up positively when contacting the FC-oil, repelling the droplets, while the FC layer stays neutral.

Two reasons make scenario (b) sound more plausible than (a). First of all, from a chemical point of view the FC surface and the FC-oil are very much the same, in contrast to the PMMA/FC-oil couple. Strong interactions are expected to occur for very different structures, rather than chemically alike ones. Secondly, charging effects might occur due to contact or friction charging between oil and sample. The phenomenological rule of Coehn states that when two materials are brought into contact, the one with the higher dielectric constant will acquire a

positive charge [A. Coehn1909]. The PMMA-FC-oil-interface displays a bigger difference between the dielectric constants than the FC-FC-oil-interface ($\varepsilon_{FC\text{-}77}$ = 1.87, $\varepsilon_{PMMA} \approx 3.4$, $\varepsilon_{FC} \approx 2$). The dielectric constant of the FC layers is assumed to be in the same range as the specific permittivity of PTFE. Hence, according to the rule of Coehn the charge occurring at the PMMA-oil-interface is predicted to be positive.

Suspensions of PMMA particles in low dielectric constant media (ε=5.5…6.6) showed considerable electrophoretic motion, even without further addition of electrostatic stabilizers [Perez2004; Royall2003]. Perez et al. found the particles to carry a positive surface potential, which can be reversed by the addition of appropriate salts. Together with the contact charging phenomena described above, we expect our PMMA samples to be positively charged. The FC-layers used in our experiments are considered to be hydrophobic and nonpolar. Generally, no interaction could be detected between hydrophobized silica particles in nonpolar media [McNamee2004], which supports the assumption that we do not expect strong interactions between the FC-layers and the FC-oil.

A direct comparison of the surface potentials of PMMA and FC layers is obtained from KFM measurements on a sample being composed of both PMMA and FC regions. An FC layer was evaporated onto one part of a PMMA sample in a PECVD process using HFP gas as described in section 2.3. To this end, the PMMA sample was partially masked with a second PMMA piece to prevent FC deposition in this area. PMMA was used to prevent any unwanted contact electrification of the sample that might occur upon contacting another material. In a series of KFM images obtained before and after immersing this sample into FC-77, the PMMA always displays a higher surface potential than the FC-coated part, see Fig. 3.4. The difference in roughness that is visible in the amplitude image helps to distinguish the two materials: the PECVD-grown FC layers typically have rougher surfaces than PMMA.

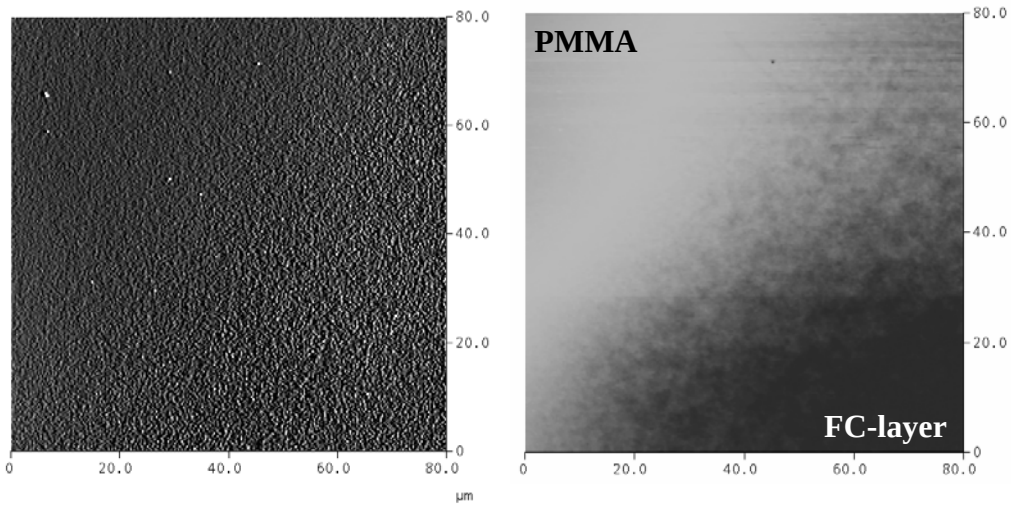

Figure 3.4 PMMA sample partially coated with a FC layer. Left: AFM amplitude image (a.u.), and right: KFM image of same area (z-scale: 2 V). Bare PMMA regions display a considerably higher surface potential than FC-coated ones, as can be resolved in the potential image. The amplitude image helps to distinguish between the two materials, as FC-layers typically show higher rougher than PMMA layers.

3.3.2 Charge Pattern Stability

The electrostatic field generated by the charge patterns is not only determined by the interactions between the pristine electret surface and the oil, but also by the stability of the local surface charges. The electrostatic field in turn defines the forces acting on the droplets. For the pristine electret-oil-interface we found striking differences between PMMA and FC-layers in general, while both types FC layers showed the same characteristics. Yet, we observed differences in the stability of the charge patterns between the two fluorocarbon-based electrets: When immersed into FC-oils, charges of either polarity were found to be reasonable stable on FC-HFP layers [Mesquida2002b] and on PMMA samples. Two interesting characteristics can be observed for the C_4F_8-based FC-layers: (a) the charges rapidly blur out in the oil, and get neutralized, and (b) this only holds for negative charges, positive ones are found to be stable.

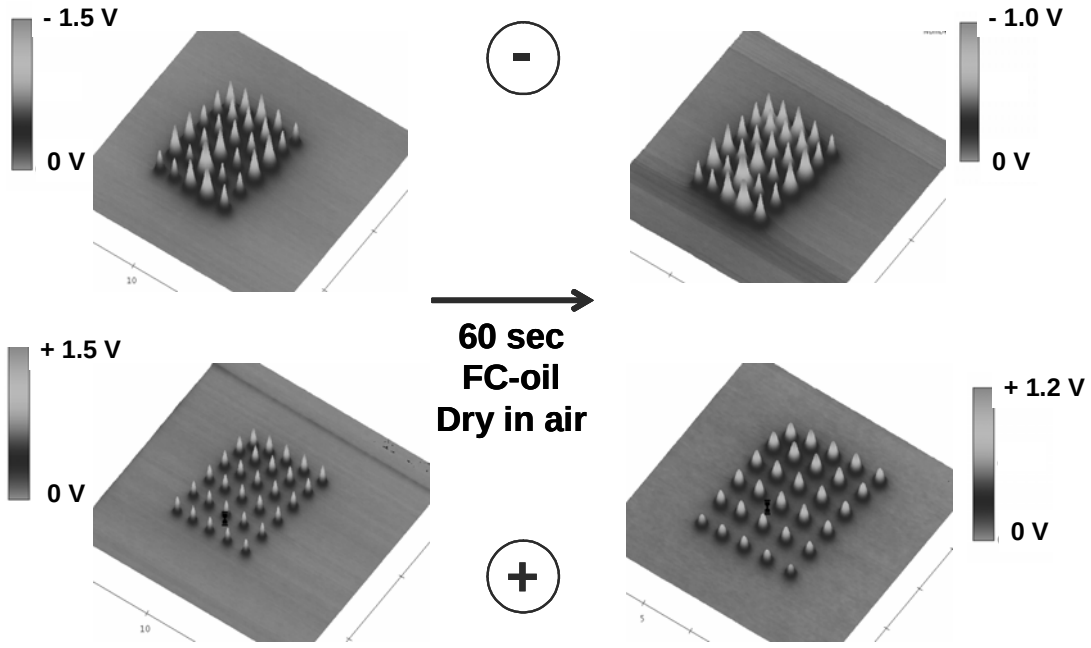

Figure 3.5 Surface charges on PMMA before and after immersion into FC-77. The samples were charged with negative (top) and positive (bottom) dot patterns of 2 µm pitch. After immersion into FC-77 for 60 sec, they were dried in air and imaged by KFM.

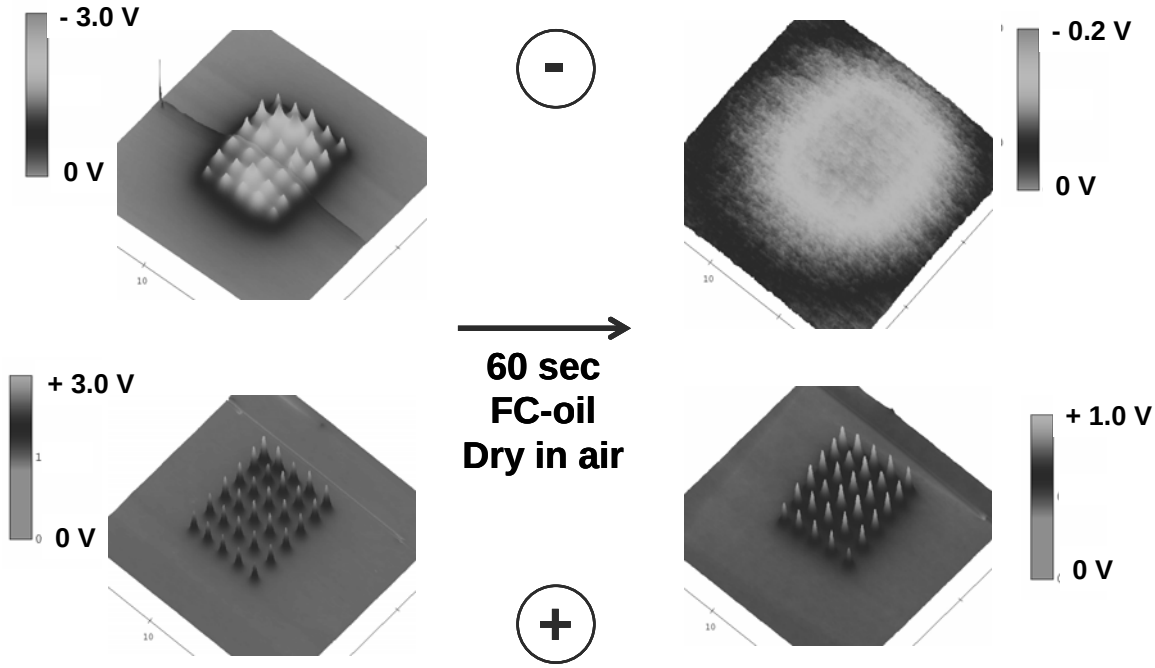

Figure 3.6 Surface charges on FC-layers before and after immersion into FC-77. The samples were charged with negative (top) and positive (bottom) dot patterns of 2 µm pitch. After immersion into FC-77 for 60 sec, they were dried in air and imaged by KFM.

We studied the stability of the local surface charges by comparing KFM images of the samples before and after immersion into FC-77. While the charge patterns of both polarities can clearly be resolved on PMMA after immersing the sample into FC-77 (Fig. 3.5), the negative charge dots can hardly be seen on the FC-layers after immersion (Fig. 3.6). Since negative charges on FC-layers do not show substantial decay when exposing the charged sample to air for a few hours, the charge decay has to occur due to the contact with the FC-oil.

As we have observed particles to deposit onto negative charges on FC-layers, the charges cannot vanish instantaneously. To estimate the time scale of charge decay on FC-samples, we slightly modified the process of sample immersion: Instead of immersing the sample into the oil and letting it dry in air in a horizontal orientation, we just dipped the FC-samples for a specific time and retracted them from the oil while holding the samples vertically. Due to the vertical orientation, the oil can immediately de-wet the sample, resulting in defined drying times of a few seconds maximum. After 10 seconds immersion, the surface potential already decreased substantially, while a considerable amount of charge is still present after 5 seconds (Fig. 3.7). Though, the charges obviously blur out at first contact with oil.

KFM studies on FC-HFP [Mesquida2002b] showed the charges of both polarities to be stable upon contact with FC-77 and PFD. Although we have no definite explanation for these differences, the different charge stabilities might be attributed to the fabrication of the FC layers. Fluorocarbon materials are generally considered to be nonpolar and hydrophobic, as well as inert to most chemicals. However, both fluorocarbon layers are no pure PTFE layers, nor do they contain only carbon and fluor, but also a certain amount of impurities like but also a certain amount of impurities like oxygen and nitrogen due to the fabrication process [Knapp1999; Mesquida2002b].

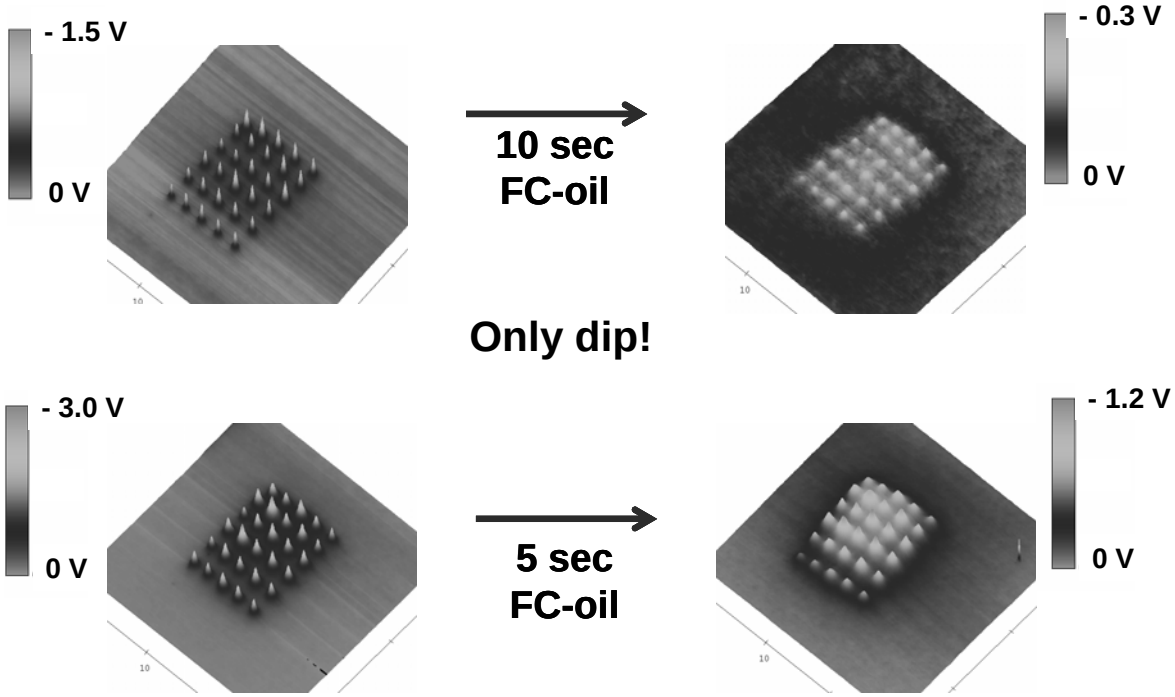

Figure 3.7 Surface charge patterns on FC-layers after dipping into FC-77. Instead of being immersed, the samples are vertically dipped into FC-77 for 5 and 10 sec, respectively. Vertical retraction allows the oil to flow off, resulting in defined contact time between oil and surface.

Charge stability in PTFE films is found to depend on plasma treatment [Tzeng2002]. Chen et al. observed that especially the negative charges behaved differently after plasma treatment, while the positive ones were widely unaffected. Impurities might lead to acidic or basic surface sites on the fluoropolymer, which might have an influence on charge stability. The observation that enhanced charge decay predominantly occurs for one polarity of surface charges, might be explained by the presence of just acidic or just basic surface groups, which change the surface properties of the fluorocarbon.

KFM studies of the charge patterns in-situ (obtained in FC-oil) might elucidate the interfacial characteristics even further. Until now, all information we have is based on measurements in air. In-situ studies in liquid will clarify if the charge decay on the FC-samples occurs upon contact with the oil or due to any phenomena during evaporation of FC-77.

However, KFM images are not easily obtained in fluorocarbon oils. Besides the general difficulties when using tapping mode in liquids, the lift mode technique requires a larger tip-sample distance which adds additional instabilities to the system (for detailed information see App. A). For these KFM studies, the AFM liquid cell (Veeco) was used. Charge patterns were written in air, but with the sample already mounted into the fluid cell, which allowed for imaging the patterns immediately after injecting PFD into the cell.

Substantial surface potential could be detected on PMMA for both polarities (Fig. 3.8 and 3.9). The dot patterns in both KFM images have the appearance of lines. This may be attributed to the cantilever being scanned in parallel to the fast-scan direction (see Fig. 3.9). Due to the low conductivity of the oil, the cantilever beam experiences the forces of an entire row of dots, leading to this line-shaped overall signal.

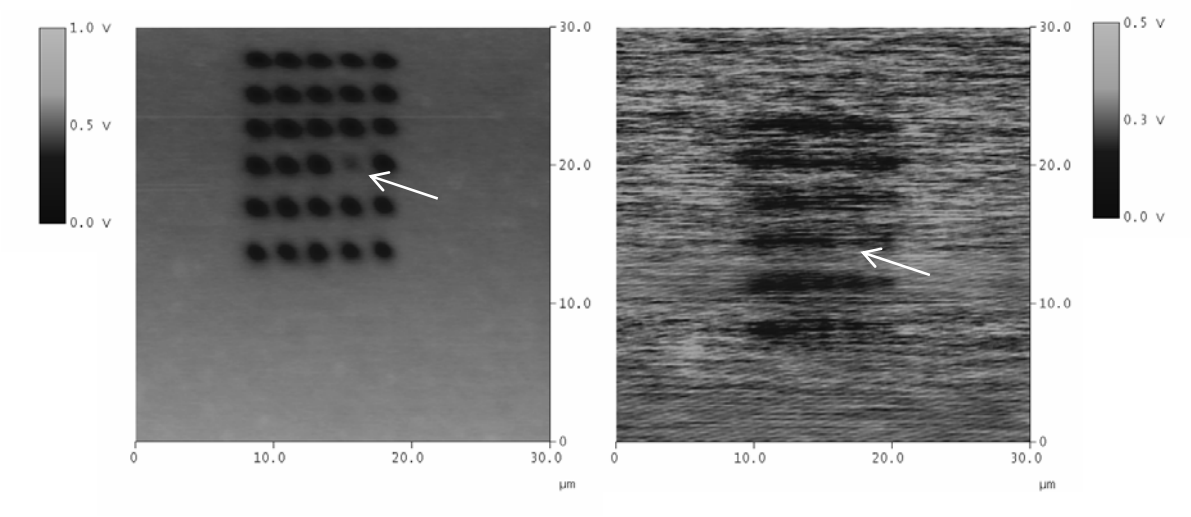

Figure 3.8 Negative charge pattern on PMMA imaged in liquid. KFM images of negatively charged dots on PMMA before (left) and after (right) filling in PFD in the liquid cell. The charge patterns were written in air, with the sample already being mounted into the fluid cell. The pattern is still resolved after filling the cell with PFD. (arrow: missing dot in both patterns)

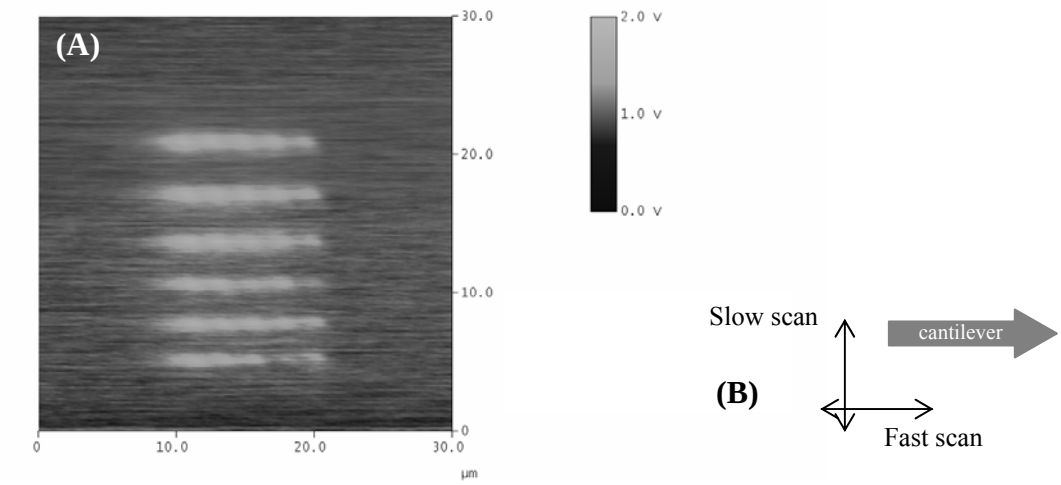

Figure 3.9 Positive charge pattern on PMMA imaged in liquid. KFM image of positively charged dots after filling in PFD into the fluid cell (A). Same sample and same process condition as in Fig. 3.8. (B) scheme of the scanning conditions for both patterns.

On FC-layers, we did not succeed with the write-in-air-image-in-oil method, because of the fast decay of the negative charges. We therefore created the charge patterns while the sample was already immersed in PFD, and imaged the patterns immediately after writing. The blurring of the negative charges and the decay in potential is clearly revealed in Fig. 3.10. The charge dots seem to get weaker in the bottom part of the pattern, which fits above observations of a decrease of potential with time, as the slow scan direction was from top to bottom.

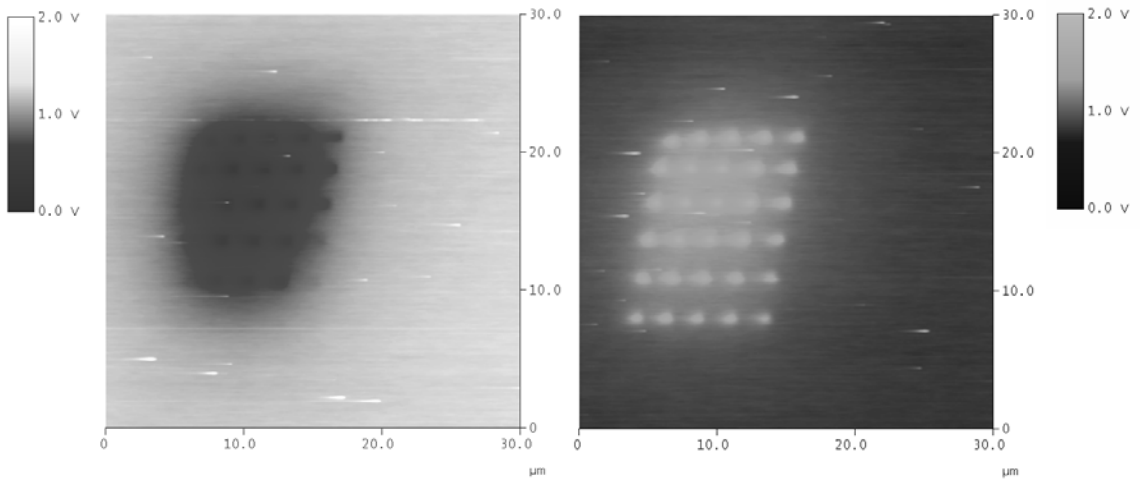

Figure 3.10 Charge patterns on FC-layers. The charge patterns were written in PFD and imaged immediately after writing due to the fast decay of the negative dots. Slow scan direction: top to bottom. The negative charges (left) already decay during the KFM scan, manifesting itself in a decreasing surface potential in scan direction.

Above KFM studies in liquid support the observations and assumptions made in the previous sections. The decrease in surface potential seen in KFM images obtained after immersion and drying can now definitely be attributed to the interaction of the electret surface with the oil.

3.4 The Electret-Emulsion System

Before discussing the deposition results, we should take a brief look at the interaction of the emulsion with the electret surface immersed in FC-oil. As model system, we simply choose a water droplet in FC-oil in close proximity to the sample. Based on the discussions in above sections, we expect the PMMA-oil interface to establish a positive surface potential, while the fluorocarbon layer-oil interface is not expected to show any distinct behaviour. We further assume the water droplets to carry a net positive charge, as discussed in section 3.2.

Coming back on the results shown in Fig. 3.1, the background coverages already suggest that the barrier for the droplets to deposit onto PMMA is significantly higher than for FC layers. Nevertheless, we have to consider the fact that these images have been obtained after drying the samples, meaning after evaporation of the FC-77. When taking the samples out of the development solution, a small droplet of emulsion remains on the surface. The difference in background coverage might also be related to drying phenomena of the evaporating droplet.

On FC layers, the FC-oil forms a nearly completely wetting layer, which evaporates quickly due to the high vapour pressure of the oil. The solvent film is observed to evaporate nearly without diminishing the sample-solvent contact area, and no contact line pinning has been detected. As PMMA is not as hydrophobic as the FC layers, the solvent is not wetting the sample completely, but instead establishes a defined contact area. This gives rise to contact line pinning, resulting in coffee-ring like structures (Fig. 3.11) formed by the beads after drying of the emulsion. For comparison, Fig. 3.12 displays an FC sample, which was partially covered by emulsion. The concentration of beads in the outer zone corresponds well to the overall background concentration. The images in Fig. 3.13 show typical background coverages observed throughout all experiments, also without local surface charges. The question now arising is if the drying characteristics

"just" force the droplets to deposit everywhere on FC layers, while on PMMA they are transported to the contact line, or is the background already established in solution?

Due to the quick evaporation of FC-77, no light microscopy images could be obtained showing the drying process itself. However, we made the observation that water droplets already deposit onto FC-layers while the sample is still wetted by the oil. During the last steps of evaporation of the oil, the droplets on, or close to, the FC sample do not move anymore. Instead, they are found to stay at a fixed position, where they finally dry, leaving the particles behind.

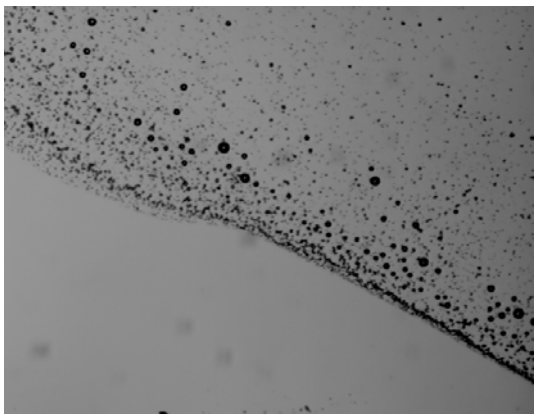

Figure 3.11 Evaporating emulsion on PMMA. Reflected light microscopy image of the rim of an emulsion droplet evaporated on PMMA. The water phase contained 330 nm silica beads for better visibility.

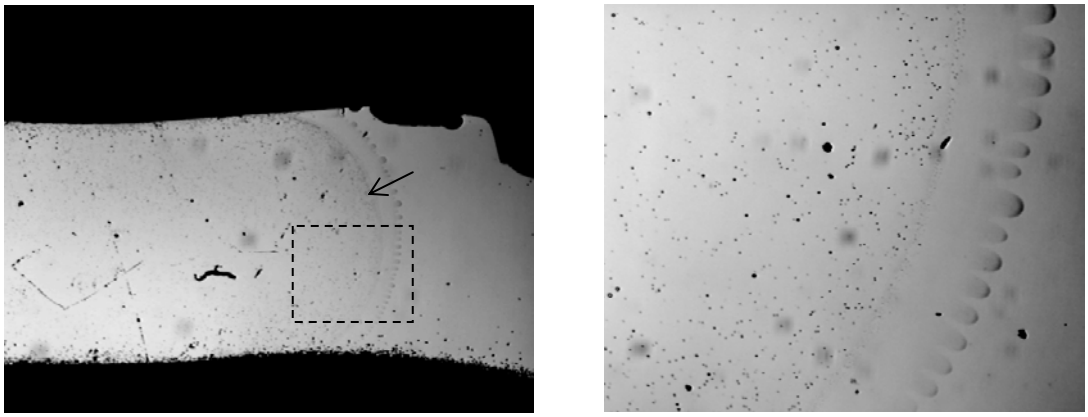

Figure 3.12 Evaporating emulsion on an FC-sample. The contact line (arrow) is not as clearly resolved as on PMMA since no coffee-ring structure was formed. The FC-sample was partially covered by an emulsion droplet (same emulsion as in Fig. 3.11). The right image is magnified region of the area marked with the rectangle.

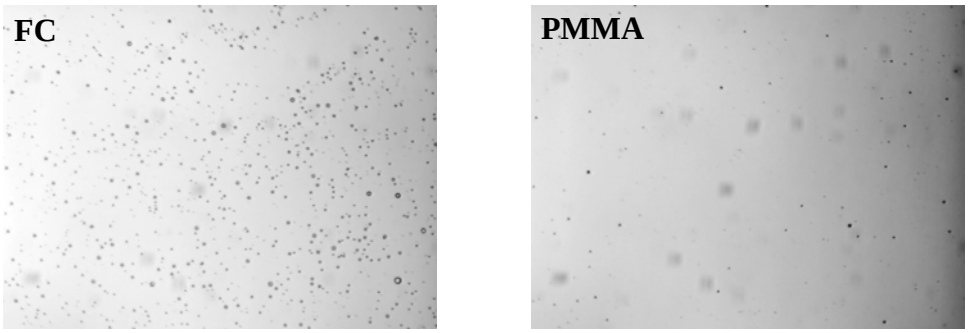

Figure 3.13 Typical background coverages of FC (left) and PMMA (right). Images were obtained inside the evaporation area after drying of the emulsion droplets (see Figs. 3.11/12).

In contrast to that, only very few water droplets or observed to approach a PMMA surface in solution, and subsequently attach. However, water droplets in close proximity to the surface show a very high lateral mobility. In Fig. 3.14, movement of two droplets right above the PMMA surface can be seen. As the same sample has already been exposed to an emulsion before, silica particles can be observed sticking on the surface. These particles serve as a reference for the two droplets being in approximately the same focal plane as the background. As we can still see them moving, they obviously do not experience any force attracting them to the PMMA.

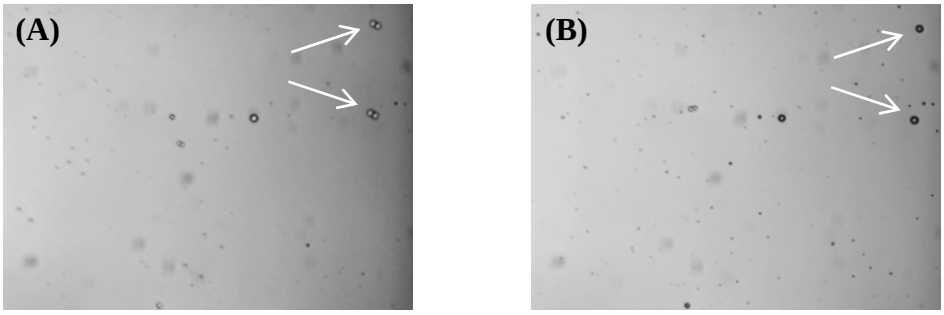

Figure 3.14 Water droplets on PMMA. (A) In-situ observation of 2 moving droplets (arrows) in emulsion close to the surface. Image (A) is composed of 2 sequential images. Particle residues of former emulsion treatments prove that we are in focus. (B) Same place as (A), image obtained immediately after evaporation of FC-77. The two droplets now adhere to the sample. Note that the background coverage did not increase considerably.

The results shown above at first sight seem to be counterintuitive to what would be expected regarding the material properties, especially the wetting characteristics of both substrates. Fluorocarbon surfaces are more hydrophobic than PMMA. Indeed, macroscopic water droplets are easily moved around with pipette on FC-layers in FC-77, while on PMMA they show stronger adhesion.

According to that, we would expect the droplets to move with the liquid during evaporation of the emulsion on FC-samples because of hydrophobicity of fluorocarbon layers. Though, the light microscopy observations show a contradicting behaviour: The droplets do not show considerable lateral movement on FC-samples and, instead, just hit the surface sometimes, where they finally adhere until the sample is fully dried. The reason for the droplets being pinned to the surface may be found in the drying process: Evaporation of FC-77 on FC-samples is very fast, and is observed more like a *layer-thinning* process instead of *droplet-shrinking*, leading to lower lateral forces acting on the droplets. Yet, a clear barrier exists for the water droplets to approach too close to the PMMA samples, manifesting itself in random-like lateral movement of the droplets even during later steps of evaporation.

With these experiments, we can exclude that the drying phenomena are the only contributions to the background formation, although it cannot be fully ignored. The barrier might be a positive overall surface charge that repels the likely charged water droplets. Once a droplet “really” hits the PMMA surface (when being attracted to local charge, for example), it is expected to adhere.

We cannot fully explain the charging of PMMA against the oil. However, when studying the literature, various origins can be thought of: First of all, we should remember that one fundamental driving force for charging is always present, namely the difference in electronic properties (Fermi levels) between two dissimilar dielectric materials. According to the rule of Coehn, the contact between FC-77 and PMMA should result in a positive PMMA surface. The chemical structure of PMMA offers another hint on the origin of a positive charge: PMMA carries basic sites on the surface, which act as proton acceptors.

As all our experiments have been conducted in ambient conditions, we will always have water present in our system, especially when working with the emulsions. The conductivity of the oil will not be significantly affected by the moisture (due to the low water solubility in FC-oils). However, the water will

readily adsorb to the PMMA surface instead. Even trace amounts of water can have a large influence on the charging of hydrophilic solids in nonpolar media [Kitahara1984; McGown1966].

Additional observations

While trying to approach macroscopic water droplets to both materials immersed in FC-77, no clear repulsion could be observed at first sight. However, a closer look revealed that at least attraction could definitely be excluded on PMMA: We approached a PMMA sample to a fixed water droplet, thereby observing the droplet shape. Neither the water nor the emulsion droplet showed any kind of reaction to the approaching PMMA, until it was literally pressed onto the surface. In contrast, when trying to retract the sample, strong deformations on the droplet surface could be observed. Upon contact with the surface, the droplet firmly adheres and cannot be removed, due to the interfacial energies of the PMMA-oil-water system. Hence, we won't find any regions on PMMA, where a water droplet deposited and detached again.

This leads us to the conclusion that some kind of barrier has to exist, that keeps the droplet at a certain distance to the PMMA sample, thereby preventing contact between the two materials. These observations manifest the assumption of a positive surface potential evolving at the PMMA-oil interface. In case of the barrier being of electrostatic origin, repulsion should even more dominant for smaller droplets, since charging of the droplets is an interfacial phenomenon.

Force curves

Additional information on the substrate-oil-interface can be obtained from force curves conducted with the AFM in FC-oil. To simulate a single droplet interacting with the sample, we were using cantilevers with spherical tips. Since the droplets are rather large in diameter, at least in the range of 500 nm, common tips at AFM cantilevers are too sharp to correctly sense the forces acting on a droplet. Thus, SiO_2 cantilevers with spherical tips of around 900 nm diameter were used (Fig. 3.15A).

To render the cantilevers hydrophilic, we exposed them oxygen plasma for 2 minutes to remove all organic contaminants. A small droplet of UHQ water was placed on a PMMA sample, before mounting it into the fluid cell. Using the coarse approach commands, the cantilever was approached to the sample, until it contacted the water droplet. After retracting the cantilever again and injected PFD into the cell, the tip was coarsely approached to another place on the PMMA surface recording the force curves.

Force curves obtained over a range of 3 μm seemed to be counterintuitive at first sight, because of showing a clearly attractive interaction between PMMA and the tip (Fig. 3.15B). Repeating the experiment with fresh materials yielded the same results. The scan-range might give a hint on what we are actually seeing in these force curves. For working in aqueous solutions, force curves measured over 3 μm definitely represent long-range interactions. Though, in nonpolar media the same distance might rather represent short-range interactions (or medium-range, depending on definition), as the double layer can easily reach a few hundred μm in nonconducting liquids [Briscoe2002a; Briscoe2002b]. Hence, the force curve in Fig. 3.15B corresponds the short-range attractions, and electrostatic interactions may be sensed over longer distances, considerably longer than a few μm.

As force curves can only be obtained over a range of a few μm, we could not obtain quantitative data for these long-range interactions. Though, already during the first approaches of the cantilever to PMMA samples strong interactions where observed already at large distances. The reactions of the cantilever during approach indicate the existence of some kind of repulsive forces (Fig. 3.16).

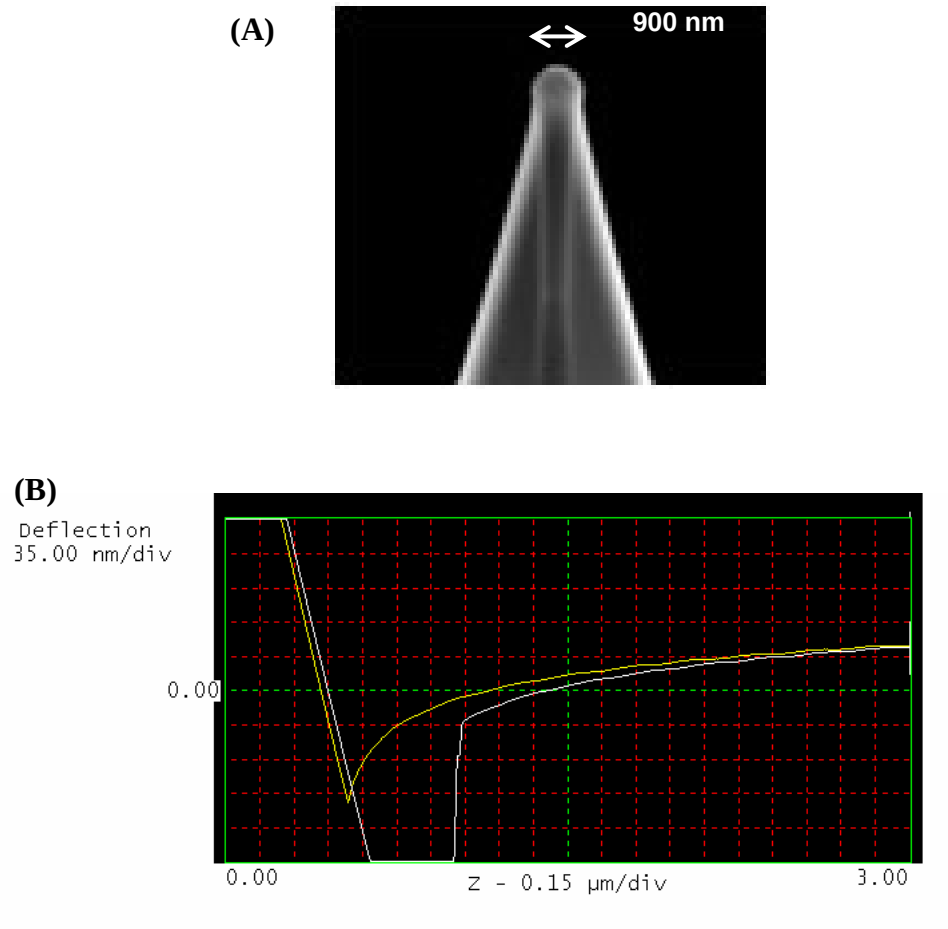

Figure 3.15 Force curve on PMMA with a sphere cantilever in PFD. Cantilevers with spherical tips of 900 nm diameter (A) were used to obtain approach- and retract-curves (B) on PMMA samples immersed in PFD. Before filling the fluid cell with PFD, the hydrophilized tips were shortly dipped into UHQ-water.

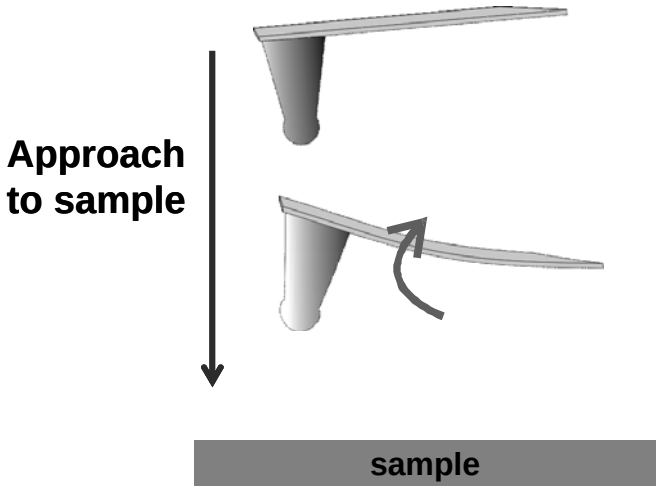

Figure 3.16 Schematics of cantilever behaviour during approach to PMMA. The cantilever was observed to bend upwards when approaching a PMMA surface in an FC-oil over a range of around 200 µm.

No significant long-range interactions have been observed when approaching the cantilever to FC-samples, neither did we find hints for extraordinary behaviour at a small scale (Fig. 3.17). This leads us to the conclusion that above observations originate from the substrate interacting with the cantilever, rather than in measuring artefacts or instabilities.

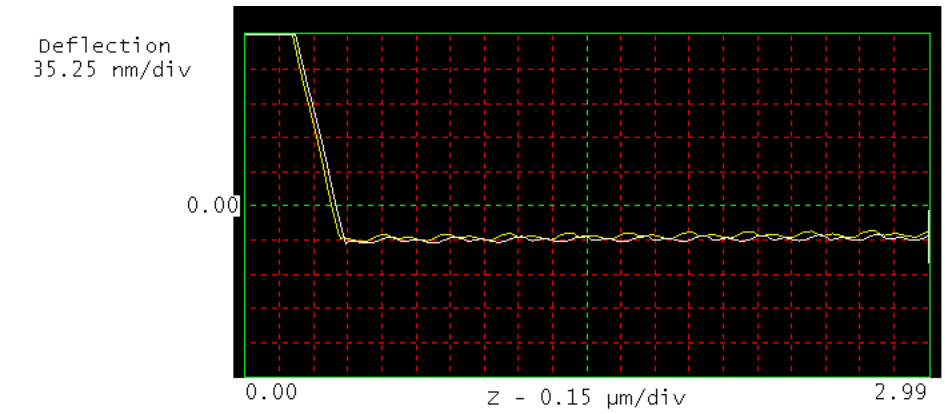

Figure 3.17 Force curve on FC with a sphere cantilever in PFD. Same cantilever and same procedure as in Fig. 3.15.

Based on above results, the long-ranged repulsion between PMMA and the water-covered (or, at least, hydrophilic) cantilever can be attributed to electrostatic repulsion. The observed short-range (or intermediate-range) attraction over 3 μm is in line with publications on attraction of similar materials in nonpolar solvents [Kanda2002], assuming both the cantilever as well as the PMMA surface to be covered by a thin water film resulting in ambient humidity.

3.5 Deposition of Particles

As explained in the introduction, we studied the basic deposition characteristics with the help of water-in-oil emulsions containing nanoscale particles, which are located within the water droplets. We employed particles of various sizes ranging from 50 to 300 nm, consisting of two different materials, silica and polystyrene (PS) (for details see App. B.2). Fluorescence labelling simplifies the detection of the smaller beads by fluorescence microscopy. Regardless of the kind of beads used, they are all suspended in pure UHQ water. This assures that we have the same emulsion properties throughout all experiments, especially concerning the charge of the droplets. As we have learned from section 3.2, the charge of the water droplets originates from preferential adsorption of hydroxide ions to the oil-water-interface. The emulsions were prepared according to the procedure described in section 3.2. Unless otherwise stated we used the following parameters: bead suspension: 20 μl, FC-77: 2.5 ml, sonication time: 1 minute, immersion time: 1 minute. The droplet size can roughly be estimated to be between 500 nm and more than one μm (see below and App. C.1). The charge patterns were written according to the procedure described in section 2. The voltage applied to the tip was chosen to yield in a specific potential difference with respect to the background, to provide a possibility for comparing the results.

Typical structures obtained by depositing silica beads onto PMMA and FC-layers are shown in Fig. 3.18. Deposition experiments on large-scale patterns (Fig. 3.18A,B), show that the beads selectively cover negative charge patterns on FC layers, while a large depletion zone is detected on and around the positive charges. This characteristic corresponds to positively charged water droplets (see section 3.2) being attracted to opposite charges on the sample surface via Coulomb forces.

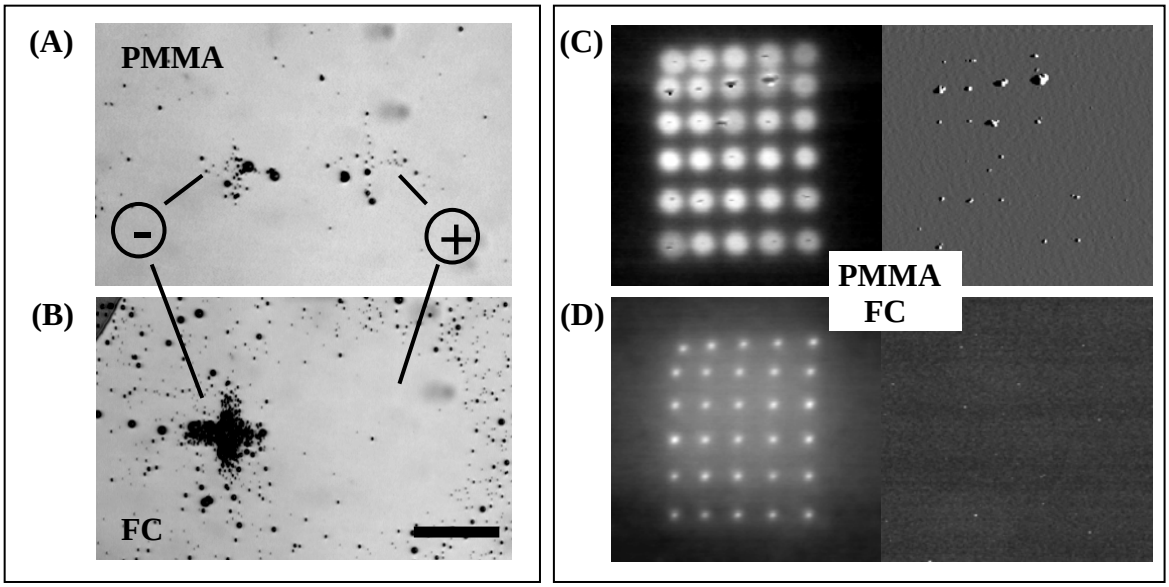

Figure 3.18 Deposition of silica beads. (A,B) Reflected light microscopy images of 330 nm silica beads on PMMA (A) and FC-film (B). Potential: +/- 3V, charge pattern: cross 40µm wide. Scale bar: 40 µm. (C,D) KFM and AFM topography (amplitude) images of 50 nm silica beads on PMMA (C) and FC (D). Potential: +2.5 V (PMMA), and +1.9 V (FC). Arrow: single bead. Samples were mounted on the same sample holder and processed simultaneously.

On PMMA surfaces, however, no clear preference for particles getting attracted to either polarity can be observed. Instead, they attach to both patterns with less coverage than on the FC layer. The background coverages observed here are typical for both substrates and correspond to the findings from above sections: whereas the basically neutral FC layers do not specifically interact with the water droplets over a long range, the positively charged PMMA surface repels the likely charged droplets. The samples shown in Fig. 3.18 were mounted onto the same holder while processing, assuring the same conditions throughout the experiment, and, therefore, comparability of results.

The AFM images of 50 nm silica beads on a positive dot pattern on PMMA (Fig. 3.18C) show that the water droplets get attracted to the dots, leaving their "cargo" behind after drying. AFM topography images show the small dots being in a size range of 60 nm, meaning that at least some droplets were loaded with a single particle (see arrow). As expected, the water droplets are repelled from positive charges on FC-layer (Fig. 3.18D).

Although a few single beads can be resolved in Fig. 3.18C, the general amount of particles per charge dots shows a certain polydispersity. However, this polydispersity might be attributed to a polydispersity in the amount of particles per emulsion droplet, rather than to a very broad distribution of droplet diameters. The larger deposits of particles in the second row are well separated from each other, suggesting that on each charge dot a single droplet has landed that did not grow considerably. Otherwise, the droplets would have merged into bigger ones upon contact, leading to larger, but more sparsely particle deposits. Furthermore, the KFM image gives a hint on the droplet diameter: The surface potential of the PMMA surface is slightly changed due to the deposition of a water droplet. Regarding the KFM image, we can assume the droplet size to be in the range of a few hundred nm. (For comments on the droplet size, see App. C.1)

The concentration of particles in the bulk suspension employed in the deposition experiment shown above was approximately adjusted to 1/5 of the original solution. Assuming a droplet size of 500 nm, each droplet would contain around 5 particles (see App. C.2), which matches with the amount of particles resolved in the AFM image above. Though, the distribution seems to be quite broad, manifesting itself in droplets loaded with definitely more than 10-20 particles as well as “unloaded” droplets (the charge dot in the middle of the top row shows the typical discharge phenomena upon contact with a droplet, without a particle deposited onto).

The approximate match between the average number of particles on a charge dot and the bulk concentration in suspension manifests the assumption that the particles are located inside the water phase, rather than assembling at the oil-water-interface. If they did so, there would be a higher concentration of beads in the suspension close the interface with the oil, from where dispersion starts. Since silica particles are known to establish a negative surface potential, the location of the particle inside the droplet might originate in electrostatic repulsion between the negatively charged oil surface and the likely charged silica particle.

Regarding above results, one unexpected characteristic shows up that needs further investigations: While the exclusive attraction of the water droplets to negative charges on FC-layers, as well as the appearance of the background on both materials, can be explained with the insights gained so far, explaining the

deposition onto both polarities on PMMA does not seem to be straightforward. Before addressing this question, we take a look at fluorescent latex beads deposited onto both substrates (Fig. 3.19). From these experiments we can conclude that the droplet charge is indeed determined by the pure oil-water-interface, since no differences in deposition characteristics can be observed when using either silica or latex beads.

Dot patterns on FC surfaces generally show very high particle coverage, which is increasing with increasing surface potential difference (Fig. 3.19D). In Fig. 3.19 C,D basically each dot is covered. However, fluorescence is not only detected on the predefined dots, but also in between and directly around the structure, compromising pattern definition.

Comparing the two substrate materials leads to the result that pattern definition is better on PMMA, while the structures on FC-layers generally show a very high coverage. This effect would not be detected during deposition experiments on large-scale structures, as mainly high pattern coverage is desired. In contrast to FC samples, on PMMA, the space between the single dots is mainly free of any particles.

A careful look at Fig. 3.18 and 3.19 reveals that around the negative structures on FC-samples no depletion regions can be found. However, this kind of zone would be expected to appear since all charged particles, in this case droplets, that are located in vicinity of the charge patterns should be attracted. The answer to that behaviour can be found in the discussions in section 3.3: The first droplets deposit immediately after immersion, when the charge dots (a) still show considerable potential, and (b) have not yet blurred out too much. When the charges start to blur out, a high overall potential can still be detected (Fig. 3.7, 5 seconds immersion), leading to attraction of the droplets to the region between the dots. Finally, after the charges have nearly vanished, the droplets will experience not special forces around these areas, resulting in random-like deposition like on the uncharged sample parts. The deposition seems to take place within a short time scale, as the charge patterns are observed to vanish within seconds!

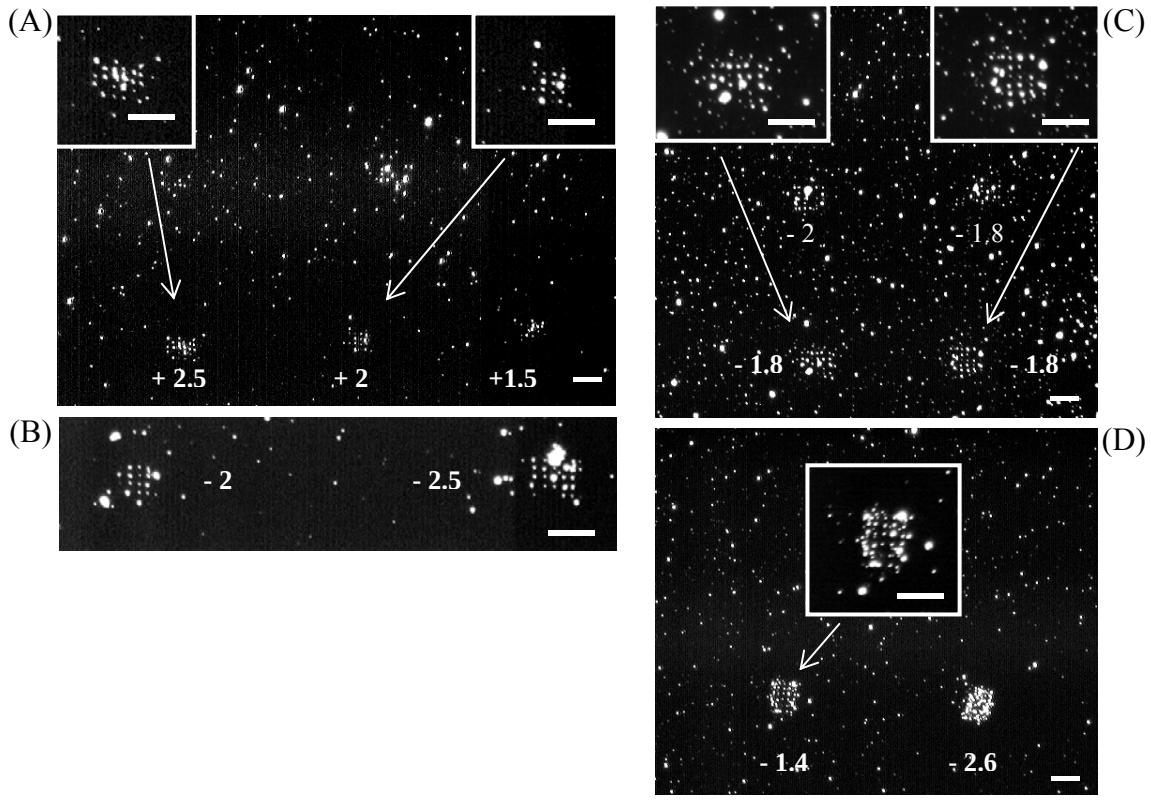

Figure 3.19 Deposition of 50 nm latex beads. Fluorescence microscopy images of 50 nm latex beads attached to dot patterns on PMMA (A,B) and FC (C,D). Samples were mounted on the same sample holder and processed simultaneously. Development conditions as described above. Numbers given in images are surface potentials in Volts. Scale bars: 10 µm.

Now let us go back to the question why the water droplets deposit onto both polarities on PMMA To this end, we need to reconsider some basic assumptions: In our process, we are dealing with electrostatic forces. But so far, we have only taken into account Coulomb interaction F_{Coul}, which leads to attraction or repulsion simply because of the charges q on the objects:

$$F_{Coul} = qE$$

Though, dielectric forces (or: polarization or gradient forces) also have to be considered, especially since we are working with droplets that are easily polarizable:

$$F_{Diel} = \frac{\pi}{4} d^3 \varepsilon_0 \varepsilon_s \frac{\varepsilon_d - \varepsilon_s}{\varepsilon_d + \varepsilon_s} \nabla E^2$$

with ε_0, ε_d ,and ε_s representing the dielectric permittivity of vacuum, the water droplets, and the solvent, respectively, and d representing the droplet diameter. While the Coulomb force only depends on the field strength E and the droplet charge q, the polarization force is directly proportional to the gradient of the square of the electric field, and acts attractive in the direction of maximum field gradient for $\varepsilon_d = \varepsilon_{water} \cong 80$ being higher than $\varepsilon_S = \varepsilon_{FC\text{-}77} = 1.86$.

Dielectric interactions explain why the droplets also may deposit onto likely charged patterns, as observed on PMMA. But, as we immersed both samples into the same emulsion, it is not yet clear why we cannot observe the same characteristics in FC-layers. Obviously, it is also the substrate material that defines the interaction forces.

In the case of PMMA, the overall repulsive electrostatic may change the deposition characteristics by reducing Coulomb interaction, manifesting itself in a weaker attractive force towards the negative charge patterns, accompanied by weaker repulsion from positive charges. The shape of the charge dots observed by KFM contains information on the field gradient (Fig 3.20). While around positive charges we can observe a sharp change in local surface potential, the field gradient around negative ones appears significantly smoother. The sharper the change in the local surface potential on the substrate, the more droplets will be attracted to pattern by polarization forces.

We will always have both forces acting on the droplets, but force ratio is influenced by the substrate material: While on PMMA the ratio is shifted towards polarization forces due to the overall background potential, resulting in pronounced deposition on positive charges, the deposition on FC-layers is dominated by Coulomb interaction. Another experimental observation that supports the assumption of dipolar attraction on PMMA is the observation that the edges of positive structures are often decorated with particles.

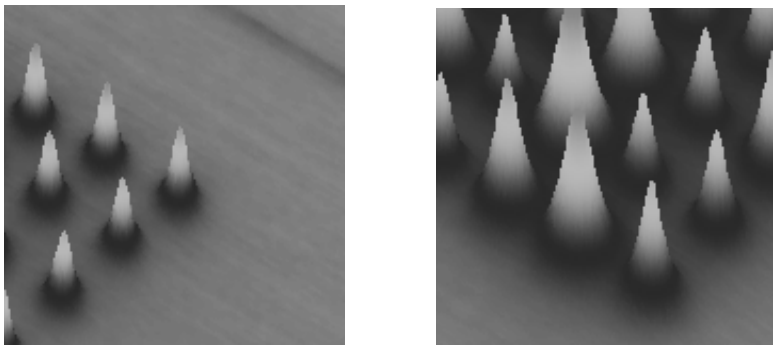

Figure 3.20 Charge dots on PMMA. KFM images of charge dots on PMMA clearly show a sharper dot definition, meaning a sharper field gradient, for positive dots (left) compared to negative ones (right). Z-scale: 1.5 V in both images. Pitch of dot patterns: 2 μm.

Also other groups who deposited particles from fluorocarbon oils observed deposition on both polarities [Fudouzi2002b; Jacobs2001].

Can we use the knowledge gained above to improve pattern definition on FC-layers?

To investigate if we can improve pattern definition we wrote a different type of charge pattern into an FC-layer: The negative charge dots were therefore applied in an area with a positively charged background (Fig. 3.21) to simulate the deposition characteristics on PMMA, where we achieved better pattern definition.

The answer to above question can be seen in Fig. 3.22: Yes, we can improve the pattern definition on FC samples! While the negative charges without additional positive background show the usual disordered deposition (Fig. 3.22C), pattern definition has significantly been improved by the use of a positive background potential (Fig. 3.22A,B). This indicates that we can improve the deposition results by combine the high selectivity of FC-samples with the excellent pattern definition of PMMA. Furthermore, the images shown in Fig. 3.22 manifest the assumption of a positive background charge on PMMA, which becomes evident when comparing particle patterns on PMMA (Fig. 3.22D) to the improved deposition results on FC.

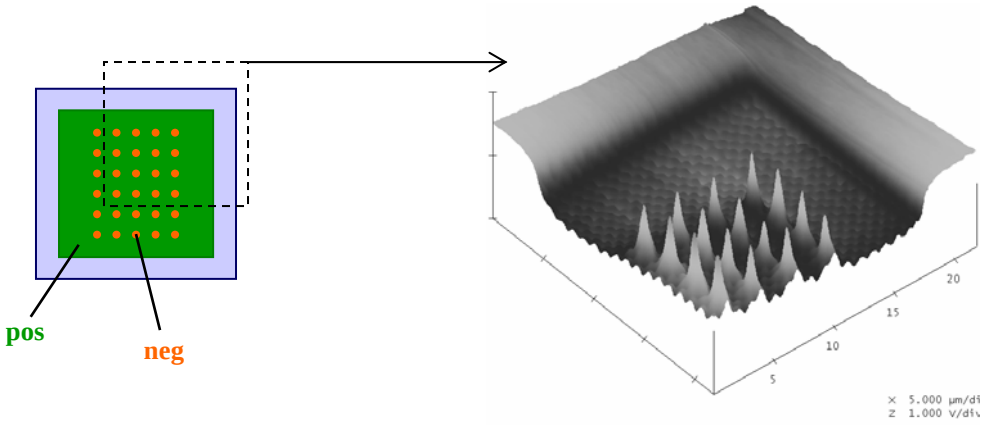

Figure 3.21 FC layers with neg charge dots on pos background; schematic (A) and KFM images (B); KFM image is inverted for better visibility; pos square, neg dots written into it.

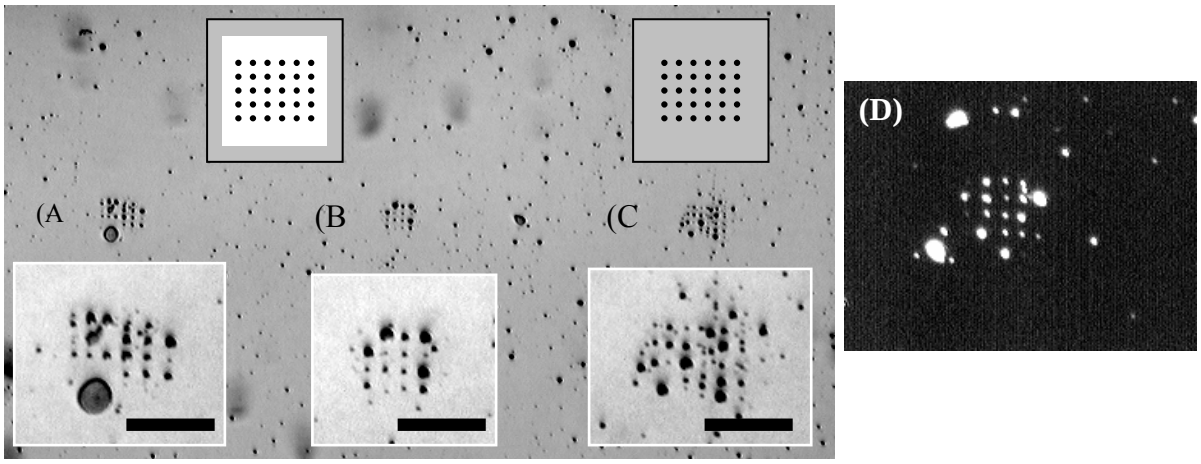

Figure 3.22 Deposition of 50 nm silica beads onto combined patterns on FC. Charge patterns: positive background charge (+0.25 V) with negatively charged dots (-1.8 V (A), -1.1 V (B)), and (C) only negative charge dots (-1.2 V). Scale bars: 10 µm. For comparison: fluorescence image of bead pattern on PMMA (D).

The results shown above further prove that deposition on FC occurs within a very short time scale. This opens additional possibilities for improving pattern definition: Since the definition obviously gets worse with time due to random-like attachment, shorter immersion times might result in well-defined patterns. Better control on the immersion time may be achieved by using microfluidic channels.

4 Fabrication of Biomolecular Structures

Organized layers of biological molecules may serve as templates to create other nanostructured materials, or as functional micropatterns for studying cell growth [Falconnet2004], to name just a few applications. Due to the very versatile role proteins have in biology (ranging from signalling, to mechanical support, to force generation) they may even be integrated into micro- or nano-scale devices, like bio-MEMS.

A crucial step is the precise immobilization of biomolecules in well defined patterns on solid surfaces while retaining their native functionality. The task of fabricating protein arrays has been addressed by various approaches, be it well-known soft-lithography-based methods [Feng2004a; Feng2004b; Jacobs2001], or even scanning-probe-based ones [Lee2003]. Further methods to selectively deposit biomolecules onto substrates have evolved during the past few years, relying on sphere lithography [Garno2002; Yap2005], nanoimprint lithography [Hoff2004], or chemical patterning of polymer films [Douvas2005].

We applied our method of electric field guided assembly to selectively pattern proteins onto solid substrates. A crucial requirement for potential use in biological applications is that the functionality of the proteins is retained. To investigating the functionality of our protein patterns, we relied on the avidin-biotin binding, a well-known protein-ligand reaction. In this thesis, we evaluated the suitability of two approaches:

- ◊ In a *direct approach*, we used the protein deposited from the emulsion directly to detect further molecules from solution (section 4.2).
- ◊ In a second approach we used the first protein layer as anchor points to deposit the functional biomolecules (the so-called *"glue"-method*). Layered structures consisting of up to three biomolecular layers were fabricated at designated positions on the sample (section 4.3).

Independent of the method and the material we used, we observed one special characteristic of the patterns: Being deposited from emulsion, the proteins are delivered to the patterns by small water droplets, which subsequently dry on the sample, resulting in ring-like structures. The origin of these rings will be discussed in section 4.4.

4.1 Proteins

Being present in biological systems, proteins are mainly suspended in aqueous solutions. At the same time, they have amphiphilic properties, meaning that they are composed of hydrophilic as well as hydrophobic domains. Thus, the hydrophilic part is exposed to the solution, shielding the hydrophobic parts. This effect leads to a complicated folding of the protein, usually termed tertiary structure.

This tertiary structure is very sensitive to the surrounding medium, the most important parameters being temperature and the pH of the solution. Minute changes in ambient conditions may already cause structural changes within the molecule, which may be reversible or irreversible, and even may deactivate the protein. Hence, proteins are typically handled in buffer solutions.

Avidin is a relatively robust protein, in the sense that its tertiary structure stays stable over a wide pH range, providing a functionality of the molecule within various types of buffer solutions. The avidin-biotin reaction is one of the strongest protein-ligand reactions found in nature due to the high affinity of the reaction ($K_a=10^{15}$). Biotin, a vitamin, fits to certain domains of the avidin molecule like a key in its lock. Nevertheless, the binding is formed only under special conditions, when both molecules are in their native, active state.

Avidin has four subunits to bind biotin, which can be randomly distributed over the surface of the molecule. When being adsorbed to a solid surface, an avidin molecule may therefore have between zero and four functional groups exposing towards the solution that allow biotin molecules to bind. Streptavidin is a slight modification of avidin, with the main difference being in the distribution of its functional groups: They are located two by two at opposite sides of the molecule, assuring that always two binding sites are available for reaction to biotin. Immunoglobulins are globular proteins, like avidin. Though, they exhibit

differences in structure in terms of immunoglobulins being more flexibly than the rather rigid avidin molecules. Detailed information on the structure of the molecules can be found in the Appendix (see App. B.3.1).

Protein adsorption at interfaces, be it solid-liquid or liquid-liquid, as well as drying the protein almost always leads to conformational changes in the molecule, especially when being adsorbed to hydrophobic surfaces. These changes in tertiary structure may be reversible or irreversible, depending on the material and the process conditions, possibly leading to protein denaturation which in turn results in loss of biological functionality. Reviews on protein characteristics at interfaces are found in references [Dickinson1999; McClements2004; T. A. Horbett1995].

Being composed of hydrophilic as well as hydrophobic parts, proteins may also serve as natural emulsifying agents [Dickinson1999; Kamyshny1997; Kamyshny1999; McClements2004]. Adsorption of proteins to liquid-liquid interfaces happens in two steps: the migration of the protein to the interface may be followed by conformational rearrangement. Unfolding of the molecules leads to the hydrophobic parts interacting with the oil, and may finally result in the formation of a network. Dynamics of protein adsorption vary over a wide range, and depend on the type of the protein [Freer2004a; b]. Globular proteins usually exhibit extremely slow dynamics of conformational rearrangement, though they sometimes adsorb within less than a minute.

4.2 Experimental Details

The experimental section contains descriptions of the processes and methods used to deposit and modify the biomolecules. Detailed information on the materials employed can be found in the Appendix (see App. B.3.2).

4.2.1 Depositing Proteins via Emulsion-Based Development

The first layer of the biomolecular structures, which serves as anchor site to attach further molecules, has been deposited with the method described in the previous section: After defining the location of the functional spots via AFM-based charge writing, the sample is developed in a water-in-oil emulsion containing the desired molecules (Fig. 4.1). For the charge writing, we relied on the same procedure as described in detail in section 2, using the same charge pattern geometries, as well as the same voltage ranges for both polarities. The protein patterns were predominantly deposited onto PMMA samples, although a few experiments have also been conducted on fluorocarbon films. We used mainly PMMA samples due to less background coverage compared to FC-samples (see section 3), and better adhesion of PMMA to the silicon support. FC-layers showed only limited adhesion to silicon when immersed into aqueous solutions.

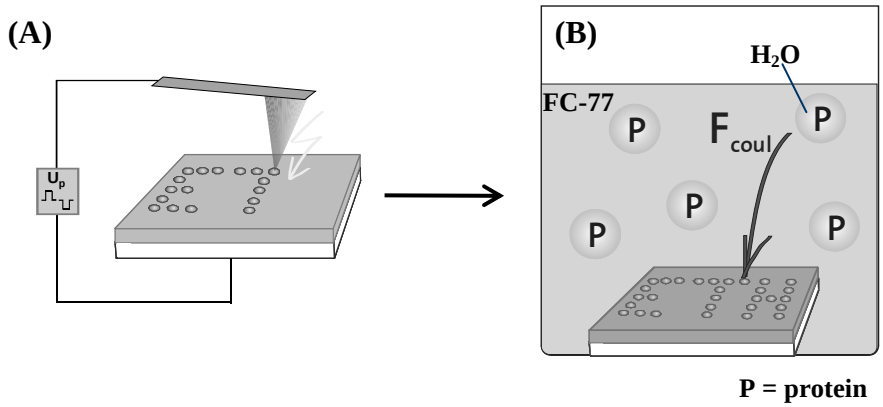

Figure 4.1 Process scheme. After writing charge patterns with a conductive AFM tip (A), the proteins are deposited from a water-in-oil emulsion (B), where water droplets transport the proteins to the predefined locations via electrostatic attraction.

For the development step, one fundamental difference regarding the emulsions employed has to be considered: In the previously described experiments the emulsion properties are determined by the pristine water/oil interface, which for the "biological emulsions" is substituted by a water/protein/oil system. In consequence, for constant development conditions throughout the series of experiments, the preparation of these emulsions has to follow a precise protocol. To this end, the concentration of proteins in the aqueous solution has to be as carefully adjusted as the amounts of the two liquid phases to be emulsified. Unless otherwise stated we have been working with concentrations of 1 mg protein per ml solution. We emulsified 20 µl of protein solution in 2 ml of FC-77 using an ultrasonic cleaner bath as described in section 3.2. In case a beaker with larger diameter was used to prepare the emulsion, the amount of oil was adjusted to yield approximately the same liquid height to obtain the same process conditions throughout all developments. Because of the emulsion as well as the proteins being very sensitive to temperature, the water in the ultrasonic cleaner has been cooled while sonicating using ice cubes in order not to exceed 25°C. To provide enough time for the proteins to assemble at the water-oil-interface, the emulsions were typically sonicated for a couple of minutes (ranging from 2 to 7 minutes). Long-term sonication would lead to substantial heating of the emulsion, if it was not cooled. Throughout the experiments, immersion times were kept constant, the exact times being described in the pertaining parts in section 4.3. After the development, the samples were taken out of the beaker and dried in air. It is important to allow sufficient time for the samples to dry thoroughly before continuing with further modification steps, to assure that both the fluorocarbon oil and the water from the deposited droplets have evaporated completely. We typically waited for at least 30 minutes before immersing the samples into further solutions.

Characterization of the samples is performed by light microscopy and AFM.

4.2.2 Washing and Rinsing Procedures

Before further modification of the patterns, the dry samples had to be re-wetted and salt as well as excess and loosely bound protein molecules had to be washed away. To this end, the substrate was rinsed in a washing solution during

approximately 5 minutes (wash (A), Fig. 4.2). The “wash (A)” step served as a rinsing step and, at the same time, as a blocking step to prevent any unspecific binding of proteins while rinsing and during further modification steps. This blocking solution was composed of approximately one part commercial blocking solution (Block Aid), consisting of a mixture of proteins, and 3 parts filtered phosphate buffered saline solution (PBS).

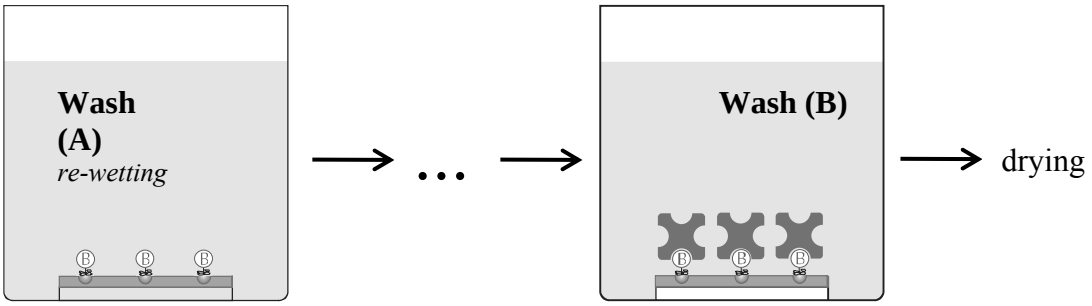

Figure 4.2 Washing and rinsing of the samples. The samples are cleaned from excess salt and loosely bound molecules by immersing them into washing solutions. The dry samples are re-wetted and cleaned in PBS solution containing a certain amount of blocking solution (Wash (A)). After the last modification step, the samples are rinsed in pure PBS, followed by two extensive rinses in UHQ water (Wash (B)).

After the patterns had been reacted with further biomolecules from solution, again excess and loosely bound molecules had to be rinsed away before drying the sample. The “wash (B)” step actually consisted of three consecutive washing steps: First, the sample was rinsed in filtered PBS for 5 to 10 minutes, followed by 2 excessive rinses in UHQ water, 5 minutes each. These last steps additionally prevented salt to crystallize on the sample while drying.

4.2.3 Direct Deposition of Avidin

The method described in section 4.2.1 was used to locally deposit avidin molecules onto PMMA and FC-HFP surfaces. To this end, a 1 mg/ml solution of avidin in PBS was emulsified in FC-77 by ultrasonication (Fig. 4.3A). If not

otherwise stated, sonication and immersion times were kept at 2 and 3 minutes. For better visualization of the deposition results, we used FITC-labelled avidin (fluo iso thio cyanate) (avidin-FITC). After drying, the samples were characterized by AFM and fluorescence microscopy regarding deposition results.

The deposited avidin molecules were subsequently tested regarding their activity. To this end, the sample was immersed into a solution containing biotin-labelled polymer beads with a diameter of 1 μm (Fig. 4.3B). Here, it was important to quickly transfer the sample from the washing solution into the bead solution, in order to prevent intermediate drying phenomena, which may lead to denaturation of the proteins. The samples were incubated in a bead solution consisting of 0.01 % (w/v) beads in 1 part commercial blocking solution and 2 parts PBS overnight. The large diameter of the beads allowed for easy characterization of the samples in reflected light microscopy.

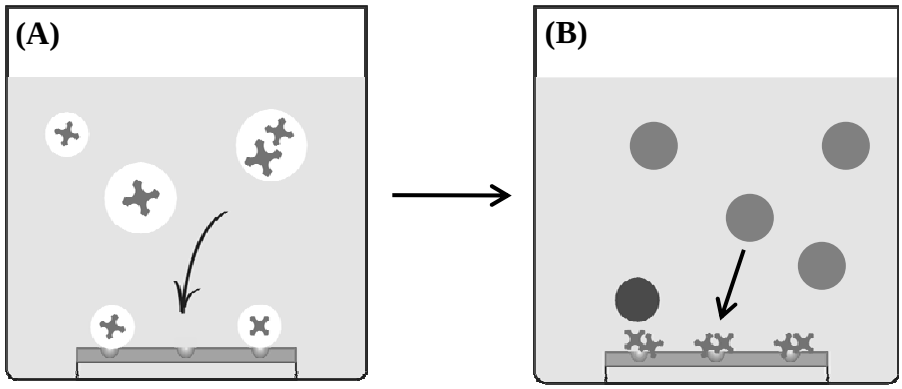

Figure 4.3 Deposition of avidin and detection with biotin-beads. Avidin-FITC is transported to the patterns via the emulsion (A). After drying and rinsing, the sample is immersed into a 0.01 % (w/v) solution of 1 μm biotin-labelled polymer beads (B).

4.2.4 Using IgG-biotin as Glue

An alternative molecule that is used to determine the anchor sites for subsequent functionalization is immunoglobulinG modified with biotin groups (IgG-biotin). In these experiments, the aqueous phase of the development emulsion consists of 1 mg/ml IgG-biotin in PBS, if not stated otherwise. The emulsion was prepared

according to section 4.2.1. If not mentioned otherwise, the mixture was sonicated for 2 minutes before immersing the samples for 3 minutes.

In most cases, PMMA samples were used as substrates, although some studies were also made on FC-samples. Either way, deposition onto positive and negative charge patterns was investigated. The deposition results were mainly studied by AFM.

The IgG-biotin spots on the sample were used as anchor points for three different types of modifications:

(a) Attaching anti-biotin to the biotin groups.
(b) Attaching FITC-labelled avidin to the biotin groups.
(c) Attaching 40 nm sized biotin-labelled beads via a streptavidin linker.

Regarding sample handling during functionalization, we used the same procedure as described in section 4.2.3.

Attaching anti-biotin

Anti-biotin is known to bind selectively to biotin. Hence, a successful binding holds for a proof that the biotin groups on the IgG are still active and accessible for subsequent reactions in aqueous solutions. To this end, the samples are immersed into a 10 μg/ml solution of fluorescently labelled anti-biotin in PBS for at least 60 minutes, and subsequently rinsed for cleaning.

Attaching avidin-FITC

Further modification of the IgG-biotin spots on the sample was achieved via specific reactions at the biotin groups. To this end, the samples were immersed into a 0.1 mg/ml solution of FITC-labelled avidin in PBS for at least 60 minutes (Fig. 4.4B).

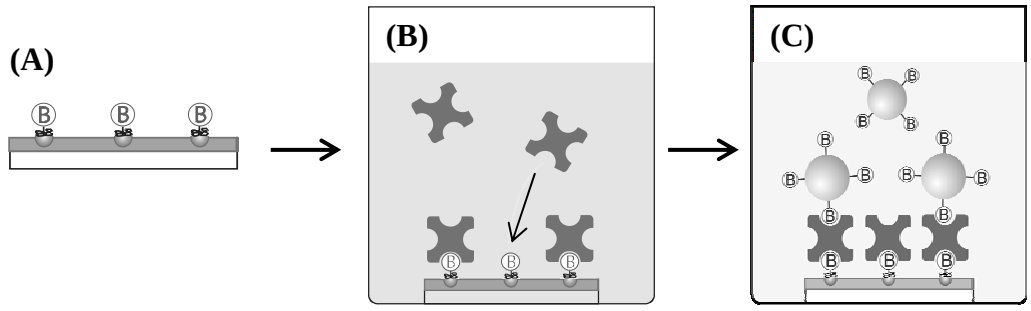

Figure 4.4 Attachment of nanoparticles via an avidin linker. The samples modified with IgG-biotin (A) were first immersed into an aqueous solution of FITC-avidin to bind avidin to the predefined spots (B). In a second solution, 1 μm biotin-labelled polymer beads can bind to the deposited avidin (C).

Additional experiments were conducted to investigate the functionality of the avidin molecules. Hence, after the avidin attached to the patterns, the samples were immersed into a 0.01 % (w/v) solution of biotin-labelled beads (Fig. 4.4C) for at least 2 hours similar to the procedure described in section 4.2.3, and subsequently rinsed for cleaning.

Attaching biotin-beads via a streptavidin linker

Layered structures were fabricated by using streptavidin molecules as linkers between the deposited IgG-biotin spots and biotinylated nano-beads. Due to its molecular structure, streptavidin is generally considered to be more suited for building up layered structures than avidin (see section 4.1).

The streptavidin linkers were applied in a procedure similar to one described above for the attachment of FITC-avidin, that is the samples were immersed into a 0.1 mg/ml streptavidin solution in PBS for 120 minutes. To track the individual process steps, we used fluorescently labelled streptavidin (alexa fluor 568).

After rinsing the sample in pure PBS, the sample was immersed into the next solution, to react the streptavidin patterns with biotin-labelled polymer beads,. The biotin-beads were attached to the patterns from PBS solution containing 0.03 % (w/v) of beads of a diameter of 40 nm and ca. 33 % commercial blocking solution (BlockAid). To distinguish streptavidin from the biotin-beads in the

fluorescence images, the fluorescent marker of the beads is chosen to emit at another wavelength as the streptavidin marker (see App. b.3.2).

4.3 Results

4.3.1 Direct Deposition of Avidin

The average droplet sizes of the avidin-emulsion were determined by laser scanning confocal microscopy (LSCM). Fig. 4.5 shows a typical section through an emulsion containing avidin-FITC, clearly revealing the fluorescence of the molecules. Based on this and similarly obtained images we estimate the droplet size to be in the range of 1μm, with smaller droplets around 400 nm, and larger ones above 1 μm being present. Though, the emulsions used for the LSCM measurements were already a few minutes "old", in contrast to the emulsions used for attaching the proteins, which haven been used immediately after preparation. Thus, the average size obtained from these images represents an upper limit.

These images further indicate that the avidin molecules are located at or close to the oil-water-interface, which meets the expectations regarding the adsorption behaviour of proteins [Dickinson1999].

Initial experiments on FC-HFP only showed deposition on negatively charged structures. Hence, only negative charge patterns have been used for studying the attachment of avidin from emulsion. Fig. 4.6 shows 4 lines onto which avidin-FITC has selectively deposited, as can be seen in the fluorescence image (Fig. 4.6B), differentiating the proteins from unspecific background information in the reflected light microscopy image (Fig. 4.6A).

The "bumps" displayed in the AFM amplitude image appear after immersing the FC-HFP samples into the emulsion (Fig. 4.6C). Since these buckling effects even occur when immersing the samples into pure FC-oil and also due to poor adhesion of the FC-layer on the substrates when immersed into aqueous solutions, further experiments were performed on PMMA substrates.

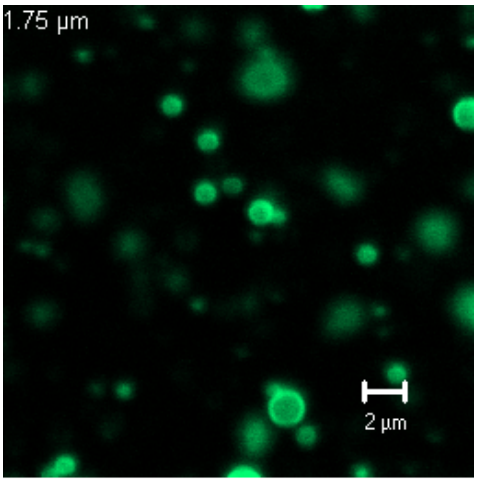

Figure 4.5 Emulsion containing avidin-FITC. Laser scanning confocal microscopy image of an avidin-emulsion.

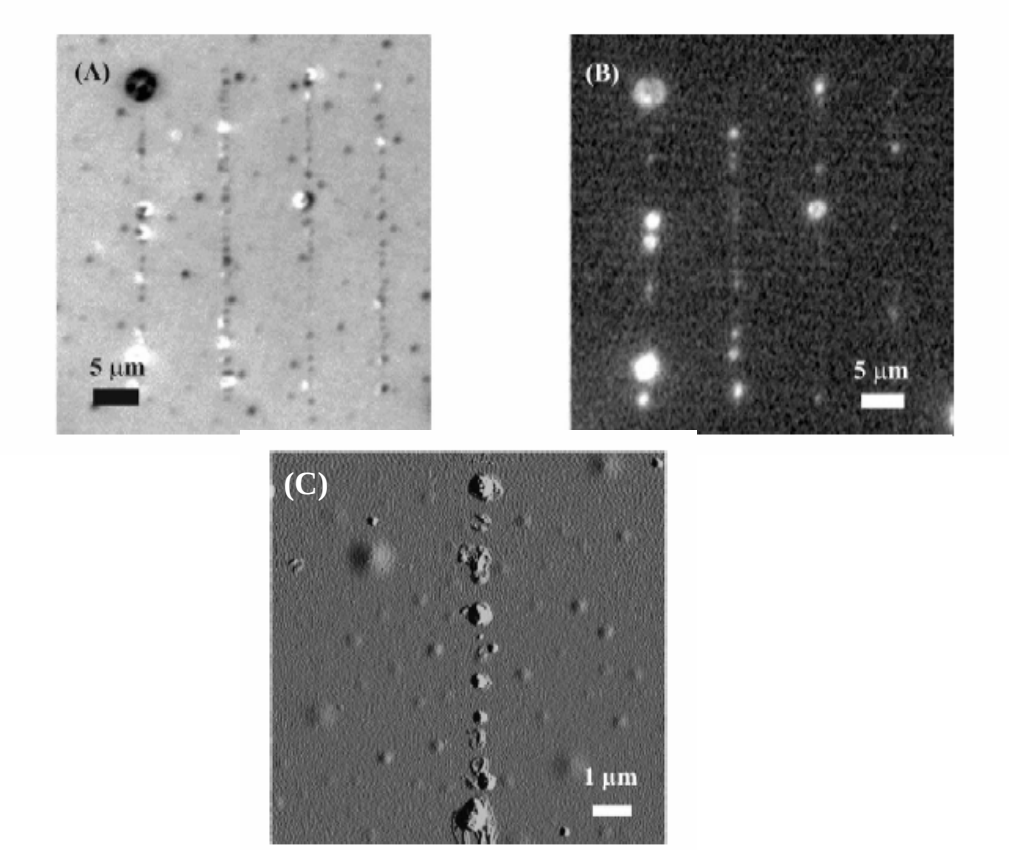

Figure 4.6 Attached protein/salt clusters on FC-HFP after dipping the sample into the emulsion (see section 4.2) for 3 min and air-drying. (A) Reflected light microscopy image, 40x magnification. (B) Fluorescence microscopy image, 40x magnification. Charge pattern: 4 negatively charged lines of 40 µm length. Pulse height: -60 V, pulse length: 1 ms, areal pulse density: 3.125 charge pulses/µm. (C) Zoom onto single line. AFM amplitude image, image size: 11 x 11 µm.

Fig. 4.7 shows FITC-avidin deposited onto a negatively charged cross on a PMMA sample. Again, fluorescence (Fig. 4.7A) proves the cross to consist of avidin-molecules. Though, these deposits may not exclusively consist of protein molecules, since we were working in a PBS buffer with a high salt concentration. As we wanted to react the avidin with other molecules or particles in aqueous solution, we first had to investigate the stability of these structures against exposure to water-based solutions. Some protein might dissolve from the surface, as it is expected for the salt.

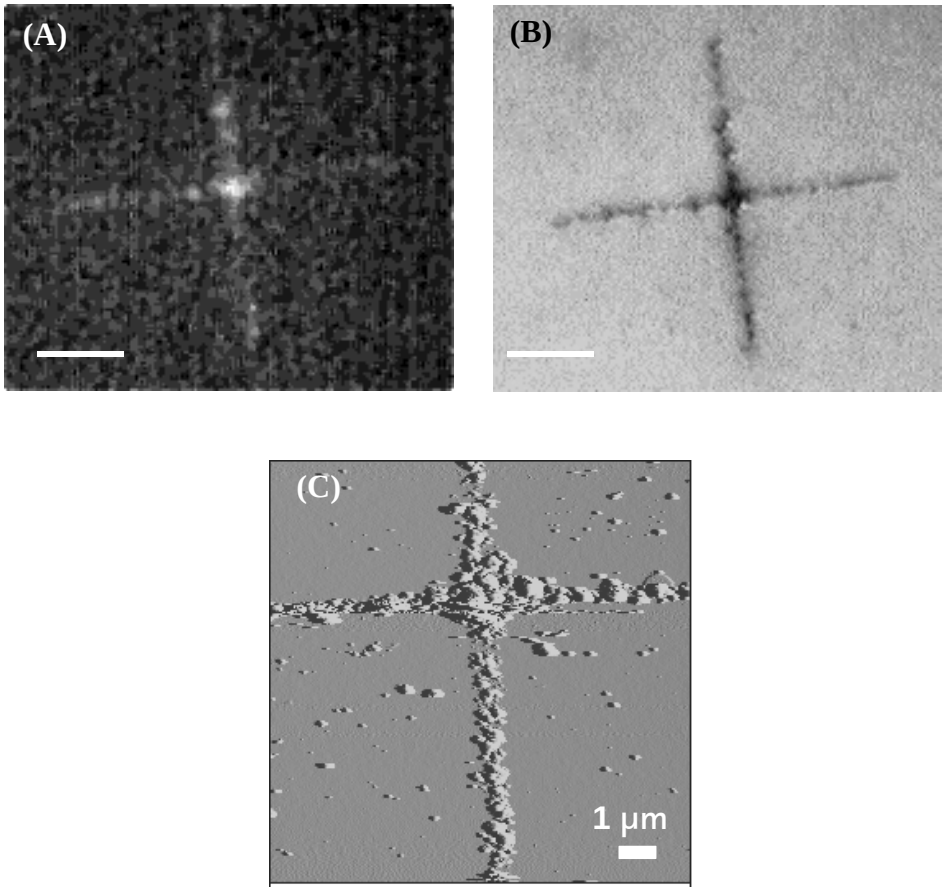

Figure 4.7 Attachment of FITC-avidin on PMMA. Fluorescence microscopy (A) and reflected light microscopy (B) images of a negatively charged cross covered with avidin. (C) AFM amplitude image (a.u.) of the same structure. Charge pattern: 40µm cross. Sonication of emulsion: 3 min, immersion: 2 min. Scale bars 10 µm.

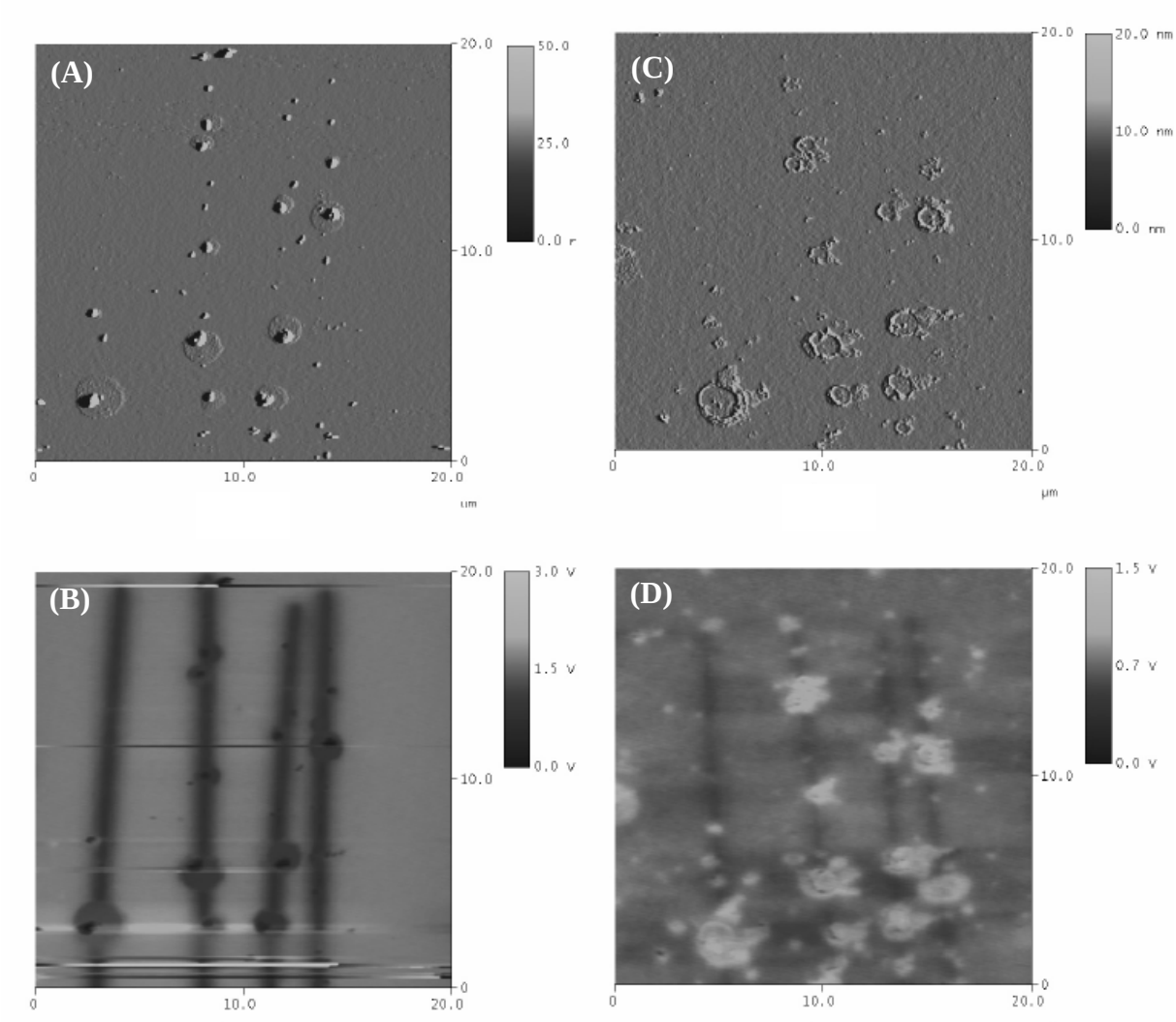

Figure 4.8 Stability of FITC-avidin during rinsing. AFM amplitude (A, C) and KFM images (B, D) of FITC-avidin on PMMA after deposition (A, B) and after rinsing (C, D). Same process conditions as in Fig. 4.7. Images obtained after rinsing in PBS for 30 min, followed by 2 rinses in UHQ-water.

After immersing a sample into pure PBS solution followed by two rinses with UHQ-water, KFM and AFM images were obtained from the same structures. Though the amount of material diminished during rinsing (Fig. 4.8C), the amplitude image still displays protein deposits. The ring-like appearance of the larger avidin spots is discussed in detail in section 4.4.

To clarify if the deposited avidin shows enough functionality to bind biotin molecules for building up further layers, the samples were incubated in a buffered aqueous solution containing biotin-beads, as described in section 4.2. Due to the

large bead diameter (1 μm), the samples could easily be characterized by light microscopy (Fig. 4.9). No specific attachment of the beads could be observed (Fig. 4.9A), although the fluorescence image clearly reveals the FITC-avidin (Fig. 4.9B).

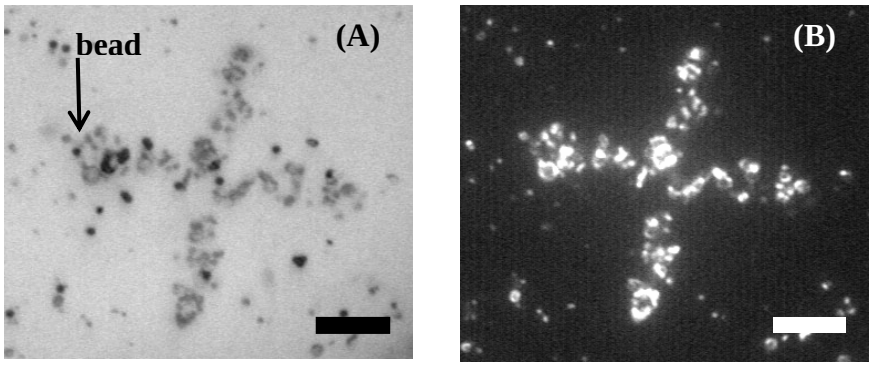

Figure 4.9 Biotin-beads on avidin structures on PMMA. Samples prepared like in Fig. 4.7 were incubated in solution of 1 μm biotin-beads. The beads are clearly resolved in the reflected light microscopy image (A), while only the FITC-avidin is detected in the fluorescence image (B). Scale bar: 10 μm.

The reason for above observation might be denatured avidin. Proteins are known to change their conformational state and denature when being dried in unspecific conditions, or when contacting hydrophobic surfaces (see section 4.1). This unfolding of avidin can have rendered the molecule inactive, making it impossible to bind to biotin. Hence, avidin cannot be used as a sensor on the micropatterns in a direct manner. Therefore, alternative ways for depositing functional structures have to be explored.

4.3.2 Using IgG-biotin as "Glue"

Deposition of IgG-biotin from emulsion

According to the emulsifying of IgG as discussed in section 4.2.1, we observed increased stability of IgG-stabilized emulsions compared to the emulsions used in

section 3.5, manifesting itself in two observations: The emulsion droplets were observed to form loose coagulates rather than to coalesce into a bigger drop, and a larger amount of protein solution could be emulsified into the oil compared with the amounts of particle suspensions, indicating better stability. Coagulation leads to ramified structures, which due to their shape, show slower rising speeds than spherical droplets of the same volume, resulting in slower de-emulsification. Due to the difficulties in determining the droplet size by light diffraction (see App. A), we have to rely on estimations based on AFM images. The drying residues are clearly resolved in amplitude images due to the protein layer that formed around the droplets and deposited onto the samples (Fig. 4.10). From various amplitude images, we estimate the droplets to have diameters around 1 μm, although we frequently observe pattern dot sizes smaller than a micron, as well as some dots even reaching 2 μm. We further assume, based on the discussion in 4.1, that the protein concentration in the outer droplet layers exceeds the concentration in bulk, like it has been observed for droplets containing avidin-FITC (Fig. 4.5).

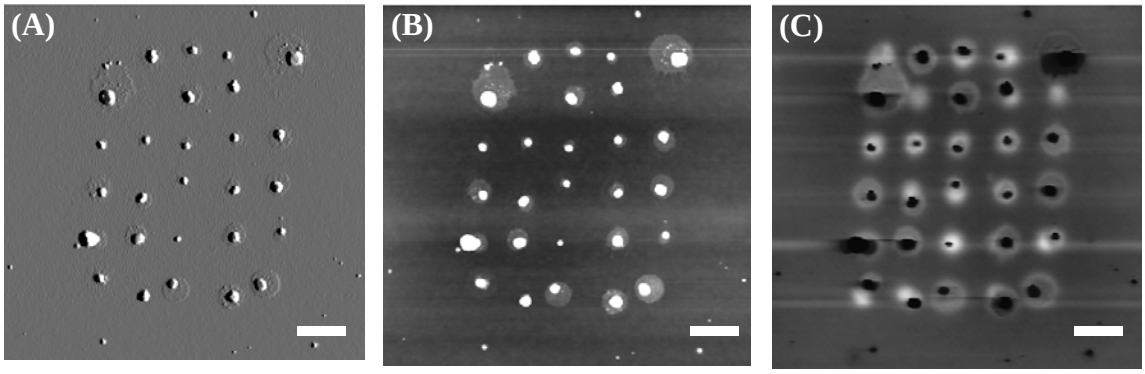

Figure 4.10 IgG deposited onto PMMA. AFM amplitude (A), topography (B) and KFM images (C) of IgG-biotin deposited onto positively charged dots on PMMA. Charge pattern: 30 dots with 2 μm pitch, 2.5 V surface potential. Z-range: (A) 15 nm, (B) 50 nm, and (C) 2 V. Process conditions as described in section 4.2. Scale bars: 2 μm.

We have studied the influence of the surface potential height of the charge dots on the deposition characteristics and have found the coverage to depend on the potential (Fig. 4.11). When using higher surface potentials in the range of 3 V, nearly 100 % coverage could be achieved on the dot patters without significant background binding around the patterns (see also Fig. 4.10), showing the high

selectivity of this method. Lower potentials lead to correspondingly less deposition (Fig. 4.11B).

Since we found the substrate material to have large influence on the particle deposition, we also conducted some deposition experiments on FC-samples. The protein loaded water droplets were generally observed to deposit onto both polarities on FC-samples, with more pronounced deposition on negatively charged structures. On PMMA, they were mainly observed to attach to positive dots.

This leads us to the following conclusion regarding the charge of the droplets: The droplets may be weakly positively charged, at least less than the pure water droplets. Due to high ionic strength of the protein solution, the conductivity inside the droplets is very high, probably leading to strong dipolar interactions. The Coulomb interactions are weakened because of the droplets carrying less charges, resulting in decreased repulsive forces between positive dots and the droplets on FC layers, thereby shifting the force balance to dielectric interaction on FC. The fact that we found hardly any deposition on negative charges on PMMA may also be attributed to decreased Coulomb attraction, while the repulsive forces from positive patterns are also decreased, leading in pronounced dielectric attraction. The same effect is assumed to be the reason for droplet deposition onto positive charges on FC-samples: the reduced Coulomb repulsion enhances dielectric attraction. Furthermore, the dielectric attraction to negative dots on PMMA is weaker anyway, due to their broader shape (Fig. 3.20), further decreasing the attractive forces.

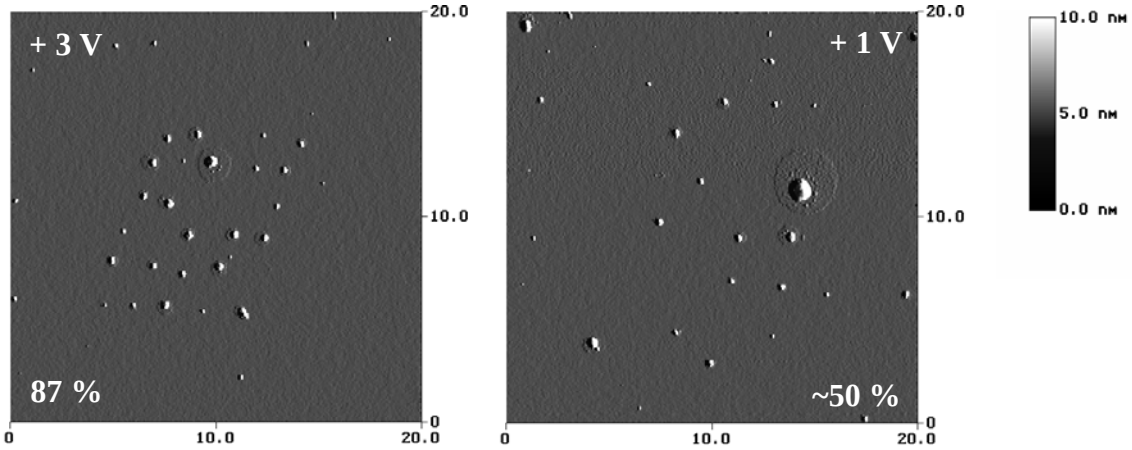

Figure 4.11 Influence of surface potential on pattern coverage. AFM amplitude images (a.u.) of IgG-biotin on positively charged dots on PMMA. The dot patterns have a pitch of 1.5 µm and are located one the same sample. Surface potentials were + 3 V (left) and + 1 V (right). Numbers given in the images are surface potential in V (top) and coverage in % (bottom). Process conditions as described in section 4.2.

The charge of the droplets is likely to depend on the sonication time, since the protein adsorption at the oil-water-interface shows strong time dependence, in terms of migration to the interface as well as in terms of real adsorption. Whereas we can assume the proteins to readily assemble at the interface within less than a minute [Freer2004a] (see section 4.1), adsorption needs more time. Adsorbed protein layers might cause a different surface charge than loosely bound ones. The charge might originate from difference in dielectric constants of the protein layer and the oil, according to the rule of Coehn [A. Coehn1909] (see section 3.1). The difference in dielectric constants is significantly bigger for the water-oil interface than for protein-oil interface, possibly leading to less charge at the protein shell.

Attaching anti-biotin to IgG-biotin

Due to the adsorption of IgG to the oil-water-interface, conformational changes are expected to occur in the molecules and this is also expected after drying the samples. Although the functionality of the biotin groups is most likely not affected by this process, these structural changes might cause the biotin to be hidden within the protein molecule. To verify that the biotin groups on the IgG-molecules are still active, as well as accessible, the samples were incubated in a fluorescently labelled anti-biotin solution. Indeed, we observed a specific attachment of anti-biotin to the previously defined IgG-biotin patterns. Figure 4.12 shows a 40 µm cross after development and subsequent attachment of anti-biotin. As can be seen in the AFM topography image to the left, the IgG-biotin deposited selectively on the positive charge pattern, clearly displaying the cross shape. The biotin activity is verified in the fluorescence image to the right: obviously, the anti-biotin bound very specifically to the IgG spots. The fluorescence image displays ring structures that are also observed in the topography image, and are discussed in detail section 4.4.

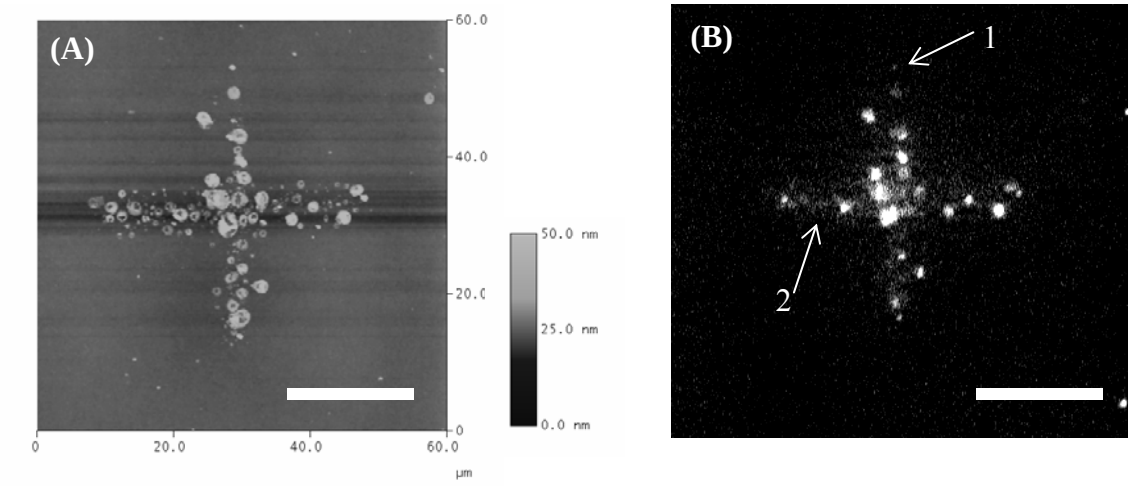

Figure 4.12 Attachment of anti-biotin to IgG-biotin on PMMA. IgG-biotin was deposited onto a positively charged cross (40 µm) on PMMA according to section 4.2, followed by the attachment of fluorescently labelled anti-biotin. (A) AFM topography image, and (B) fluorescence image. Scale bars: 20 µm.

Fluorescence is observed to be generally brighter on higher IgG spots (compare the topography and fluorescence images). Nevertheless, signals are still detected for very small (arrow 1), and very flat (arrow 2) spots.

These results hold for a proof that *(a)* not all of the biotin is buried in the probably denatured IgG chains, and *(b)* the biotin is still active. Furthermore, they show that pattern definition is retained even after immersion into various aqueous solutions, as fluorescence is exclusively detected on the cross pattern.

Attaching avidin-FITC to IgG-biotin

For building up layered structures on the IgG-biotin patterns, we take advantage of the high specificity of the above described avidin-biotin binding. Hence, the samples were incubated in an avidin solution. This way, fluorescently labelled avidin molecules have been selectively attached to the previously defined anchor spots, as is seen in Fig. 4.13. Fluorescence can be clearly detected on the predefined patterns, which were a 40x40 μm cross (Fig. 4.13A) and seven 40 μm long lines (Fig. 4.13B), respectively. The line width is in the range of 800 nm, as also shown in previous experiments [Naujoks2004]. The fact that hardly any fluorescence can be detected in the background is a sign that the avidin specifically bound to the biotin (bound to the IgG) on the sample surface. Due to use of a blocking solution in the earlier rinsing step, the avidin is prevented from binding to the background. The fluorescent spots in the background of Fig. 4.13A originate from avidin bound to randomly deposited IgG.

Figures 4.13(C) and (D) show deposition results of dot patterns located on the same sample. While the “ETH” letters are still detectable, the dot array is harder to resolve. Based on the results obtained on the larger structures, we attribute the poor visibility to a low fluorescence signal, rather than to bad pattern coverage. The fluorescence might be weak because of the shape of the IgG dots on the sample displaying more a ring-like structure rather than a filled circle. For small droplets this ring may be very thin, resulting in a weak signal.

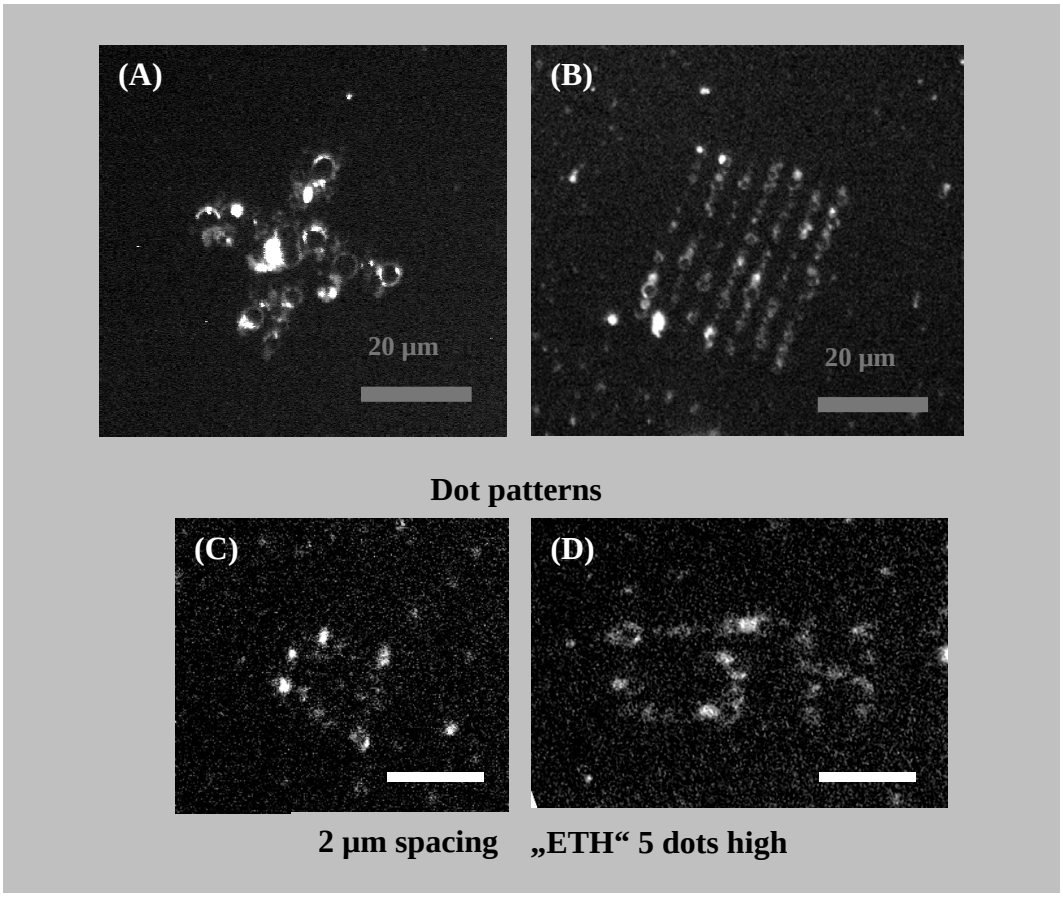

Figure 4.13 IgG-biotin reacted with FITC-avidin. Fluorescence microscopy images of IgG-biotin deposited onto PMMA and reacted with avidin-FITC. (A) Cross shaped pattern (40 µm x 40 µm). (B) Line pattern (each 40 µm long). (C) dot pattern (30 dots, 2 µm pitch), and (D)“ETH” written with single dots. Scale bars: 20 µm (A, B) and 10 µm (C, D).

Attaching biotin-beads

Further modification of the structures with 1 µm sized biotin-beads from aqueous solution did not yield satisfactory results, as is shown in Fig. 4.14. Due to their size, the beads are easily detected in the reflected light microscopy image (Fig. 4.14A, see arrow). Only few beads attached to the pattern, although the fluorescence image (Fig. 4.14B) clearly reveals the fluorescent avidin molecules on the cross pattern. Polymer beads, as used in this experiment, might also show self-fluorescence. Yet, when comparing both images it gets evident, that the

detected fluorescence originates from the FITC-avidin (see the two arrows), which, at least, fluoresces significantly stronger than the polymer beads.

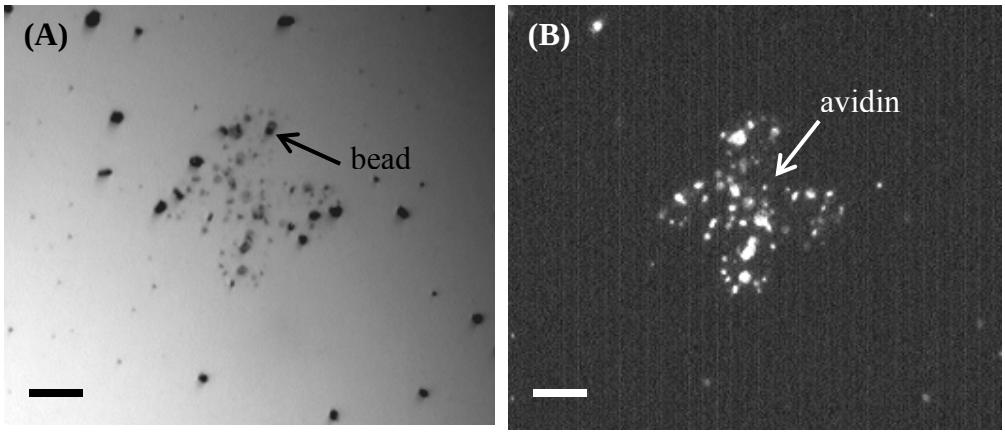

Figure 4.14 Biotin-beads on avidin on IgG. The biotin-labelled polymer beads (1 µm) are clearly resolved in the reflected light microscopy image (A), while the location of the avidin molecules can be found in the fluorescence image (B). Pattern: 30 µm cross on PMMA. Scale bars: 10 µm.

Comparing this image with a light microscopy image obtained before re-wetting the sample and modifying it with avidin and biotin-beads corroborates this interpretation (Fig. 4.15). The large contrast in the right images originates from the salt crystals still being present on the sample, as the image has been obtained before rinsing.

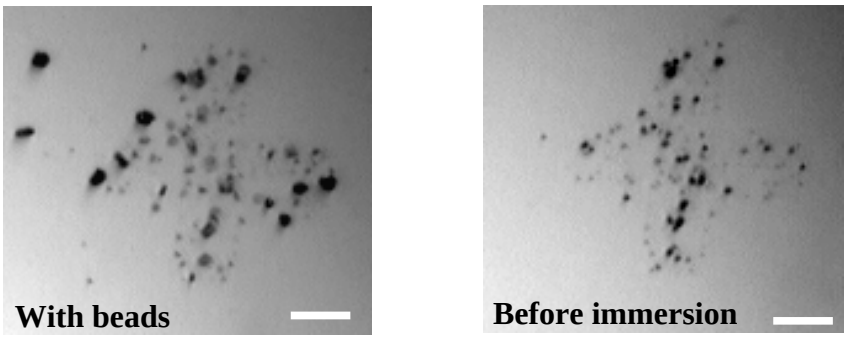

Figure 4.15 Avidin pattern before and after immersion into the bead solution. Same pattern as in Fig. 4.14, imaged after deposition of IgG from emulsion (right) and after bead deposition (left). Scale bars: 10 µm.

These results bring up the question why so little successful binding of the biotin beads to the avidin molecules could be achieved. Several possible reasons have to be considered:

I. The biotin on the beads is not active.
II. The avidin on the pattern might not be functional (anymore).
III. Most of the biotin-binding sites of avidin are already blocked (by biotin groups sticking out of the IgG chains).
IV. The biotin beads are too big to be caught.

Since some binding of the beads is observed on the pattern, the biotin on the beads is assumed to be functional. Additionally, the beads are often detected in very close proximity to a fluorescent spot, suggesting that it attached to an area modified with avidin. As the sample has not been dried while transferring it from the avidin to the biotin-bead solution, a denaturation of the avidin seems unlikely. Also the fact that a blocking solution was used for binding the avidin suggests the avidin to be in an active state to allow for specific binding reactions. An avidin molecule has four binding sites for biotin (see section 4.1), which are not necessarily arranged symmetrically on the molecule. This means that all binding sites can possibly face to the IgG layer, leaving no reactivity to the solution-facing side of the molecule. Hence too few functional groups are present on the avidin facing inside the solution for catching a biotin-bead. As the beads are 1 μm in diameter, just a few avidin-biotin bonds might not provide enough strength to hold the particle at the substrate, especially while drying the sample, when strong shear forces are present (see App. D).

Dot patterns before and after immersion into aqueous solutions

AFM images of the patterns before and after immersion into the avidin solution might elucidate the situation a little bit. The left part of Fig. 4.16 shows the typical deposition characteristics as discussed earlier in this section. After washing and modification of this pattern, only rings are left as IgG-biotin spots (Fig. 4.16, right), as has also been seen for the avidin spots in section 4.3.1. The centre of the as-deposited salt/protein cluster is substantially higher than the outer circle (Fig. 4.16A). However, as this part of the former droplet is rinsed away in the subsequent washing and modification steps (Fig. 4.16B), it is assumed to mainly consist of salt from solution, with some protein incorporated in the crystal. During rinsing, the protein shells of the former droplets seem to break up, exposing the salt/protein crystal from the inside to the solution. The former upper part of this protein layer then seems to get deposited next to the droplet (see arrow in Fig. 4.16B), probably still connected to the rest of the residue. However, they clearly show the ring-like structure, which even applies for dots smaller than 500 nm.

The fact that the docking sites for the biotin-beads have a ring-like geometry, instead of a filled circle, favours the assumption that too small a number of free avidin sites are available for binding a 1 μm bead.

Based on above findings, 2 modifications are made to the experiments: Streptavidin will be used as a linker molecule for further modification, and smaller biotin-beads will be employed. The four biotin binding sites of streptavidin are located face to face on opposite sides of the molecule, rendering it more suitable for building up layered structures (see section 4.1).

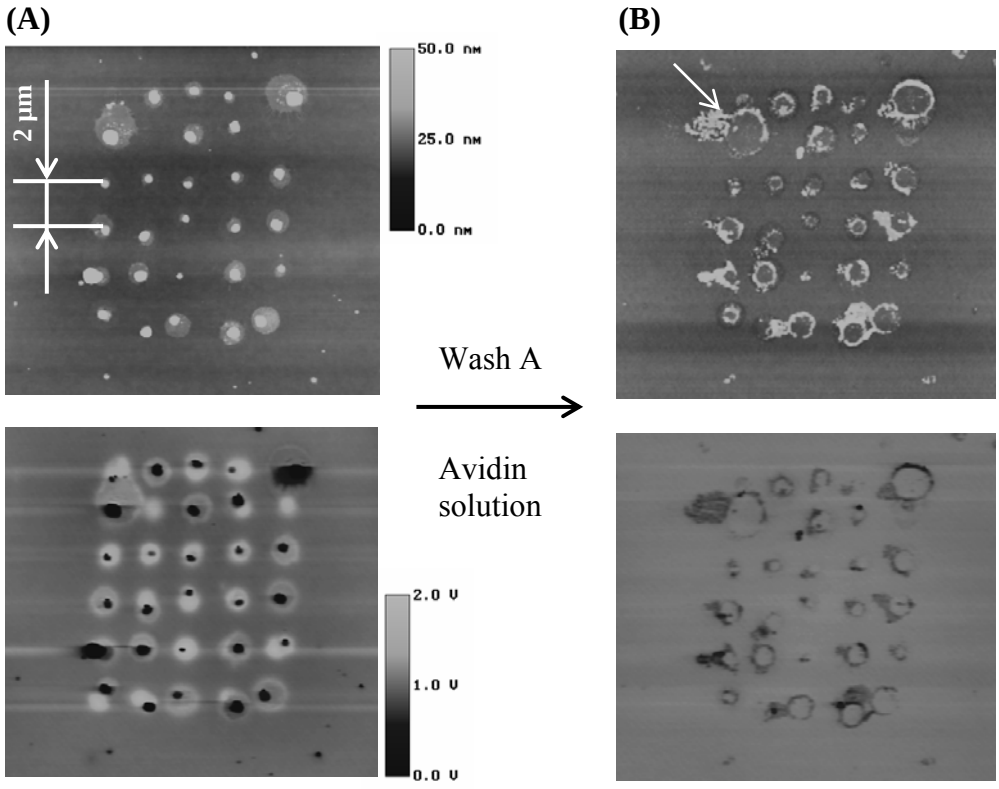

Figure 4.16 Stability IgG patterns to rinsing. AFM topography (top) and KFM images (bottom) of IgG-biotin on a positive dot pattern on PMMA. Images were obtained after deposition of IgG-biotin (A) and after modification with avidin (B).

Attaching biotin-beads via a streptavidin linker

Due to different fluorescence markers for the streptavidin and biotin-bead "layers", we can visualize the result of each reaction step individually, after the whole process of functionalization has been completed. To this end, we record fluorescence images at different excitation wavelengths and use different filters for detection. Fig. 4.17 shows images taken of one and the same pattern. The more discrete spots appearing in the right image account for the biotin beads being imaged, whereas the more homogeneous circles in the left image correspond to streptavidin on IgG-biotin. According to the images, both functionalization steps have been carried out successfully.

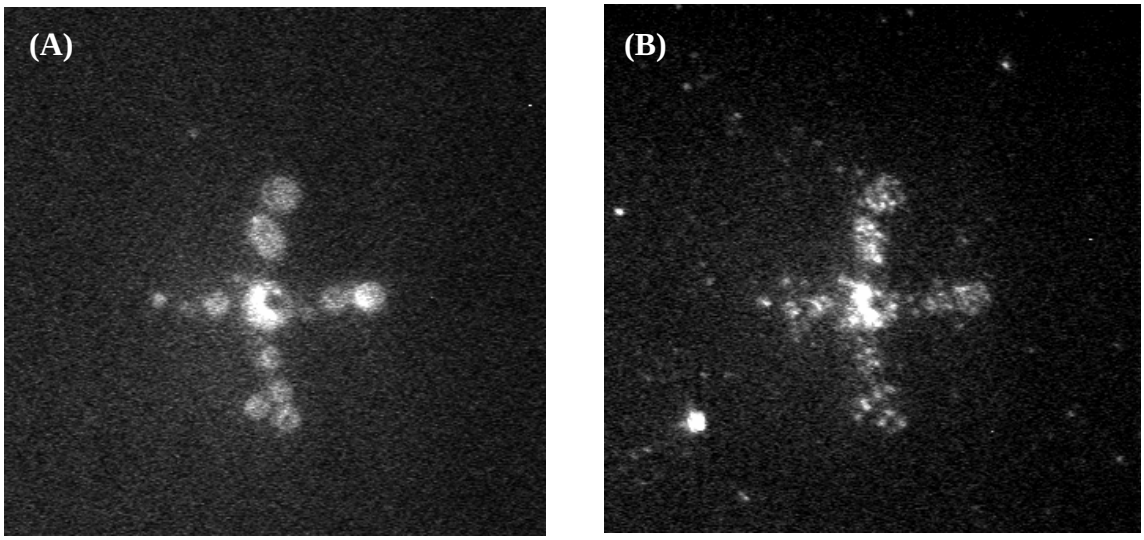

Figure 4.17 Biotin beads attached via a streptavidin linker (I). Fluorescence microscopy images of streptavidin (A) and the 40 nm biotin-beads (B). Pattern: positively charged 40 μm cross on PMMA. Scale bar 20 μm., excitation, emission

In both of the two images, signals occur that cannot be found in the other one, for example the bright spot in the bottom left corner of the bead image. This observation suggests that no significant cross-talk between the signals exists, allowing for separate characterization after sample processing.

An AFM topography image of another cross pattern on the same sample as discussed above is shown in Fig. 4.18. The 40 nm sized beads are clearly revealed in the image. It is evident, that they preferentially attached to the IgG-biotin spots. Observation of the ring structures shows the biotin-beads to be deposited on the rim; an effect, which is important to keep in mind for the analysis of the ring structures in section 4.4.

Although the results shown above prove that the method itself is feasible, the structures shown are rather large. To answer the question whether this procedure of layered assembly also works on a smaller scale, we also investigated the process on 2 μm spaced dot patterns, instead of using the ample cross structures. One of these dot patterns is shown in Fig. 4.19.

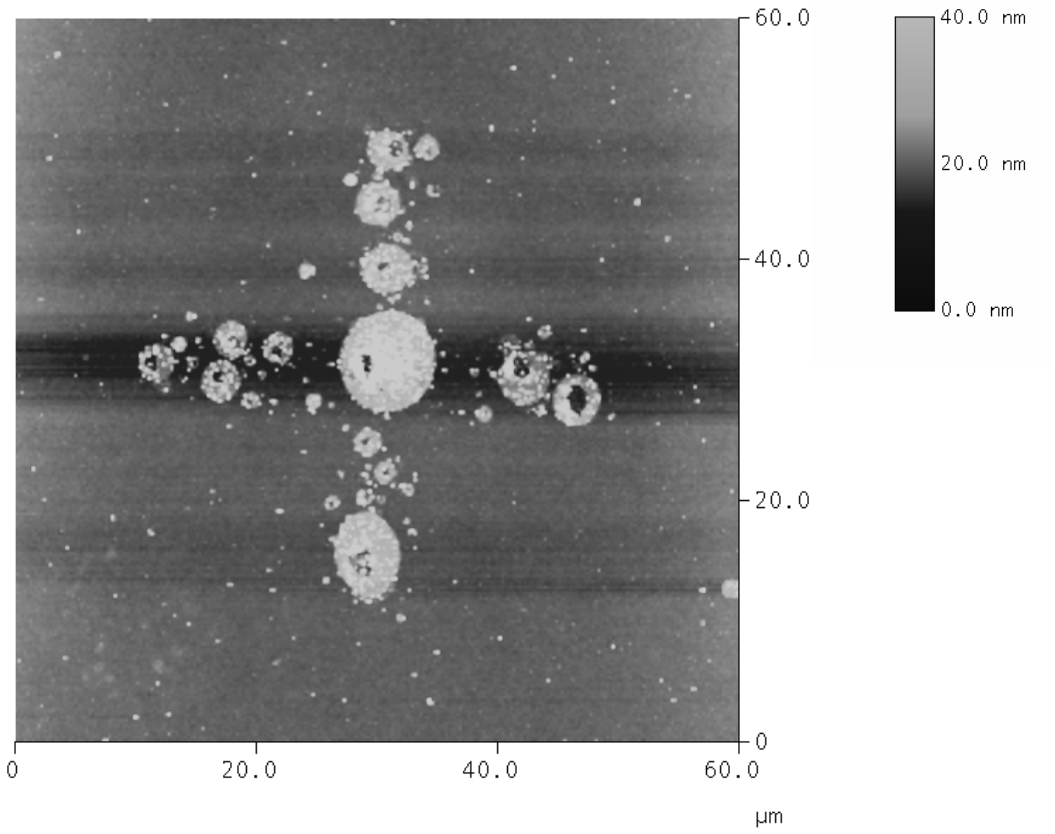

Figure 4.18 Biotin beads attached via a streptavidin linker (II). AFM topography of a 40 µm cross, same sample as in Fig. 4.17. Single beads are resolved via the z-scale.

Again, we find the biotin-beads to mainly populate the rims of the deposited IgG rings, whereas a few beads per spot are detected. Even the very small spots, which hardly can be displayed in the 25 µm AFM scan (see arrow in Fig. 4.19A), are active to bind the biotin-labelled beads. This is verified by zooming into the spot marked in A (Fig. 4.19B). Besides the ring-like structure that is detected also on the small scale, the hill on the ring catches our attention: A single biotin bead has been attached to the IgG spot.

Above results prove that even at small scales enough biotin groups on the deposited IgG are available for further functionalization steps.

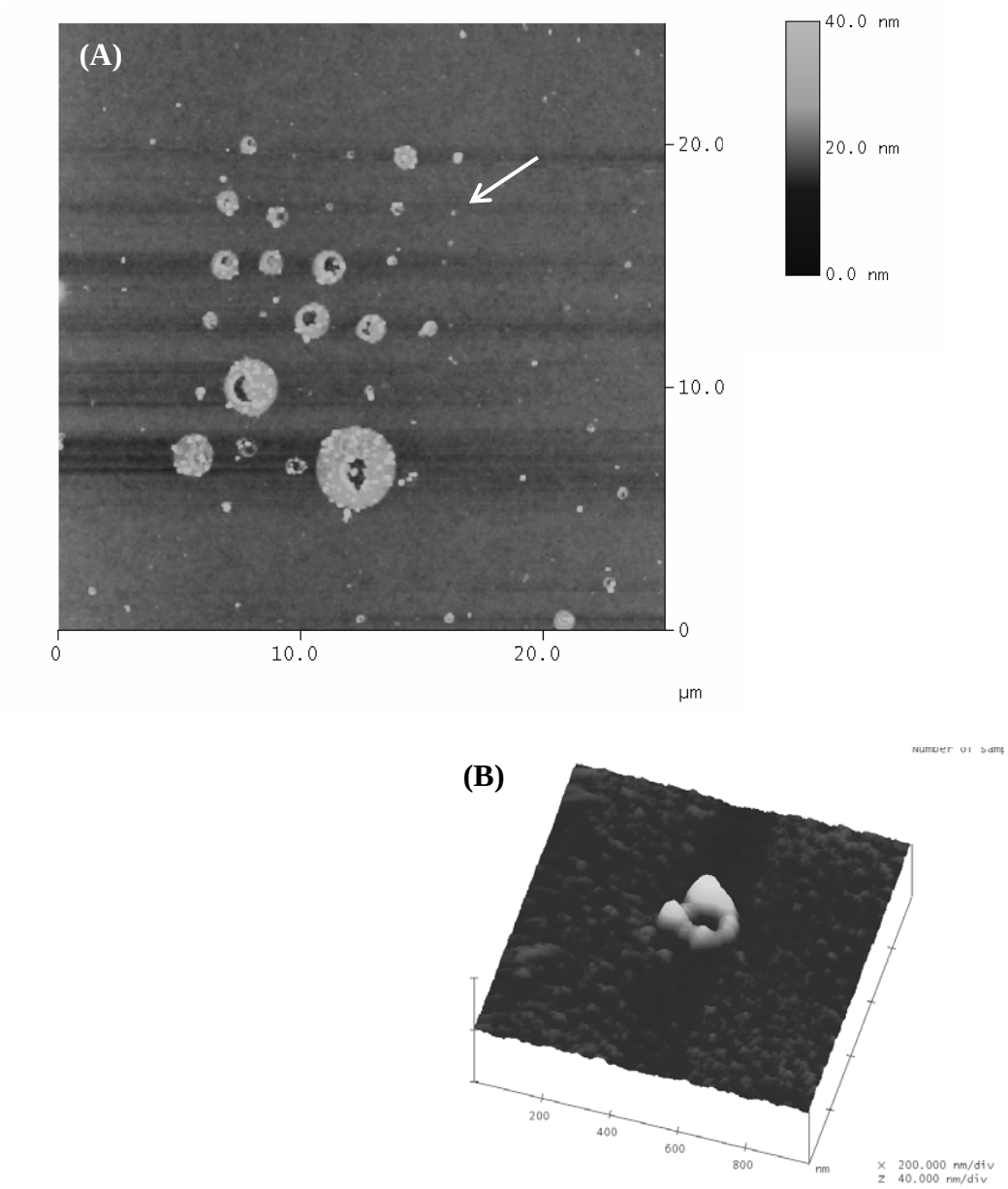

Figure 4.19 Biotin beads attached via a streptavidin linker (III). AFM topography image of biotin-beads on IgG and streptavidin on a dot pattern, same sample as in Figs. 4.17/18. A single biotin-bead is displayed in the 3D image (B); zoom into the dot marked with the arrow in (A).

4.4 Ring Structures OR Model for "Drying Step"

The formation of the ring-like deposits throughout all experiments involving the protein emulsions, may have a number of reasons. The rings may originate from the evaporation process of the droplet, from some charging phenomena, or they may have their origin in some biological processes. However, we can think of basically two scenarios that might lead to the rings:

(1) The protein layers at the surface of the droplets already open while it is still in solution, approaching the sample. This would need the action of long-ranged electrostatic forces.

(2) The droplet lands on the sample in its "native" state, that is in the conformation it had in emulsions, and deformation and / or re-arrangement of the shell starts after deposition.

The fact that we could not detect any significant or systematic differences between droplets deposited (a) onto different samples, and (b) onto neutral or charged surfaces, makes scenario (1) sound more plausible for us (Fig. 4.20). The droplets may carry a surface charge (see sections 4.3.1 and 4.3.2), especially if we consider them to be surrounded by a protein layer. This layer might establish a charge in contact with oil based on contact charging. Cell membranes, which also consist of proteins at a liquid-liquid-interface, were found to have dielectric constants ranging from 5 to 9 [Enikov2004], which would indicate a positive charge on the droplet. However, the layer would break up because of repulsive forces, rather than attractive ones. Since we observed these rings to occur independently of the charge of the surface (positive, negative, neutral), we can widely exclude long-range electrostatic interaction causing deformation of the protein layer.

Although we consider the droplet to "deform" after having landed on the substrate, the mechanism is still unclear. There are a number of effects to think of, so we will start with some general considerations and observations:

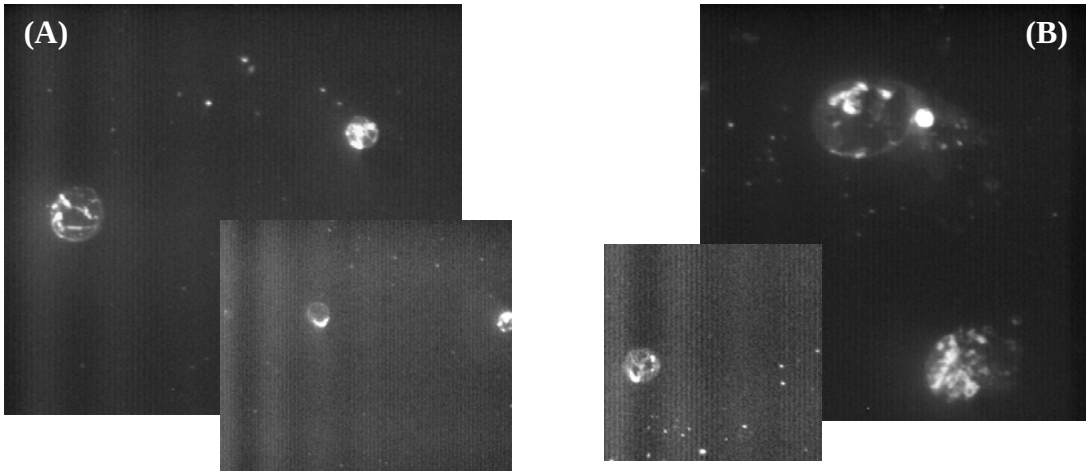

Figure 4.20 Fluorescence images of dried emulsion droplets on FC (A) and PMMA (B). We used fluorescently labelled IgG.

First of all, the amount of protein in one droplet may simply not be enough to cover the whole area contacting the sample. Throughout our experiments we have observed circles with different degrees of “solidity” (the extent to which they seem to be filled with a protein layer). For example the circles in Fig. 4.19 appear to be nearly filled, in contrast to the rings in Fig. 4.16. Based on the concentration of the protein solutions, and the assumption that the concentration in an emulsion droplet corresponds to the bulk concentration, we can state the following: The number of protein molecules per droplet should be sufficient to cover the whole contact area (see App. C.3 for a detailed calculation) for larger droplets, while for smaller droplets there might be a lack of molecules. Yet, rings are observed for all droplet sizes, albeit more or less pronounced!

Both proteins used in our studies are globular proteins, yet exhibiting different conformations. Avidin displays a more rigid structure, while IgG consists of flexible chains, which would suggest increased adsorption or assembly of IgG at the interface. On the other hand, avidin might feel a stronger force to migrate to the interface. Avidin is positively charged in PBS solutions, leading to attraction the negatively charged oil surface. In contrast to that, the isoelectric point of IgG falls into the range of the PBS pH, resulting in no or very little charge of the IgG-

biotin molecule, thus giving it no electrostatically driven force to migrate to the oil-water-interface. For the following model, we assume both IgG and avidin to assemble at the interface, while we cannot predict the adsorption behaviour. Most probably, both layers are still in flexible state, as conformational changes usually occur after longer periods of time [Dickinson1999; Freer2004b], giving the protein molecules enough possibilities to move within the layer.

But what is the driving force for the re-arrangement of the protein layer? IgG is found to show only little affinity for PMMA, resulting in no or very little adsorption from solution [Douvas2005; Martynova1997]. Although the conformational structure of the IgG molecule at the oil-water-interface might have changed, it may still feel some kind of repulsion regarding the PMMA surface. Magdassi et al. observed IgG to widely keep its biological properties when adsorbed at oil-water-interfaces [Kamyshny1997; Kamyshny1999]. Thus, we can assume the IgG molecules that hit the sample to be dissolved into the PBS solution inside the droplet again.

The IgG adsorbs at the oil-water-interface exposing its hydrophobic parts to the oil. If these hydrophobic moieties now hit the PMMA surface, they might want to stay in contact with the oil, leading to a migration of molecules within the layer towards the oil-water-interface. This movement might originate in the PMMA being less hydrophobic than the FC-oil, especially when it is covered by a thin water film, which will be the case, as we are working in ambient conditions. Another driving force for this layer to break up might be hydrophilic interactions between the water inside the droplet and the thin water film on the PMMA sample, leading to an attraction of both phases, pushing the IgG molecules away. Opening of the layer might be an easy task, since we did not allow sufficient time for a network to form [Dickinson1999], so that we will not have a continuous layer.

Thus, considering the final evaporation stages, the droplet may be considered as a droplet of protein solution on a solid substrate. Evaporation of this droplet typically leads to coffee-ring like structures [Deegan2000a]. Yakhno et al. even observed buffered IgG solutions to separate into salt and proteins that way, the salt being located in the inner part of the droplet residue, while the IgG molecules assembled at the outer rim [Yakhno2005].

To conclude this section, we have shown that protein can be selectively deposited onto various kinds of solid substrates, and may serve as anchor sites for subsequent deposition of functional biomolecules. Selectivity during the deposition process from emulsion is achieved simply by electrostatic forces, without the need for passivating the surface against unwanted deposition in this process step. We reproducibly obtained resolutions in the range of one μm, whereas smaller spots detected on our samples indicate that better resolutions may be achieved. Pattern definition and resolution is widely retained in the modification steps, which can be conducted in aqueous environment. The formation of the ring-like patterns may be controlled by using different protein concentrations in the droplets or by conducting the evaporation in controlled atmosphere. The structure of particle deposits during droplet evaporation has been shown to depend on the solvent evaporation rate [Deegan2000b].

5 Conclusions and Outlook

This thesis concentrates on the assembly of nanoscale objects on a solid surface guided by electrostatic forces that are generated by local surface charges written by an AFM tip. The driving forces of the deposition process have been studied in detail and the process has been applied to selectively position proteins, thereby creating a basis for site-directed layered assembly of biomolecular structures.

Charge patterns are created by applying voltage pulses of either polarity to a conductive AFM tip scanning over the surface in ambient conditions. To circumvent problems such as abrasion of conductively coated tips, we used highly doped silicon tips. The same tips have been used for characterizing the charge patterns by means of KFM. For the deposition of particles we used a water-in-oil emulsion: charged water droplets transport particles or molecules to the charge patterns through a nonpolar oil phase.

The electrets applied in this study, PMMA and FC layers, are known to store charges at the surface. As aqueous solutions and polar solvents in general rapidly neutralize these surface charges, particle deposition has to take place in a nonconducting, nonpolar medium. To this end, aqueous solutions containing particles or proteins have been emulsified in a fluorocarbon liquid by ultrasonication. For the deposition, we take advantage of the positive charge that spontaneously forms on the surface of water or air domains in nonpolar media.

To gain deeper understanding of the deposition process, we first investigated the interactions between the pristine materials before studying the deposition of water droplets onto local charges. Since some materials are known to establish surface charges in nonpolar media, we started with studying the characteristics of the oil-substrate interface. One important parameter is the stability of surface charges when immersed into the oil. KFM measurements of charge patterns after

immersion into pure FC-oil showed that charges of both polarities are stable on PMMA, while negative charges on FC-layers showed only limited stability. These observations are supported by KFM studies conducted in-situ, i.e. while the samples are immersed in PFD. While substantial surface potential could be detected on positive charges on FC-layers, negative charges blurred out and vanished within tens of seconds.

However, the phenomenological rule of Coehn predicts the PMMA surface to acquire a positive charge when immersed into the fluorocarbon oils, whereas fluorocarbon layers are not expected to show any special behaviour in contact with PFD or FC-77. Light microscopy observations of uncharged PMMA and FC samples after immersion into a water-in-oil emulsion show a significant difference in overall coverage with beads: On FC layers, we observed substantially more background than on PMMA. Combined with the observation that the water droplets carry a positive charge, one may think of electrostatic repulsion between the droplets and the positively charged PMMA surface. Indeed, we observed some kind of barrier that keeps the water droplets at a certain distance from the PMMA surface in solution, while no force could be observed that keeps them from depositing onto FC samples. Force curves, obtained in PFD on both substrates with hydrophilic spherical cantilevers, support the hypothesis of electrostatic repulsion between water and PMMA in nonpolar media. We did not observe any special behaviour when approaching the cantilever to an FC surface. Yet, during the approach to PMMA samples strong interactions already became apparent in the long range regime.

As model system to study the deposition characteristics, we chose 50 nm silica and latex nanoparticles dispersed in aqueous suspensions. Since both bead suspensions are delivered in pure UHQ water without the addition of ions or stabilizers, we could assure a positive droplet charge. In accordance with above considerations, the substrate material was observed to have a strong qualitative and quantitative influence on the deposition results. The results obtained on FC layers met our expectations, that is the droplets only got attracted to negative charge patterns by Coulomb forces. The positive charge induced at the PMMA-oil-interface shifts the balance of dielectric and Coulomb force acting on the

droplets in the direction of dielectric interaction, which manifested itself in the deposition on charge patterns of both polarities.

With these insights, we were able to significantly improve pattern definition on FC layers by writing negative charge dot patterns into a homogeneous positive background charge. Apart from repelling the droplets around the negative dots, the positive charge stabilized the negative charge dots.

Using the same method, we deposited proteins onto local surface charges. We utilized these proteins as docking sites for functionalized particles and molecules to create layered biomolecular structures. By binding 40 nm sized biotin-labelled beads to predefined locations via a streptavidin linker, we verified the functionality of the previously deposited IgG-biotin. All assembly steps following the initial deposition of the docking proteins can conveniently be conducted in aqueous solutions.

Using emulsified water droplets as transporters offers great flexibility in the choice of particles to be deposited, since most nanoparticles and especially biomolecules are water-soluble. They neither have to show special affinity to the substrate material, nor do they have to be dispersible or even soluble in the oil. Thus, although the choice of the medium interacting with the electret is very limited due to the stability of the local surface charge, the method is applicable to a wide range of materials.

In our process, we take advantage of several phenomena occurring due to inherent properties of the materials themselves or their interfaces:

- ◊ Electrical charges occur spontaneously at the oil-water-interface and lead to selective deposition of the droplets.
- ◊ On PMMA, the positive potential emerging upon contact with the FC oils results in low nonspecific background coverage.
- ◊ The good stabilizing properties of IgG proteins lead to emulsions with better stability.
- ◊ Upon separation of the metastable emulsions, larger water droplets rise upwards due to the significant density difference between the two liquids, thus preventing large droplets from hitting the sample surface.

The resolution achievable with this method mainly depends on the emulsion droplet size. Although we observed individual 50 nm sized particles deposited onto single charge dots, the resolution in terms of pitch or minimal distance between objects still depends on the droplet size, which is currently limited to few hundred nm.

Although the assembly process itself is accomplished within seconds to minutes due the electrostatic fields acting on a large amount of particles in parallel, it still suffers from the slow charge writing speed. Conductive stamps have the advantage of allowing the parallel fabrication of an extended and complex charge pattern in one step. Yet, serial methods based on AFM are advantageous if different particles have to be attached at different locations, e.g. for biosensor-arrays. Additionally, the AFM allows for in-situ characterization of the charge patterns directly after writing using the same tip.

5.1 Outlook

In this thesis, we have investigated the mechanism of electric field guided assembly of nanoscale objects on solid surfaces. Due to its great flexibility, the process developed may offer a promising approach in nanoscale fabrication. However, further investigations are needed to find methods for improving resolution and pattern definition.

One possibility to improve the resolution of particle structures is to increase the resolution of the charge patterns. This may be accomplished by using granular or nanocrystalline materials as substrates [Decossas2005; Kazimierski2003; Maffeis2004; Wilks2004]. For example, Wilks et al. reported on locally charging nanocrystalline SnO2 surfaces using the tip of a scanning tunneling microscope by injecting electrons into individual 8 nm SnO_2 nanocrystals [Wilks2004], while Decossas et al. used Ge nanoislands embedded in silicon as eletrects [Decossas2005].

The use of smaller charge patterns also requires smaller droplets to take advantage on a higher pattern resolution. By finding the right surfactants for the water-in-FC-oil system, the size of the water droplets is expected to decrease significantly.

Nonetheless, we expect better pattern definition and a decrease in structure size, at least to some extent, using the known emulsions in a changed “reaction environment”. Microfluidic devices, instead of beaker chemistry, may provide more control over the deposition, particularly when pumping small amounts of emulsion into a geometrically defined reaction chamber, followed by rinsing steps, if necessary.

Suspensions, where resolution only depends on the particle size, provide an alternative route to emulsion-based deposition. Although dispersing particles in nonpolar media is not straightforward, organically dispersible nanoparticles might offer an alternative. Such particles can be fabricated in various sizes and shapes today [Selvakannan2004].

One might think of various applications of this versatile method, like depositing catalysts to locally induce reactions or nucleation. Examples might be the fabrication of nanotubes or nanowires, or the growth of metallic particles by locally reacting the corresponding metal salt. As incorporating particles into emulsions may involve difficulties, the particles might be produced in the disperse phase of the emulsion, perhaps even induced after the droplet has landed on the corresponding spot on the sample surface.

Appendix

A KFM in FC-oils

KFM imaging of samples immersed in one of the FC-oils showed to be difficult. Especially when working with PMMA samples, we had significant problems in obtaining any useful signal. These difficulties might be attributed to two phenomena: Firstly, we were using fluorocarbon oils instead of aqueous solution, while the liquid cell is mainly designed for the latter. The large difference in viscosity (the viscosity of PFD being approximately 5 times higher than that of water) leads to increased damping. Secondly, the cantilever might be difficult to excite because it already feels the electrostatic field generated by the positive surface potential of the PMMA sample. In KFM, the excitation is switched from mechanical to electrical. However, with the built-in *interleave* function, the electrical excitation is limited to U_{AC} = +/- 10 V, which might simply be not sufficient to overcome the overall electrostatic forces, resulting in the cantilever being "stuck" either directly on the sample or far away. This assumption is manifested by the fact that we sometimes could not observe any response of the cantilever at all. However, sufficiently stable imaging was achieved with one kind of cantilever (see below). All images shown in section 3 were obtained with this type of lever.
Hence, we expect to overcome this problem by the right choice of cantilever, or by using higher excitation amplitudes.

Cantilever properties:

Length L: 250 µm
Width w: 35 µm
Thickness t: 1 µm
Resonance frequency f_{res}: 20 kHz
Force constant k: 0.08 N/m

B Material properties

B.1 Solvents

	Water	FC-77	PFD
Chemical formula	H_2O	*(a)*	$C_{10}F_{18}$
Electrical resistivity ρ/Ωcm	$18 \cdot 10^6$	$1.9 \cdot 10^{15}$	$1 \cdot 10^{17}$
Relative dielectric constant ε_r	81	1.86	1.863
Rel. density d/(water=1)	1	1.78	1.908
Refractive index n	1.33	1.28	1.31
Surface tension $\sigma/(10^{-3}$N/m)	72.75	15	17.6
Boiling point T_B/°C	100	97	142
Dyn. viscosity $\eta/(10^{-3}$Ns/m^2)	1.0	1.4	5.1
Vapour pressure p_V/mbar	23.3	56	8.8

*(a)*Fluorinert ™ (FC-77), mixture of fully fluorinated n-alkanes, primarily with 7 carbons

Suppliers: FLUOROCHEM LTD., Old Glossop, UK (PFD, FC-77) and INTERELEC ELECTRONICS AG, Rüschlikon, CH (FC-77)

B.2 Particle suspensions

Particle material	SiO_2	SiO_2	PS *(a)*
Diameter D/nm	330	50	50
Standard deviation	< 10 %	10 nm	< 15 %
Surface functionality	hydroxyl	hydroxyl	plain
Density $d/(10^3$g/m$^3)$	1.96	1.96	1.05
Concentration c/(weight-%)	10 %	5 %	2.5 %
Concentration c_N/(number/ml)	$2.7 \cdot 10^{12}$	$3.9 \cdot 10^{14}$	$3.64 \cdot 10^{14}$
Art.-nr.	SS02N/5630 *(b)*	24040 *(c)*	17149 *(c)*
Comments			fluorescent *(d)*

All particle suspensions present as aqueous suspensions in pure UHQ water.

(a) PS = polystyrene, latex.

Suppliers: *(b)* BANGS LABORATORIES INC., Fishers IN, USA, *(c)* POLYSCIENCES INC., Warrington PA, USA.

(d) Fluoresbrite® YG, excitation: 441 nm, emission: 486 nm.

B.3 Biomolecules

B.3.1 Molecular structures

Avidin / Streptavidin

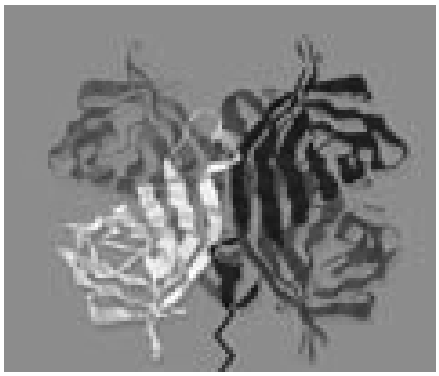

Streptavidin

Biotin

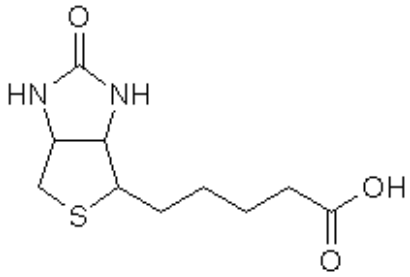

ImmunoglobulinG (IgG)

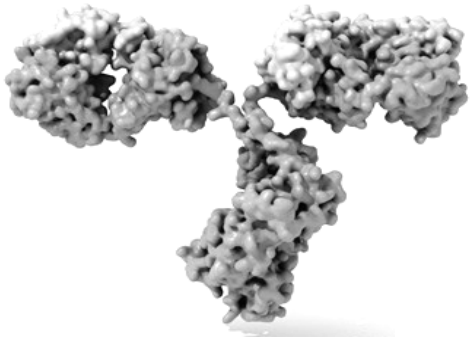

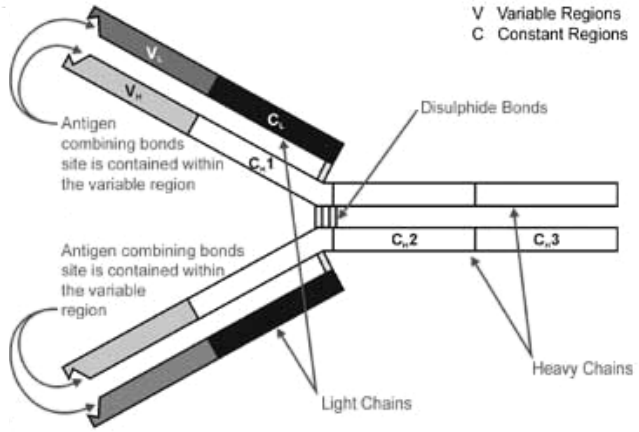

B.3.2 Materials

All protein and particle solutions used in the experiments presented in section 4 were used without further purification, and were diluted to the intended concentration with pure phosphate buffered saline (PBS). PBS tablets were purchased from Sigma-Aldrich (Fluka, 79382) and dissolved in UHQ water to yield a solution containing 137 mM NaCl, 2.7 mM KCl and 10 mM phosphate buffer (pH = 7.4 at 25°C).

Fluorescently labelled avidin (*avidin-FITC*) (from chicken egg white) was purchased from Sigma-Aldrich (Sigma, A2901) as lyophilized powder and diluted in PBS. Avidin-FITC contains 2-4 mol fluorescein isothiocyanate (FITC) per mol avidin. *Streptavidin* (Alexa Fluor® 568 conjugate) was purchased from Molecular Probes (S-11226) as lyophilized powder and diluted with PBS. Excitation and emission wavelengths of Alexa Fluor® 568 are 578 nm and 603 nm, respectively. Both immunoglobulins (*IgG-biotin* and *IgG-FITC*) were purchased from Sigma-Aldrich (Sigma, B-8520 and F-9137) as IgG fractions from antiserum in buffered aqueous solution (0.01 M PBS), containing 15 mM sodium azide (IgG-biotin) or 0.01 % thimerosal (IgG-FITC). Both molecules were provided as whole molecule of anti-mouse IgG produced in rabbit. Fluorescently labelled *anti-biotin* (monoclonal 2F5) was purchased from Molecular Probes (A31801) as Alexa Fluor® 488 conjugate in PBS, pH 7.2, plus 5 mM sodium azide.

Both types of *biotin-labelled polymer beads* (FluoSpheres®, biotin-labelled microspheres) were purchased from Molecular Probes as 1% solids in 50 mM sodium phosphate, 50 mM

NaCl, pH 7.5 plus 0.02% Tween 20 and 2–5 mM sodium azide. The 1 μm sized beads (F-8769) were nonfluorescent, while the beads of 40 nm diameter (F-8766) were Yellow-Green (YG) labelled.

The *blocking solution* (BlockAid™) was purchased from Molecular Probes (B-10710) and consisted of a mixture of proteins dissolved in PBS containing 0.02% thimerosal as a preservative.

For all experiments ultrapure water (UHQ water) was used with a resistivity greater than 18 MΩcm.

C Details of the emulsions

C.1 Droplet sizes

Determination of the droplet sizes of the emulsions used in the experiments was difficult using dynamic light scattering in a commercially available set-up (Zetasizer Nano ZS, Malvern) due to several reasons: Firstly, the apparatus required too much time to calibrate the set-up before starting a measurement (the sample already has to be inserted), so that easily 2 to 4 minutes could have passed until a measurement was started, and another 2 or 3 minutes until it was completed. As we used the emulsions for the development immediately after preparation due to their instability, the emulsion characterized in the Zetasizer did not correspond at all to the emulsions we used for developing our samples. Secondly, the emulsion droplets deposited onto the walls of the cuvette practically immediately after filling the cuvette, which disturbs the measurement signal as well as it contributes to the droplet size signal, giving a wrong impression of the size distribution. Thirdly, the size distribution is determined around 7 to 10 mm above the bottom of the cuvette. Since larger droplets rise faster, we expect this signal to constitute an upper limit of the droplet size. However, this also does not correspond to the emulsion that is close to the charge patterns, since we fully immerse the sample into the beaker, laying it flat at the bottom.

Hence, we so far have to rely on indirect methods to estimate the droplet size, like AFM images (see text). For future investigations, one might think of modifying the cuvette walls, thereby preventing adhesion of the water droplets. When using emulsions with improved stability, time becomes a less crucial factor, leading to less crucial measurement conditions.

C.2 Particle emulsions

(as used for particle deposition experiments described in section 3.5)

For the particle deposition experiments, following bead suspensions were used:

- Polystyrene beads, 50 nm diameter, 2.5% (w/v) in UHQ water, and
- Silica beads, 50 nm diameter, 5.34% (w/v) in UHQ water.

The concentrations correspond to 3.64×10^{14} beads / ml (PS) and 4.19×10^{14} beads / ml (silica), respectively. The suspensions were diluted to 1:5 of the original solution.

Table 1 Amount of beads per droplet for polystyrene and silica suspensions.

		number of beads per drop			
Droplet diameter	**droplet volume**	**Polystyrene**		**Silica**	
[µm]	**[µl]**	**original**	**1/5**	**original**	**1/5**
0.1	5.24E-13	0.19	0.04	0.22	0.04
0.2	4.19E-12	1.52	0.30	1.76	0.35
0.3	1.41E-11	5.15	1.03	5.92	1.18
0.4	3.35E-11	12.20	2.44	14.04	2.81
0.5	6.54E-11	23.82	4.76	27.42	5.48
0.6	1.13E-10	41.17	8.23	47.39	9.48
0.7	1.80E-10	65.37	13.07	75.25	15.05
0.8	2.68E-10	97.58	19.52	112.33	22.47
0.9	3.82E-10	138.94	27.79	159.93	31.99
1	5.24E-10	190.59	38.12	219.39	43.88
1.1	6.97E-10	253.68	50.74	292.01	58.40
1.2	9.05E-10	329.34	65.87	379.10	75.82
1.3	1.15E-09	418.73	83.75	482.00	96.40
1.4	1.44E-09	522.98	104.60	602.00	120.40
1.5	1.77E-09	643.24	128.65	740.43	148.09
1.6	2.14E-09	780.66	156.13	898.61	179.72
1.7	2.57E-09	936.37	187.27	1077.85	215.57
1.8	3.05E-09	1111.52	222.30	1279.47	255.89
1.9	3.59E-09	1307.26	261.45	1504.78	300.96
2	4.19E-09	1524.72	304.94	1755.10	351.02

Conclusions

1. The concentration of beads inside the water droplets approximately corresponds to the concentrations in bulk solutions, based on a comparison of the theoretical number of particles per drop (see table 1) and the average number of particles found on a dot pattern.
2. The number of beads that are found in average on the patterns suggest a droplet size of around half a µm.
3. Depositing single beads seems possible, since the smaller droplets contain around 0.5 to 3 beads in average (see marked fields in table 1).

C.3 Protein emulsions

For the experiments presented in section 4, solutions containing approximately 1 mg proteins per ml have been used for preparing the emulsion.

The calculations presented in table 2 are based on following assumptions

1. The concentration of proteins inside the droplets corresponds to the bulk concentration in solution. $C(IgG_{droplet}) = C(IgG_{bulk})$
2. The area covered by one protein molecule has been calculated with dimensions of 7 x 7 nm of the IgG molecule, which are the dimensions it has in solution
3. The contact area confined by the droplet and the PMMA is based on a 90° contact angle, and therefore corresponds to the surface are of a circle with the droplet radius.

Molecular Weight of IgG: Mw = 160000 g/mol

Conclusions

Although we use high protein concentrations (in terms of "biological" considerations), the area that may be covered by the molecules is very small (see table 2). However, the actual area covered will be higher due to the following reasons:

- ◊ There will be no closed packing achieved due to the geometric structure of the molecules.
- ◊ The dimensions of the molecules themselves will be larger due to unfolding when depositing onto the surface.

Nevertheless, there won't be sufficient biological "material" available to fully cover the PMMA surface exposed to the solution (see column A_{prot}/A_{drop} in table 2).

Though, the fact that we observed rings instead of a uniform, sparse coverage all over the PMMA/water contact area, leads to the conclusion that evaporation effects and the lack in surface affinity of the IgG to PMMA are the main reasons for the formation of the rings.

Table 2 Amount of protein molecules per droplet and the theoretical area to be covered by the molecules.

Droplet diameter [µm]	droplet volume [µl]	Amount of protein [mg]	Amount of protein [mol]	Number of protein molecules	Area covered by the proteins A_{prot} [nm2]	Droplet contact area A_{drop} [nm2]	A_{prot} / A_{drop}
0.1	5.24E-13	1.05E-15	6.54E-24	3.94	1.93E+02	7.85E+03	0.02
0.2	4.19E-12	8.38E-15	5.24E-23	31.54	1.55E+03	3.14E+04	0.05
0.3	1.41E-11	2.83E-14	1.77E-22	106.44	5.22E+03	7.07E+04	0.07
0.4	3.35E-11	6.70E-14	4.19E-22	252.29	1.24E+04	1.26E+05	0.10
0.5	6.54E-11	1.31E-13	8.18E-22	492.76	2.41E+04	1.96E+05	0.12
0.6	1.13E-10	2.26E-13	1.41E-21	851.48	4.17E+04	2.83E+05	0.15
0.7	1.80E-10	3.59E-13	2.24E-21	1352.12	6.63E+04	3.85E+05	0.17
0.8	2.68E-10	5.36E-13	3.35E-21	2018.33	9.89E+04	5.03E+05	0.20
0.9	3.82E-10	7.63E-13	4.77E-21	2873.75	1.41E+05	6.36E+05	0.22
1	5.24E-10	1.05E-12	6.54E-21	3942.04	1.93E+05	7.85E+05	0.25
1.1	6.97E-10	1.39E-12	8.71E-21	5246.86	2.57E+05	9.50E+05	0.27
1.2	9.05E-10	1.81E-12	1.13E-20	6811.85	3.34E+05	1.13E+06	0.30
1.3	1.15E-09	2.30E-12	1.44E-20	8660.67	4.24E+05	1.33E+06	0.32
1.4	1.44E-09	2.87E-12	1.80E-20	10816.97	5.30E+05	1.54E+06	0.34
1.5	1.77E-09	3.53E-12	2.21E-20	13304.40	6.52E+05	1.77E+06	0.37
1.6	2.14E-09	4.29E-12	2.68E-20	16146.61	7.91E+05	2.01E+06	0.39
1.7	2.57E-09	5.14E-12	3.22E-20	19367.26	9.49E+05	2.27E+06	0.42
1.8	3.05E-09	6.11E-12	3.82E-20	22990.00	1.13E+06	2.54E+06	0.44
1.9	3.59E-09	7.18E-12	4.49E-20	27038.48	1.32E+06	2.84E+06	0.47
2	4.19E-09	8.38E-12	5.24E-20	31536.35	1.55E+06	3.14E+06	0.49

Mw=	160000	g/mol	
NA=	6.023E+23		
dimension of IgG:	7x7x5	49	nm2

D Forces acting on the polymer beads

The polymer beads deposited onto the protein patterns are attached to the sample via avidin-biotin bonds with a bond strength in the range of 10 to 200 pN for a single bond [Zhu2002].

The drag force acting on the particle due to the streaming liquid is defined by:

$$F_{drag} = \frac{\pi}{8} c_d \rho_l d_p^2 u_l^2$$

with the dimensionless drag coefficient c_d, density of the medium (liquid) ρ_l in kg/m^3, the particle diameter d_p in m, and the velocity of the streaming liquid u_l in m/s.

However, even when assuming a high streaming velocity of the liquid of 1 cm/s the resulting drag force is in the range of 10^{-11} N ($F_{drag} = 4.7 \cdot 10^{-11}$ N), and thus one order of magnitude smaller than a single bond. Hence, even a single bond could hold the bead at the sample surface.

Though, the evaporating liquid causes capillary forces to act on the particles during evaporation. Immersion capillary forces acting laterally on the particles have been reported to be in the range of $F_{cap} = 6 \cdot 10^{-9}$ N or larger for µm sized particles in a water film [Denkov1992; Hu2004; Kralchevsky1992]. Hence, several avidin-biotin bonds (more than 30) would be needed to overcome capillary interactions. In conclusion, the large polymeric biotin-beads might have been detached from the protein patterns while drying the sample, if too few avidin-biotin bonds established.

References

[A. Coehn1909] A. Coehn, U. R., Ann Phys **4. Folge**(30), 777 (1909).

[A. Klinkenberg1958] A. Klinkenberg, J. L. v. d. M. (1958). Electrostatics in the petroleum industry. New York, Elsevier.

[Agarwal2003] Agarwal, G., R. R. Naik and M. O. Stone, Journal of the American Chemical Society **125**(24), 7408-7412 (2003).

[Amjadi2001] Amjadi, H. and C. P. Franz, Journal of Electrostatics **50**(4), 265-277 (2001).

[Barrett1991] Barrett, R. C. and C. F. Quate, Journal of Applied Physics **70**(5), 2725-2733 (1991).

[Beattie2004] Beattie, J. K. and A. M. Djerdjev, Angewandte Chemie-International Edition **43**(27), 3568-3571 (2004).

[Binks2000] Binks, B. P. and S. O. Lumsdon, Langmuir **16**(23), 8622-8631 (2000).

[Binks2001] Binks, B. P. and S. O. Lumsdon, Langmuir **17**(15), 4540-4547 (2001).

[Boer2001a] Boer, E. A., L. D. Bell, M. L. Brongersma and H. A. Atwater, Journal of Applied Physics **90**(6), 2764-2772 (2001a).

[Boer2001b] Boer, E. A., M. L. Brongersma, H. A. Atwater, R. C. Flagan and L. D. Bell, Applied Physics Letters **79**(6), 791-793 (2001b).

[Bouaidat2004] Bouaidat, S., C. Berendsen, P. Thomsen, S. G. Petersen, A. Wolff and J. Jonsmann, Lab on a Chip **4**(6), 632-637 (2004).

[Briscoe2002a] Briscoe, W. H. and P. Attard, Journal of Chemical Physics **117**(11), 5452-5464 (2002a).

[Briscoe2002b] Briscoe, W. H. and R. G. Horn, Langmuir **18**(10), 3945-3956 (2002b).

[Ciunel2005] Ciunel, K., M. Armelin, G. H. Findenegg and R. von Klitzing, Langmuir **21**(11), 4790-4793 (2005).

[D. F. Evans1999] D. F. Evans, H. W. (1999). The Colloidal Domaain- Where Pysics, Chemistry, Biology, and Technology Meet. New York, Wiley VCH.

[Dagata1998] Dagata, J. A., T. Inoue, J. Itoh and H. Yokoyama, Applied Physics Letters **73**(2), 271-273 (1998).

[Dagata2004a] Dagata, J. A., F. Perez-Murano, C. Martin, H. Kuramochi and H. Yokoyama, Journal of Applied Physics **96**(4), 2386-2392 (2004a).

[Dagata2004b] Dagata, J. A., F. Perez-Murano, C. Martin, H. Kuramochi and H. Yokoyama, Journal of Applied Physics **96**(4), 2393-2399 (2004b).

[Decossas2005] Decossas, S., J. Vitiello, T. Baron, F. Mazen and S. Gidon, Applied Physics Letters **86**(3), (2005).

[Deegan2000a] Deegan, R. D., Physical Review E **61**(1), 475-485 (2000a).

[Deegan2000b] Deegan, R. D., O. Bakajin, T. F. Dupont, G. Huber, S. R. Nagel and T. A. Witten, Physical Review E **62**(1), 756-765 (2000b).

[Denkov1992] Denkov, N. D., O. D. Velev, P. A. Kralchevsky, I. B. Ivanov, H. Yoshimura and K. Nagayama, Langmuir **8**(12), 3183-3190 (1992).

[Dickinson1999] Dickinson, E., Colloids and Surfaces B-Biointerfaces **15**(2), 161-176 (1999).

[Douvas2005] Douvas, A. M., P. S. Petrou, S. E. Kakabakos, K. Misiakos, P. Argitis, E. Sarantopoulou, Z. Kollia and A. C. Cefalas, Analytical and Bioanalytical Chemistry **381**(5), 1027-1032 (2005).

[Enikov2004] Enikov, E. T. and A. Palaria, Nanotechnology **15**(9), 1211-1216 (2004).

[Exerowa1969] Exerowa, D., Kolloid-Zeitschrift and Zeitschrift Fur Polymere **232**(1), 703-& (1969).

[Exerowa2003] Exerowa, D., N. V. Churaev, T. Kolarov, N. E. Esipova, N. Panchev and Z. M. Zorin, Advances in Colloid and Interface Science **104**, 1-24 (2003).

[Falconnet2004] Falconnet, D., A. Koenig, T. Assi and M. Textor, Advanced Functional Materials **14**(8), 749-756 (2004).

[Feder1976] Feder, J., Journal of Applied Physics **47**(5), 1741-1745 (1976).

[Feng2004a] Feng, J., C. Y. Gao, B. Wang and J. C. Shen, Colloids and Surfaces B-Biointerfaces **36**(3-4), 177-180 (2004a).

[Feng2004b] Feng, X. Z., S. Hou, Q. L. Chan, L. K. Wang, M. Qin and P. D. Han, Chemical Research in Chinese Universities **20**(6), 826-832 (2004b).

[Fowkes1972] Fowkes, F. M., Journal of Adhesion **4**(2), 155-& (1972).

[Fowkes1982] Fowkes, F. M., H. Jinnai, M. A. Mostafa, F. W. Anderson and R. J. Moore, Acs Symposium Series **200**, 307-324 (1982).

[Freer2004a] Freer, E. M., K. S. Yim, G. G. Fuller and C. J. Radke, Journal of Physical Chemistry B **108**(12), 3835-3844 (2004a).

[Freer2004b] Freer, E. M., K. S. Yim, G. G. Fuller and C. J. Radke, Langmuir **20**(23), 10159-10167 (2004b).

[Fudouzi2001] Fudouzi, H., M. Kobayashi and N. Shinya, Journal of Nanoparticle Research **3**(2-3), 193-200 (2001).

[Fudouzi2002a] Fudouzi, H., M. Kobayashi and N. Shinya, Langmuir **18**(20), 7648-7652 (2002a).

[Fudouzi2002b] Fudouzi, H., M. Kobayashi and N. Shinya, Advanced Materials **14**(22), 1649-1652 (2002b).

[Fujihira1999] Fujihira, M., Annual Review of Materials Science **29**, 353-380 (1999).

[Fujiwara1996] Fujiwara, I., S. Kojima and J. Seto, Japanese Journal of Applied Physics Part 1-Regular Papers Short Notes & Review Papers **35**(5A), 2764-2769 (1996).

[Garno2002] Garno, J. C., N. A. Amro, K. Wadu-Mesthrige and G. Y. Liu, Langmuir **18**(21), 8186-8192 (2002).

[Gemma1995] Gemma, N., H. Hieda, K. Tanaka and S. Egusa, Japanese Journal of Applied Physics Part 2-Letters **34**(7A), L859-L862 (1995).

[Ginger2004] Ginger, D. S., H. Zhang and C. A. Mirkin, Angewandte Chemie-International Edition **43**(1), 30-45 (2004).

[H.F. Eicke1987] H.F. Eicke, G. D. P. (1987). Interfacia Phenomena in Apolar Media. New York, Marcel Dekker.

[Hoeppener2002] Hoeppener, S., R. Maoz, S. R. Cohen, L. F. Chi, H. Fuchs and J. Sagiv, Advanced Materials **14**(15), 1036-+ (2002).

[Hoff2004] Hoff, J. D., L. J. Cheng, E. Meyhofer, L. J. Guo and A. J. Hunt, Nano Letters **4**(5), 853-857 (2004).

[Hu2004] Hu, M. H., S. Chujo, H. Nishikawa, Y. Yamaguchi and T. Okubo, Journal of Nanoparticle Research **6**(5), 479-487 (2004).

[Israelachvili1984] Israelachvili, J. N., M. Tirrell, J. Klein and Y. Almog, Macromolecules **17**(2), 204-209 (1984).

[Jacobs1997] Jacobs, H. O., H. F. Knapp, S. Muller and A. Stemmer, Ultramicroscopy **69**(1), 39-49 (1997).

[Jacobs1998] Jacobs, H. O., P. Leuchtmann, O. J. Homan and A. Stemmer, Journal of Applied Physics **84**(3), 1168-1173 (1998).

[Jacobs2001] Jacobs, H. O. and G. M. Whitesides, Science **291**(5509), 1763-1766 (2001).

[Jones1999] Jones, J. T., P. M. Bridger, O. J. Marsh and T. C. McGill, Applied Physics Letters **75**(9), 1326-1328 (1999).

[Kamyshny1997] Kamyshny, A. and S. Magdassi, Colloids and Surfaces B-Biointerfaces **9**(3-4), 147-155 (1997).

[Kamyshny1999] Kamyshny, A., S. Magdassi and P. Relkin, Journal of Colloid and Interface Science **212**(1), 74-80 (1999).

[Kanda2002] Kanda, Y., T. Yamamoto and K. Higashitani, Advanced Powder Technology **13**(2), 149-156 (2002).

[Kane1999] Kane, R. S., S. Takayama, E. Ostuni, D. E. Ingber and G. M. Whitesides, Biomaterials **20**(23-24), 2363-2376 (1999).

[Kazimierski2003] Kazimierski, P., Journal of Non-Crystalline Solids **325**(1-3), 206-212 (2003).

[Keir2002] Keir, R. I., Suparno and J. C. Thomas, Langmuir **18**(5), 1463-1465 (2002).

[Kikukawa1995] Kikukawa, A., S. Hosaka and R. Imura, Applied Physics Letters **66**(25), 3510-3512 (1995).

[Kitahara1984] Kitahara, A. (1984). Nonaqueous systems. Electrical Phenoena at Interfaces. A. W. A. Kitahara. New York, Marcel Dekker**:** 123 ff.

[Knapp2002] Knapp, H. F., P. Mesquida and A. Stemmer, Surface and Interface Analysis **33**(2), 108-112 (2002).

[Knapp1999] Knapp, H. F. and A. Stemmer, Surface and Interface Analysis **27**(5-6), 324-331 (1999).

[Kralchevsky1992] Kralchevsky, P. A., V. N. Paunov, I. B. Ivanov and K. Nagayama, Journal of Colloid and Interface Science **151**(1), 79-94 (1992).

[Kressmann1996] Kressmann, R., G. M. Sessler and P. Gunther, Ieee Transactions on Dielectrics and Electrical Insulation **3**(5), 607-623 (1996).

[Krinke2002] Krinke, T. J., K. Deppert, M. H. Magnusson and H. Fissan, Particle & Particle Systems Characterization **19**(5), 321-326 (2002).

[Krinke2001] Krinke, T. J., H. Fissan, K. Deppert, M. H. Magnusson and L. Samuelson, Applied Physics Letters **78**(23), 3708-3710 (2001).

[Lambert2004] Lambert, J., M. Saint-Jean and C. Guthmann, Journal of Applied Physics **96**(12), 7361-7369 (2004).

[Lee2003] Lee, K. B., J. H. Lim and C. A. Mirkin, Journal of the American Chemical Society **125**(19), 5588-5589 (2003).

[Li2001] Li, Y., B. W. Maynor and J. Liu, Journal of the American Chemical Society **123**(9), 2105-2106 (2001).

[Maffeis2004] Maffeis, T. G. G., G. T. Owen, M. Penny, H. S. Ferkel and S. P. Wilks, Applied Surface Science **234**(1-4), 2-10 (2004).

[Maillard2001] Maillard, M., L. Motte and M. P. Pileni, Advanced Materials **13**(3), 200-204 (2001).

[Mamatkulov2004] Mamatkulov, S. I., P. K. Khabibullaev and R. R. Netz, Langmuir **20**(11), 4756-4763 (2004).

[Mamin1992] Mamin, H. J. and D. Rugar, Applied Physics Letters **61**(8), 1003-1005 (1992).

[Maoz1999] Maoz, R., S. R. Cohen and J. Sagiv, Advanced Materials **11**(1), 55-61 (1999).

[Marinova1996] Marinova, K. G., R. G. Alargova, N. D. Denkov, O. D. Velev, D. N. Petsev, I. B. Ivanov and R. P. Borwankar, Langmuir **12**(8), 2045-2051 (1996).

[Martynova1997] Martynova, L., L. E. Locascio, M. Gaitan, G. W. Kramer, R. G. Christensen and W. A. MacCrehan, Analytical Chemistry **69**(23), 4783-4789 (1997).

[Maynor2001] Maynor, B. W., Y. Li and J. Liu, Langmuir **17**(9), 2575-2578 (2001).

[McClements2004] McClements, D. J., Current Opinion in Colloid & Interface Science **9**(5), 305-313 (2004).

[McGown1966] McGown, D. N. L. and G. D. Parfitt, Discussions of the Faraday Society(42), 225-& (1966).

[McNamee2004] McNamee, C. E., Y. Tsujii and M. Matsumoto, Langmuir **20**(5), 1791-1798 (2004).

[Mesquida2002a] Mesquida, P. (2002a). Zurich, ETH Zurich.

[Mesquida2002b] Mesquida, P., H. F. Knapp and A. Stemmer, Surface and Interface Analysis **33**(2), 159-162 (2002b).

[Mesquida2001] Mesquida, P. and A. Stemmer, Advanced Materials **13**(18), 1395-1398 (2001).

[Mesquida2002c] Mesquida, P. and A. Stemmer, Scanning **24**(3), 117-120 (2002c).

[Mesquida2002d] Mesquida, P. and A. Stemmer, Microelectronic Engineering **61-2**, 671-674 (2002d).

[Mishchuk2004] Mishchuk, N. A., A. Sanfeld and A. Steinchen, Advances in Colloid and Interface Science **112**(1-3), 129-157 (2004).

[Morita1993a] Morita, S., Y. Sugawara and Y. Fukano, Japanese Journal of Applied Physics Part 1-Regular Papers Short Notes & Review Papers **32**(6B), 2983-2988 (1993a).

[Morita1993b] Morita, S., Y. Sugawara, Y. Fukano, T. Uchihashi, T. Okusako, A. Chayahara, Y. Yamanishi and T. Oasa, Japanese Journal of Applied Physics Part 2-Letters **32**(12B), L1852-L1854 (1993b).

[Morrison1993] Morrison, I. D., Colloids and Surfaces a-Physicochemical and Engineering Aspects **71**(1), 1-37 (1993).

[Morrison2002] Morrison, I. D. (2002). Cooloidal Dispersions - Suspensions, Emulsions, and Foams. New York, John WIley and Sons.

[N. Naujoksto be published in 2005] N. Naujoks, P. M., A. Stemmer (to be published in 2005). Electrical-SPM -based fabrication techniques. S. K. A. Gruverman, Springer.

[Naujoks] Naujoks, N. and A. Stemmer, Journal of Nanosciene and Nanotechnology **in press**,

[Naujoks2003] Naujoks, N. and A. Stemmer, Microelectronic Engineering **67-8**, 736-741 (2003).

[Naujoks2004] Naujoks, N. and A. Stemmer, Colloids and Surfaces a-Physicochemical and Engineering Aspects **249**(1-3), 69-72 (2004).

[Naujoks2005] Naujoks, N. and A. Stemmer, Microelectronic Engineering **78-79**, 331-337 (2005).

[Nonnenmacher1991] Nonnenmacher, M., M. P. Oboyle and H. K. Wickramasinghe, Applied Physics Letters **58**(25), 2921-2923 (1991).

[Nyffenegger1997] Nyffenegger, R. M. and R. M. Penner, Chemical Reviews **97**(4), 1195-1230 (1997).

[Olthuis1992] Olthuis, W. and P. Bergveld, Ieee Transactions on Electrical Insulation **27**(4), 691-697 (1992).

[Perez2004] Perez, A. T. and E. Lemaire, Journal of Colloid and Interface Science **279**(1), 259-265 (2004).

[Petsev2004] Petsev, D. N. (2004). Emulsions: Structure Stability and Interactions. New York, Elsevier.

[Pickering1907] Pickering, S. U., J. Chem. Soc **91**
2001
(1907).

[Piner1999] Piner, R. D., J. Zhu, F. Xu, S. H. Hong and C. A. Mirkin, Science **283**(5402), 661-663 (1999).

[Ray2005] Ray, M. A., H. Kim and L. Jia, Langmuir **21**(11), 4786-4789 (2005).

[Royall2003] Royall, C. P., M. E. Leunissen and A. van Blaaderen, Journal of Physics-Condensed Matter **15**(48), S3581-S3596 (2003).

[Sakai2004] Sakai, T., Y. Takeda, F. Mafune and T. Kondow, Journal of Physical Chemistry B **108**(20), 6359-6364 (2004).

[Schönenberger1992] Schönenberger, C., Phys. Rev. B **45** (7), 3861 (1992).

[Selvakannan2004] Selvakannan, P., S. Mandal, R. Pasricha and M. Sastry, Journal of Colloid and Interface Science **279**(1), 124-131 (2004).

[Sessler1987] Sessler, G. M. (1987). Electrets. . Berlin, Springer.

[Sjöblom1996] Sjöblom, J. (1996). emulsions and emulsion stability. New YOrk, Marcel Dekker.

[Stemmer2002] Stemmer, A., P. Mesquida and N. Naujoks, Chimia **56**(10), 573-575 (2002).

[Stern1988] Stern, J. E., B. D. Terris, H. J. Mamin and D. Rugar, Applied Physics Letters **53**(26), 2717-2719 (1988).

[Sugawara1994] Sugawara, Y., Y. Fukano, T. Uchihashi, T. Okusako, S. Morita, Y. Yamanishi, T. Oasa and T. Okada, Journal of Vacuum Science & Technology B **12**(3), 1627-1630 (1994).

[Suzuki2004] Suzuki, M., T. Yasukawa, Y. Mase, D. Oyamatsu, H. Shiku and T. Matsue, Langmuir **20**(25), 11005-11011 (2004).

[T. A. Horbett1995] T. A. Horbett, J. L. L. (1995). proteins at interfaces II - Fundamentals and applications. Washington, ACS.

[Terris1995] Terris, B. D. and R. C. Barrett, Ieee Transactions on Electron Devices **42**(5), 944-949 (1995).

[Terris1990] Terris, B. D., J. E. Stern, D. Rugar and H. J. Mamin, Journal of Vacuum Science & Technology a-Vacuum Surfaces and Films **8**(1), 374-377 (1990).

[Tzeng2002] Tzeng, S. D., C. L. Wu, Y. C. You, T. T. Chen, S. Gwo and H. Tokumoto, Applied Physics Letters **81**(26), 5042-5044 (2002).

[Uchihashi1997] Uchihashi, T., A. Nakano, T. Ida, Y. Andoh, R. Kaneko, Y. Sugawara and S. Morita, Japanese Journal of Applied Physics Part 1-Regular Papers Short Notes & Review Papers **36**(6A), 3755-3758 (1997).

[Uchihashi1994a] Uchihashi, T., T. Okusako, Y. Sugawara, Y. Yamanishi, T. Oasa and S. Morita, Japanese Journal of Applied Physics Part 2-Letters **33**(8A), L1128-L1130 (1994a).

[Uchihashi1994b] Uchihashi, T., T. Okusako, T. Tsuyuguchi, Y. Sugawara, M. Igarashi, R. Kaneko and S. Morita, Japanese Journal of Applied Physics Part 1-Regular Papers Short Notes & Review Papers **33**(9B), 5573-5576 (1994b).

[Umeda1994] Umeda, N., K. Makino, T. Takahashi and A. Takayanagi, Journal of Vacuum Science & Technology B **12**(3), 1600-1603 (1994).

[Vellenga1965] Vellenga, S. J. and Klinkenb.A, Chemical Engineering Science **20**(11), 923-& (1965).

[W.H. Briscoe2004] W.H. Briscoe, R. G. h., Progr. Colloid Polym Sci **123**, 147 (2004).

[Wilks2004] Wilks, S. P., T. G. G. Maffeis, G. T. Owen, K. S. Teng, M. W. Penny and H. Ferkel, Journal of Vacuum Science & Technology B **22**(4), 1995-1999 (2004).

[Wright1998] Wright, W. M. D. and D. G. Chetwynd, Nanotechnology **9**(2), 133-142 (1998).

[Yakhno2005] Yakhno, T., V. Yakhno, A. Sanin, O. Sanina and A. Pelyushenko, Nonlinear Dynamics **39**(4), 369-374 (2005).

[Yap2005] Yap, F. L. and Y. Zhang, Langmuir **21**(12), 5233-5236 (2005).

[Zheng2004] Zheng, L. F., S. D. Li, J. P. Brody and P. J. Burke, Langmuir **20**(20), 8612-8619 (2004).

[Zhu2002] Zhu, C., M. Long, S. E. Chesla and P. Bongrand, Annals of Biomedical Engineering **30**(3), 305-314 (2002).

Curriculum Vitae

Personal Data

Name:	Nicola Naujoks
Date of Birth:	8th of June 1977
Place of Origin:	Hannover, Germany
Nationality:	German

Education

1983 – 1985	Grundschule (Primary School), Pattensen, Germany
1985 – 1987	Grundschule (Primary School), Laatzen, Germany
1987 – 1989	Orientierungsstufe, Laatzen, Germany
1989 – 1996	Gymnasium (Secondary School), Laatzen, Germany Degree: Abitur
1996 – 2001	Technische Universität Clausthal (TU Clausthal) Clausthal-Zellerfeld, Germany Degree: Diploma in Process Engineering (Dipl.-Ing.)
2001 – 2005	Nanotechnology Group Eidgenössische Technische Hochschule Zürich (ETH) (Swiss Federal Institute of Technology) Ph.D. in the field of Nanotechnology Thesis advisors: Prof. Dr. A. Stemmer (ETH Zürich) and Dr. Patrik Hoffmann (EPF Lausanne).